

CONSTRUCTION OF POLYPHOSPHORAMIDATES WITH ACID-TRIGGERED
BACKBONE DEGRADATION

A Dissertation

by

HAI WANG

Submitted to the Office of Graduate and Professional Studies of
Texas A&M University
in partial fulfillment of the requirements for the degree of

DOCTOR OF PHILOSOPHY

Chair of Committee,	Karen L. Wooley
Committee Members,	Hongcai Zhou
	Zhilei Chen
	Quentin Michaudel
Head of Department,	Simon W. North

December 2018

Major Subject: Chemistry

Copyright 2018 Hai Wang

ABSTRACT

This dissertation focuses on the development of advanced synthetic methodologies to afford well-defined polyphosphoramidates (PPAs) containing acid-labile backbone linkages (phosphoramidate). By applying these methodologies, a library of monomers and corresponding polymers could be produced with various functionalities, hydrophilicities, and degradation rates. Further, PPA-based pH-responsive drug delivery systems were developed and exhibited accelerated drug release profiles under acidic conditions compared to neutral conditions, which was demonstrated to enhance the efficacy of an anticancer drug.

In the first study, highly water-soluble PPAs with acid-labile backbone linkages were prepared readily under basic conditions *via* organobase-catalyzed ring-opening polymerization (ROP) of a five-membered-ring monomer. The ROP kinetics were explored, demonstrating these polymerizations proceeded in a controlled manner under basic conditions *via* the selective cleavage of P–O bonds during the ROP. Degradation studies demonstrated these PPAs underwent rapid backbone degradation under acidic conditions through the cleavage of P–N bonds, yielding oligomers within several days at pH 5 (17.5% P–N bond cleavage after 3 d, $DP_n = 90$). Compared to months required for their polyphosphoester analogs, which share the same structures except for the P–N linkages, PPAs exhibited significantly faster degradation under acidic conditions.

In the second study, the methodology to afford PPAs was advanced to allow for the preparation of well-defined functional PPA-based block copolymers that co-assembled with the anticancer drug camptothecin (CPT) to achieve well-dispersed nanotherapeutics. The nanotherapeutics allowed the aqueous suspension of CPT at concentrations up to 1600× higher than the aqueous solubility of the drug. Encapsulation of CPT by the polymer inhibited premature

hydrolysis of CPT at pH 7.4 and enabled accelerated CPT release at pH 5.0 (4× faster than at pH 7.4). The performance of CPT-loaded nanotherapeutics was evaluated *in vitro* and revealed enhanced efficacy relative to free CPT in cancer cells and similar toxicity in healthy cells.

In the third study, the synthesis towards α -amino acid-based PPAs *via* ROP was carefully evaluated. The hydrolytic degradation of the resulted highly water-soluble PPAs was studied, which revealed a faster degradation rate compared to its analogs without methyl carboxylate groups. Furthermore, the introduction of methyl carboxylate groups endowed the amino acid-based PPAs with intumescence, which made it a potential candidate for advanced coatings.

DEDICATION

To my family, friends, and Professor Karen L. Wooley who have always inspired and encouraged me.

ACKNOWLEDGEMENTS

I would first like to thank my advisor, Professor Karen L. Wooley. It was her email on March 30th, 2012 helped me make my most important decision of life to come to Texas A&M University for my Ph.D. degree. I also clearly remember my first conversation with Karen on August 3rd, 2012, after which I was fortunate to become a member of the group. During the past 6 years, I have experienced success and failure in both my life and research. It was Karen that taught me to dig into the nature of chemistry, supported me when I was in turbulence, encouraged me when I lost my passion and confidence. Every time I look back, I appreciate what I have learned from her and this group. To me, she is much more than an advisor for research, but an advisor for life. I believe it is not just a coincidence that I actually share the same birthday with one of her sons. Together I would like to specifically thank Professor Craig J. Hawker, who helped me tremendously start graduate school and led me to Karen. His enthusiasm also inspired my research and I always benefit from his suggestions for delivering presentations.

Secondly, I would like to thank my committee Professors Hongcai Zhou, Zhilei Chen, Quentin Michaudel, and Steven E. Wheeler (former committee member). Their advice and support have also guided my research. I would like to thank my all my collaborators for their insightful discussions and help, particularly Professor Shiyi Zhang, my friend and mentor who guided me to the world of polyphosphoesters and polyphosphoramidates. I am also extremely grateful to the Wooley group, it has been a wonderful experience to be a team with all of them. I would like to offer particular thanks to those current and former members who gave me help and valuable advice on both my life and my research: Dr. Lu Su, Dr. Fuwu Zhang, Dr. Jingwei Fan, Dr. Jiong Zou, Dr. Wenjun Du, Dr. Simcha Felder, Dr. Kevin Wacker, Dr. Ashlee Jahnke, Dr. Justin Smolen, Mr.

Richen Li, Ms. Mei Dong, Ms. Yue Song, Mr. Yen-Nan Lin, Mr. David Khoi Viet Tran, Mr. Chris H. Komatsu, Mr. Eric Leonhardt, Mr. Benjamin Demor, Ms. Brooke Versaw, Mr. Andy Moutray, Ms. Sherry Melton.

Finally, I would like to thank my family for their unconditional love, trust, and support.

CONTRIBUTORS AND FUNDING SOURCES

Contributors

This dissertation was supervised by a committee of researchers at Texas A&M: Prof. Karen L. Wooley (advisor) of the Departments of Chemistry, Chemical Engineering, and Materials Science and Engineering; Prof. Hongcai Zhou (committee member) of the Departments of Chemistry, and Materials Science and Engineering; Prof. Quentin Michaudel (committee member) of the Departments of Chemistry; Prof. Steven E. Wheeler (former committee member) of the Departments of Chemistry; Prof. Zhilei Chen (committee member) of the Departments of Microbial Pathogenesis and Immunology.

In Chapter II, synthesis of monomers and polymers were performed with the help of Dr. Lu Su and Mr. Richen Li both of the Department of Chemistry. Degradation studies were performed with the help of Dr. Shiyi Zhang, Dr. Jingwei Fan and Dr. Fuwu Zhang all of the Department of Chemistry. Electrospray ionization mass spectrometry experiments were performed by Mr. Tan P. Nguyen of the Department of Chemistry. Matrix-assisted laser desorption ionization time-of-flight mass spectrometry experiments were performed by Laboratory for Biological Mass Spectrometry of Texas A&M University.

In Chapter III, thermal characterization and transmission electron microscopy experiments were performed by Ms. Mei Dong of the Department of Chemistry. Cytotoxicity study was carried by Ms. Sarosh Khan and Dr. Mahmoud Elsabahy both of the Department of Chemistry. Dynamic light scattering study and drug release study were performed with the help of Dr. Lu Su and Mr. Richen Li both of the Department of Chemistry. Characterizations of the polymers were performed with the help of Ms. Yue Song and Mr. Yen-Nan Lin both of the Department of

Chemistry. Matrix-assisted laser desorption ionization time-of-flight mass spectrometry experiments were performed by Ms. Nari Kang and Mr. Christopher Houston Komatsu both of the Department of Chemistry.

In Chapter IV, synthesis of monomers and polymers were performed with the help of Ms. Mei Dong and Mr. Richen Li both of the Department of Chemistry.

All other experiments were carried out independently by the student.

Funding Sources

The work in Chapter II, III and IV were made possible by financial support from the National Science Foundation (DMR-1507429 and DMR-1309724) and the Welch Foundation through the W. T. Doherty-Welch Chair in Chemistry (A-0001).

The contents are solely the responsibility of the authors and do not necessarily represent the official views of the National Science Foundation, or the Welch Foundation.

NOMENCLATURE

BYOMP	(4 <i>S</i>)-2-(But-3-yn-1-yloxy)-4-methyl-1,3,2-oxazaphospholidine 2-oxide
BYPC	3-Yn-1-yl phosphorodichloridate
CDCl ₃	Deuterated chloroform
conc.	Concentration
conv.	Conversion
COSY	Homonuclear correlation spectroscopy
CPT	Camptothecin
CPT@PPA	Camptothecin-loaded polyphosphoramidates nanoparticles
CuAAC	Copper(I)-catalyzed azide-alkyne cycloaddition
\mathcal{D}	Dispersity index
D_{av}	Average diameter
D ₂ O	Deuterium oxide
DBU	1,8-Diazabicyclo[5.4.0]undec-7-ene
DCM	Dichloromethane
DCTB	Trans-2-[3-(4- <i>tert</i> -butylphenyl)-2-methyl-2-propylidene]malonitrile
$D_{h(\text{number})}$	Number-average hydrodynamic diameter
DLS	Dynamic light scattering
DMF	<i>N,N</i> -Dimethylformamide
DNA	Deoxyribonucleic acid
DP_n	Degree of polymerization
DSC	Differential scanning calorimetry

EOMP	(4 <i>S</i>)-2-ethoxy-4-methyl-1,3,2-oxazaphospholidine 2-oxide
ESI-MS	Electrospray ionization mass spectrometry
FT-IR (ATR)	Fourier-transform infrared (attenuated total reflection)
HPLC	High performance liquid chromatography
HRMS	High resolution mass spectrometry
IC ₅₀	Half maximal inhibitory concentration
KTFA	Potassium trifluoroacetate
[M] ₀ /[I] ₀	Monomer/initiator feed ratio
MALDI-Tof MS	Matrix-assisted laser desorption ionization time-of-flight mass spectrometry
MEOPC	Methyl (4 <i>S</i>)-2-ethoxy-1,3,2-oxazaphospholidine-4-carboxylate 2-oxide
MLS	Methyl L-serinate
MLS·HCl	Methyl L-serinate hydrochloride
M_n	Number average molar mass
$M_{n, \text{NMR}}$	Number average molar mass determined by end group analysis by ¹ H NMR spectroscopy of the polymer
M_w	Weight average molar mass
MS/MS	tandem mass spectrometry
MWCO	Molecular weight cutoff
NCA <i>s</i>	<i>N</i> -carboxyanhydrides
NEt ₃	Triethylamine
NMR	Nuclear magnetic resonance
PBS	Phosphate buffered saline

PBYOMP	(4 <i>S</i>)-2-(but-3-yn-1-yloxy)-4-methyl-1,3,2-oxazaphospholidine 2-oxide
PEOMP	Poly((4 <i>S</i>)-2-ethoxy-4-methyl-1,3,2-oxazaphospholidine 2-oxide)
PEMEP	Poly(4-methyl-2-oxo-2-ethyl-1,3,2-dioxaphospholane)
PMEOPC	Poly(methyl (4 <i>S</i>)-2-ethoxy-1,3,2-oxazaphospholidine-4-carboxylate 2-oxide)
PMOEPS	Poly(2-((2-methoxyethyl)amino)-1,3,2-dioxaphospholane 2-oxide, <i>N</i> -methoxyethyl phospholane amidate)
PTA	Phosphotungstic acid
PPA	Polyphosphoramidates
PPE	Polyphosphoester
ROMP	Ring-opening metathesis polymerization
ROP	Ring-opening polymerization
SEC	Size exclusion chromatography
TBD	1,5,7-Triazabicyclo[4.4.0]dec-5-ene
TEM	Transmission electron microscopy
T_g	Glass transition temperature
TGA	Thermogravimetric analysis
THF	Tetrahydrofuran

TABLE OF CONTENTS

	Page
ABSTRACT.....	ii
DEDICATION.....	iv
ACKNOWLEDGEMENTS.....	v
CONTRIBUTORS AND FUNDING SOURCES.....	vii
NOMENCLATURE.....	ix
TABLE OF CONTENTS.....	xii
LIST OF FIGURES.....	xiv
LIST OF TABLES.....	xviii
CHAPTER I INTRODUCTION.....	1
CHAPTER II POLYPHOSPHORAMIDATES THAT UNDERGO ACID- TRIGGERED BACKBONE DEGRADATION.....	9
2.1 Introduction.....	9
2.2 Experimental Section.....	10
2.3 Results and Discussion.....	19
2.4 Conclusions.....	31
CHAPTER III ACID-TRIGGERED POLYMER BACKBONE DEGRADATION AND DISASSEMBLY TO ACHIEVE RELEASE OF CAMPTOTHECIN FROM FUNCTIONAL POLYPHOSPHORAMIDATE NANOPARTICLES.....	33
3.1 Introduction.....	33
3.2 Experimental Section.....	35
3.3 Results and Discussion.....	47
3.4 Conclusions.....	57
CHAPTER IV CONSTRUCTION OF POLYPHOSPHORAMIDATES WITH ACID-TRIGGERED BACKBONE DEGRADATION USING α -AMINO ACIDS AS BUILDING BLOCKS.....	59
4.1 Introduction.....	59
4.2 Experimental Section.....	61
4.3 Results and Discussion.....	67

4.4 Conclusions.....	77
CHAPTER V CONCLUSIONS AND FUTURE WORK.....	78
5.1 Conclusions.....	78
5.2 Future Work.....	80
REFERENCES	83

LIST OF FIGURES

	Page
Figure I-1. Structures of DNA, RNA and PPEs.....	2
Figure I-2. a) Reported synthetic approach for PPEs <i>via</i> tin (II) 2-ethylhexanoate. b) Reported synthetic approach for PPEs <i>via</i> a organobase catalyst DBU.....	3
Figure I-3. The structure of poly(methyl ethylene phosphate) and the half-life of its hydrolytic degradation under different conditions.	4
Figure I-4. a) Reported synthetic approach for PPAs <i>via</i> Atherton-Todd reaction. b) Polymerization of cyclic phosphoramidate monomer <i>via</i> organobase-catalyzed ROP and cleavage of the side-chain moieties to afford polyphosphate.....	5
Figure I-5. Polymerization of (4 <i>S</i>)-2-ethoxy-4-methyl-1,3,2-oxazaphospholidine 2-oxide to afford polymers bearing phosphoramidate linkages along the backbone and its hydrolytic degradation under acidic conditions.	6
Figure I-6. Co-assembly of PPAs with CPT to afford nanotherapeutics, and its distinct release mechanism under different pH values.....	7
Figure I-7. ROP to afford α -amino acid-based PPAs and its hydrolytic degradation.	8
Figure II-1. Synthesis and polymerization of (4 <i>S</i>)-2-ethoxy-4-methyl-1,3,2- oxazaphospholidine 2-oxide (EOMP), 1, to afford polymers (PEOMP) bearing phosphoramidate linkages along the backbone, 2.	10
Figure II-2. COSY spectrum of EMOP in CDCl ₃ . Protons at the same position but belonging to different isomers were assigned as H _{x1} and H _{x2} , H _{c1} and H _{c2} for example. If signals of the protons labelled as H _{x1} and H _{x2} overlapped with each other and were not distinguishable, H _x would be used as the assignment, H _b for example. Enantiotopic protons were assigned as H _{c1} and H _{c1'} and H _{c2} and H _{c2'} . Signals of the protons labelled as H _f were overlapped with those of protons labelled as H _{c2'} , H _{d2} and H _{c1'}	14
Figure II-3. FT-IR spectra of EOMP and PEOMP ($DP_n = 90$).....	14
Figure II-4. TGA trace of PEOMP ($DP_n = 90$).....	16
Figure II-5. ³¹ P NMR spectrum of the model reaction mixture for the ring opening of EOMP with [M] ₀ /[I] ₀ of 1, at a monomer concentration of 2.2 M (same as the polymerization) after 5 min.....	16
Figure II-6. SEC traces of the chain extension experiment of EOMP. Initial PEOMP achieved with [M] ₀ /[I] ₀ of 50, at a monomer concentration of 2.2 M. Extended	

PEOMP achieved with addition of EOMP with $[M]_0/[I]_0$ of 50, at a monomer concentration of 1.5 M.	18
Figure II-7. NMR spectra of EOMP in $CDCl_3$ (ppm): a) 1H NMR (500 MHz) (see detailed assignments in Fig. S1.), b) ^{13}C NMR (126 MHz), c) ^{31}P NMR (202 MHz). NMR spectra of PEOMP in $CDCl_3$ (ppm): d) 1H NMR (500 MHz), e) ^{13}C NMR (126 MHz), f) ^{31}P NMR (202 MHz).	20
Figure II-8. a) Plot of M_n and \bar{D} vs monomer conversion for the polymerization of EOMP using TBD as the catalyst and 4-methylbenzyl alcohol as the initiator, obtained from a combination of SEC, 1H NMR and ^{31}P NMR spectroscopic analyses. The ratio of monomer : initiator : TBD was 100 : 1 : 2. b) Plots of monomer conversion ($\ln([M]_0/[M])$) vs time obtained from ^{31}P NMR spectra. c) SEC traces (DMF as eluent, 1 mL/min) of the ROP of EMOP vs time. d) MALDI-ToF MS spectrum of PEMOP ($DP_n = 10$).	23
Figure II-9. a) Kinetics of PEOMP degradation at different pH values, as monitored by ^{31}P NMR spectroscopy. b) Transition of ^{31}P NMR resonances of PEOMP over a period of conversion at pH 3.0. c) Progress of the degradation of PEOMP at pH 3.0, as monitored by SEC.	26
Figure II-10. a) Scheme of hydrolytic degradation of homopolymer 2. ESI-MS analysis (negative ion mode, tested m/z range 50-2000) of the degradation products of 2 under different conversions, b) 40%, c) 62% and d) 94%, obtained from ^{31}P NMR spectra.	28
Figure II-11. MS/MS spectrum of E_2 (positive ion mode).	29
Figure II-12. Analysis of series H in Figure II-10c (negative ion mode).	30
Figure II-13. a) MS/MS spectrum of H_1 (positive ion mode). b) MS/MS spectrum of H_5 (positive ion mode).	30
Figure II-14. Analysis of series I and I' (negative ion mode).	31
Figure III-1. a) Hydrolysis of CPT. b) Polymerization of EOMP, 5, to afford PEOMP, 1, with acid-triggered backbone degradation. c) Synthesis, and polymerization of BYOMP, 3, to afford alkyne-functionalized polyphosphoramidates, PBYOMP, 6. d) One-pot sequential polymerization of 5 and 3 to afford the amphiphilic diblock copolymer PEOMP- <i>b</i> -PBYOMP, 2.	35
Figure III-2. COSY spectrum of BYOMP in $CDCl_3$. Protons at the same position but belonging to different isomers were assigned as H_{x1} and H_{x2} , H_{f1} and H_{f2} for example. If signals of the protons labeled as H_{x1} and H_{x2} overlapped with each other and were not distinguishable, H_x would be used as the assignment, H_b and H_c for example. Enantiotopic protons were assigned as H_{d1} and $H_{d1'}$ and H_{d2} and $H_{d2'}$.	

Signals of the protons labeled as H _g were overlapped with those of protons labeled as H _{d2} , H _{e2} , and H _{d1}	40
Figure III-3. FT-IR spectra of BYOMP, PBYOMP, PEOMP- <i>b</i> -PBYOMP, and PEOMP.....	41
Figure III-4. TGA traces of PEOMP, PBYOMP, and PEOMP- <i>b</i> -PBYOMP.....	43
Figure III-5. a) Plot of M_n and \bar{D} vs monomer conversion for the polymerization of BYOMP using TBD as the catalyst and 4-methylbenzyl alcohol as the initiator, obtained from a combination of SEC, ¹ H NMR and ³¹ P NMR spectroscopic analyses. The ratio of monomer : initiator : TBD was 100 : 1 : 2. b) Plots of monomer conversion (ln([M] ₀ /[M])) vs time obtained from ³¹ P NMR spectra.	50
Figure III-6. MALDI-Tof MS spectrum of PBYOMP ($DP_n = 8$).....	50
Figure III-7. SEC traces of PEOMP and PEOMP ₄₉ - <i>b</i> -PBYOMP ₉₈ . PEOMP was synthesized with [M] ₀ /[I] ₀ = 50 at [M] = 2.2 M. Chain extension of BYOMP from PEOMP macroinitiator at [M] ₀ /[I] ₀ = 100 at [M] = 2.0 M yielded PEOMP- <i>b</i> -PBYOMP.....	53
Figure III-8. a) TEM images of PPA micelles negatively stained by 1 wt% phosphotungstic acid aqueous solution (10 μL) with an average diameter (D_{av}) of 22 ± 4 nm (counting > 50 nanoparticles). b) Number-, volume- and intensity-based hydrodynamic diameter of PPA micelles in nanopure water measured by DLS.	54
Figure III-9. a) Schematic representation of the formation of CPT@PPA by physical encapsulation of CPT into PPA . b) Number-, intensity- and volume-based hydrodynamic diameter distributions of CPT@PPA in nanopure water measured by DLS. c) TEM images of CPT@PPA negatively stained by 1 wt% phosphotungstic acid aqueous solution (10 μL), $D_{av} = 24 \pm 4$ nm (counting > 50 nanoparticles). The dark spots are artifacts from phosphotungstic acid.	54
Figure III-10. a) Release of CPT from CPT@PPA (10 wt%) at pH 5.0 and pH 7.4, that studied by a dialysis method over 2.5 d at 37 °C in citric acid – Na ₂ HPO ₄ and PBS buffers, respectively, measured in triplicates. Cytotoxicity of CPT, PPA micelles, and CPT@PPA in (b) SJS-A-1 and (c) MC3T3 cells. Cell viabilities are reported as an average of three measurements.	56
Figure IV-1. a) Well-defined PPAs achieved through ROP of cyclic monomers derived from a β-amino alcohol, which were able to undergo accelerated degradation under acidic conditions. b) ROP of a novel cyclic monomer derived from methyl L-serinate to afford well-defined PPAs with acid-labile linkages along the backbone.....	61
Figure IV-2. ³¹ P NMR (202 MHz, CDCl ₃) of the crude products achieved by the two-step trial synthesis. Representative structures of impurities and the product are labeled to the corresponding peaks.	64
Figure IV-3. TGA trace of PMEOPC ₆₉	66

Figure IV-4. a) Two-step trial synthesis of MEOPC from MLS·HCl salt. b) One-step synthesis of MEOPC from MLS·HCl salt with proposed reaction process and intermediates.	69
Figure IV-5. ³¹ P NMR (202 MHz, CDCl ₃) of the crude products achieved by the one-step synthesis.	70
Figure IV-6. a) ¹ H NMR (500 MHz, CDCl ₃) of PMEOPC. b) ¹ H NMR (500 MHz, CDCl ₃) of MEOPC.	71
Figure IV-7. a) ¹³ C NMR (126 MHz, CDCl ₃) of PMEOPC. b) ¹³ C NMR (126 MHz, CDCl ₃) of MEOPC.	71
Figure IV-8. Plots of monomer conversion (ln([M] ₀ /[M])) vs time obtained from ³¹ P NMR spectra.	74
Figure IV-9. ³¹ P NMR (202 MHz, CDCl ₃) of the crude products achieved by the one-step synthesis.	74
Figure IV-10. A piece of char of PMEOPC after TGA.	75
Figure IV-11. Kinetics of PMEOPC degradation at different pH values, as monitored by ³¹ P NMR spectroscopy.	76
Figure V-1. a) Proposed route to achieve polyphosphonamidates. b) Proposed route to achieve polyphosphordiamidates.	80
Figure V-2. a) Drug conjugation for PPAs <i>via</i> thiol-ene reaction. b) Dye conjugation for PPAs <i>via</i> CuAAC.	81
Figure V-3. Schematic synthesis and degradation of PPA hydrogels based on an α-amino acid.	82

LIST OF TABLES

	Page
Table II-1. Polymerization of EOMP Catalyzed by TBD under Different Conditions ^a	21
Table III-1. Polymerization of BYOMP catalyzed by TBD under different conditions ^a	49
Table III-2. Comparison of the IC ₅₀ values of CPT, PPA micelles and CPT@PPA in OVCAR-3, RAW264.7, and SJSA-1 cell lines.....	57
Table IV-1. Polymerization of MEOPC catalyzed by TBD under different conditions ^a	72

CHAPTER I

INTRODUCTION

Polymeric materials have enabled many of the major technological advances of the last 50 years. Polymers are used in a variety of important applications including electronics, engineering materials, transportation, biomedical devices, and packaging. Polymers are probably the most widely used materials, which can be found in almost every circumstance of our daily life. Recently, there has been considerable interest in the development of synthetic polymers that share similar compositions and architectures with those of polymers found in Nature.¹⁻³ These synthetic analogs are expected to possess the ability for natural clearance mechanisms, and explored for their biological and environmental applications, for instance, tissue engineering,⁴ regenerative medicine,⁵ gene therapy,⁶ controlled drug delivery⁷ *etc.*

Genetic information of all living organisms is stored on RNA and DNA, which are polyphosphodiester made from phosphoric acid and ribose/deoxyribose. Synthetic polyphosphoesters (PPEs), which share similar structures with RNA and DNA (Figure I-1), have received significant attention due to their good biocompatibility and biodegradability, among other favorable characteristics.⁸ By taking advantage of the pentavalent phosphorus atom, reactive pendent groups such as alkene, alkyne, hydroxyl, and carboxyl groups can be easily introduced as side-chain functionalities.^{8,9} The mechanical and chemical properties of PPEs can be manipulated in a straightforward manner by alteration of the backbone or the side chains, giving them extraordinary structural versatility and making them promising candidates in biomedical applications.¹⁰

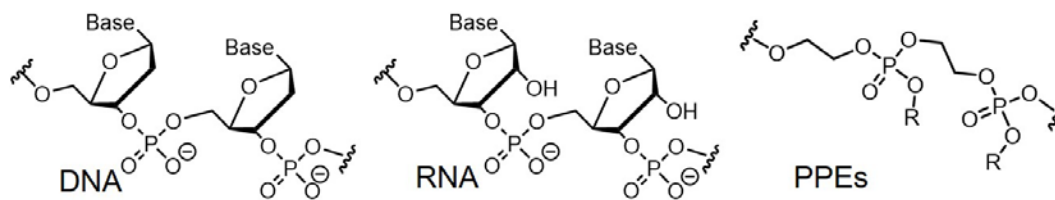


Figure I-1. Structures of DNA, RNA and PPEs.

PPEs could be prepared by various polymerization techniques. In the early stage of the development, PPEs were mainly prepared by condensation polymerization, which had little control over the polymerization and resulted in polymers with broad dispersity (\mathcal{D}).¹¹⁻¹³ In addition, harsh reaction conditions (high temperatures, acidic side products, *etc.*) are often necessary for condensation polymerization to yield polymers with high molar mass, which limit the introduction of functional groups and impede many applications for PPEs.

Efficient and controlled polymerization techniques are needed to precisely construct the architectures of PPEs and adjust the characteristics of the polymer to match specific applications. During the past decades, controlled ring-opening polymerization (ROP) has been developed to allow the selective introduction of functional groups in the α - or ω - position with precise control over the polymer microstructure. Many different types of polymers could be synthesized *via* ROP, including polyesters, polyamides, polyethers, polycarbonates, polyacetals, *etc.*¹⁴ In general, a cyclic monomer with high ring strain is required for ROP. Six-membered cyclic phosphoester were found to yield only PPE with low molar mass and oligomers due to the low ring strain. In comparison, the high ring strain (15-30 kJ·mol⁻¹) makes five-membered cyclic phosphoester suitable monomers for ROP.⁸

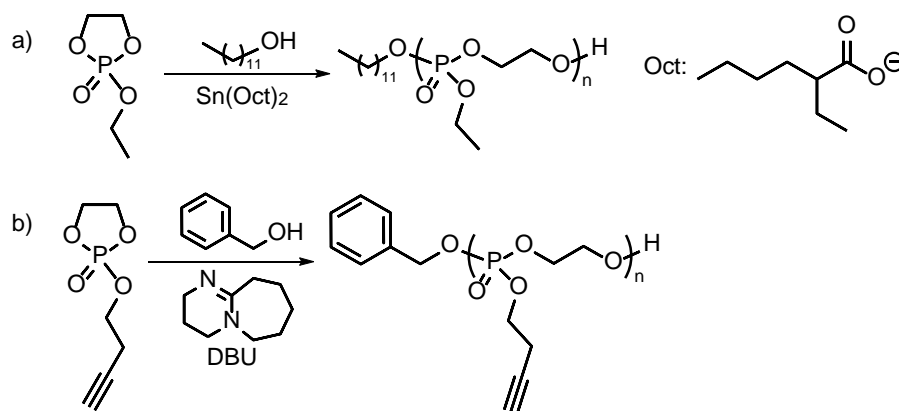
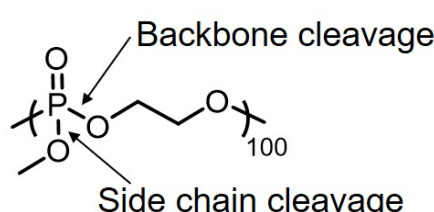


Figure I-2. a) Reported synthetic approach for PPEs *via* tin (II) 2-ethylhexanoate. b) Reported synthetic approach for PPEs *via* an organobase catalyst DBU.

Metal catalysts, for example, tin (II) 2-ethylhexanoate, have proven to be among the most efficient catalysts for ROP by an insertion mechanism. PPEs were achieved with a narrow \bar{D} and a controlled molar mass by the catalysis of tin (II) 2-ethylhexanoate (Figure I-2a).¹⁵ However, the toxicity of metal-based catalysts raised concern for this kind of materials to be used in biomedical applications. Organobase catalysts, *e.g.*, 1,8-diazabicyclo[5.4.0]undec-7-ene (DBU) and 1,5-diazabicyclo[5.4.0]undec-5-ene (TBD), showed excellent control in the ROP of lactide and other cyclic monomers, were considered as promising candidates for the ROP of cyclic phosphoester (Figure I-2b).¹⁶⁻²² They were firstly investigated by Iwasaki and Yamaguchi to afford PPEs.²³ The ultrafast organobase-catalyzed ROP offered great control over the molar mass, \bar{D} , compositions, and structures of PPEs, and also eliminates the usage of metal compounds, to fulfill the requirements of biomedical and environmental applications.²⁴ Later, Clément *et al.* found that the performance of DBU can be improved by the addition of a thiourea co-catalyst.²⁵

The hydrolytic degradation of PPEs has been studied by many researchers, which reveal that PPEs can be very stable under acidic conditions but degrade fast in the presence of a base.²⁶



The chemical structure shows a phosphate group (P=O, P-O) linked to an ethylene chain (-CH2-CH2-O-), which is further linked to another phosphate group. Arrows indicate 'Backbone cleavage' at the P-O bond and 'Side chain cleavage' at the C-O bond. The number 100 is shown at the end of the ethylene chain.

	pH	$t_{1/2, \text{ side chain (h)}}$	$t_{1/2, \text{ backbone (h)}}$	$t_{1\%, \text{ backbone (h)}}$
	12.30	6	5	0.1
	9.60	219	429	6
	7.30	5121	15161	220
	3.15	2778	13188	191
	1.50	1750	9579	139

Figure I-3. The structure of poly(methyl ethylene phosphate) and the half-life of its hydrolytic degradation under different conditions.

A typical water-soluble example is poly(methyl ethylene phosphate). As shown in Figure I-3, the half-life of both the side chain and backbone cleavage is much smaller under basic conditions than that under neutral and acidic conditions.²⁷ These observations are likely due to the stability of phosphoester bond under acidic conditions. In addition, under basic conditions, the side chain and backbone cleave at similar rates, while the side chains cleavage is more preferred, however with a much slower rate, under acidic condition. Meanwhile, phosphoramidate bonds are acid-labile,²⁸ and switching the side chain linkages from phosphoester bonds to phosphoramidates results in polyphosphoramidates (PPAs), which is expected to have further accelerated side chain cleavage under acidic conditions. This unique degradation mechanism could be exploited to achieve pH-responsive systems, such as drug carriers with acid-triggered release.

As reported previously, PPAs are conventionally prepared by the polymerization of 4-methyl-2-oxo-2-hydro-1,3,2-dioxaphospholane in the presence of metal catalyst triisobutylaluminum, followed by the modification of the resulting poly(1,2-propylene H-phosphonate) using amines via an Atherton-Todd reaction (Figure I-4a).²⁹ After the development of this method toward PPAs, a family of PPAs with different pendant amino groups was

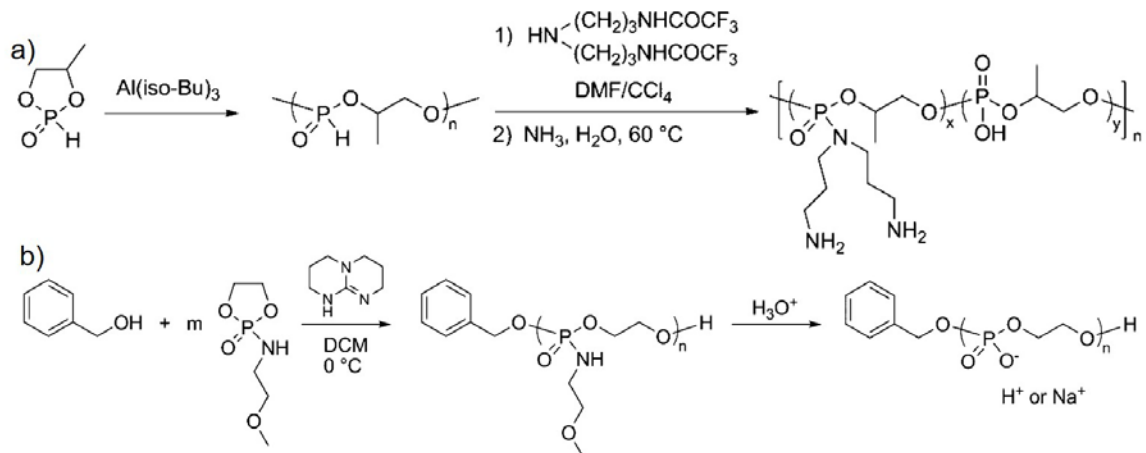


Figure I-4. a) Reported synthetic approach for PPAs *via* Atherton-Todd reaction. b) Polymerization of cyclic phosphoramidate monomer *via* organobase-catalyzed ROP and cleavage of the side-chain moieties to afford polyphosphate.

synthesized and applied for the delivery of nucleic acids.³⁰⁻³⁴ Because of the limited reactivity of the Atherton-Todd reaction, at least 25% of the PH groups were converted into phosphates rather than phosphoramidate bonds, which resulted in a random copolymer.³³ The lack of a simple and reliable synthetic route to functional PPA constitutes a significant barrier to the widespread application of this degradable polymer platform.

We took advantage of the state-of-the-art ROP technique to afford PPEs and expanded the synthetic methodology to the direct synthesis of acid-labile PPAs (Figure I-4b).⁹ The achieved PPAs could undergo selective cleavage of the side-chains and afford polyphosphates. However, the response of the achieved PPAs to pH was only mild, only 20% of the side-chain moieties could be cleaved at pH 3 after 5 d. Fully cleavage of the side chain moieties could be only achieved at harsh conditions (pH 1), which left room for further improvement. This study inspired us to explore the possibility of synthesizing PPAs with acid-labile backbone linkages. The introduction of acid-labile linkages along the polymer backbone could lead to rapid degradation of the polymer

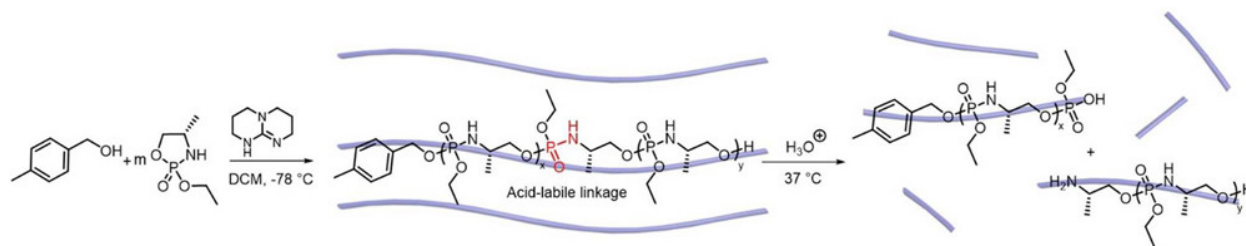


Figure I-5. Polymerization of (4*S*)-2-ethoxy-4-methyl-1,3,2-oxazaphospholidine 2-oxide to afford polymers bearing phosphoramidate linkages along the backbone and its hydrolytic degradation under acidic conditions.

under acidic conditions and a sharp decrease in molar mass even with partial conversion of the linkages. Till today, few examples with well-defined polymers containing acid-labile backbone linkages have been reported,³⁵ and it will be advantageous to achieve well-defined PPAs with acid-labile backbone linkages due to their good biocompatibility, biodegradability, and versatility to incorporate functionalities.

This dissertation is focused on the design and development of PPAs with backbone acid-labile linkages. In Chapter II, the synthetic methodologies to directly synthesize PPAs with acid-labile backbone linkages are reported, together with a demonstration of their hydrolytic degradability, evaluated under acidic conditions (Figure I-5). The introduction of acid-labile linkages along the polymer backbone led to rapid degradation of the polymer backbone upon the environmental stimuli. An oxazaphospholidine monomer bearing a phosphoramidate linkage was designed and synthesized to afford the PPAs *via* organobase-catalyzed ROP in a controlled manner. The hydrolytic degradation of the PPAs was studied, revealing the breakdown of the polymer backbone through cleavage of the phosphoramidate linkages under acidic conditions.

In Chapter III, fundamental synthetic methodology was advanced to allow for the preparation of well-defined functional PPA-based block copolymers that co-assembled with

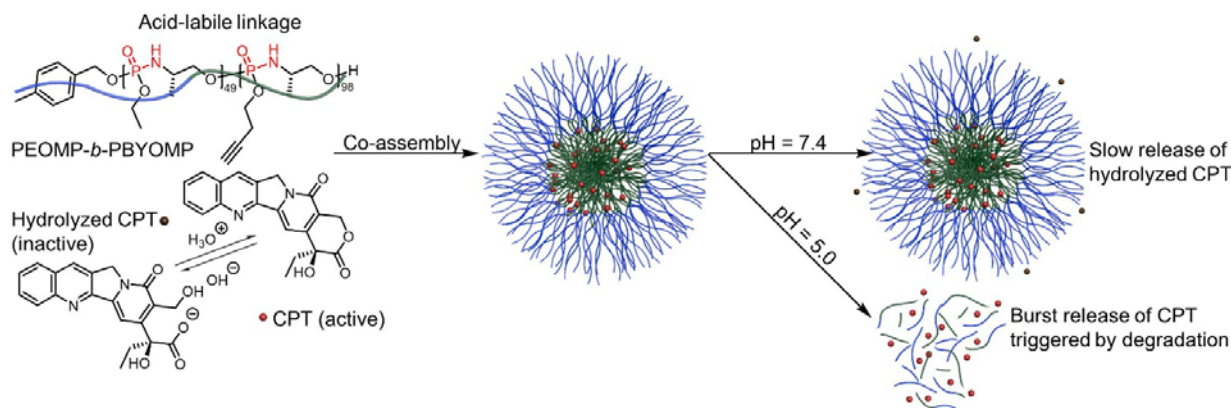


Figure I-6. Co-assembly of PPAs with CPT to afford nanotherapeutics, and its distinct release mechanism under different pH values.

Camptothecin (CPT) into nanoparticles, which underwent coincident acid-triggered polymer backbone degradation, nanoparticle disassembly and CPT release (Figure I-6). CPT is a promising anticancer drug, yet its therapeutic potential has been limited by poor water solubility and facile hydrolysis of the lactone form into an inactive carboxylate form at neutral pH. Encapsulation of CPT by the PPA polymer inhibited premature hydrolysis of CPT at pH 7.4 and enabled accelerated CPT release at pH 5.0 (*ca.* 4× faster than at pH 7.4). Two degradable oxazaphospholidine monomers, with one carrying an alkyne group, were synthesized to access well-defined block PPAs (dispersity, D , < 1.2) *via* sequential organobase-catalyzed ROP. The resulting amphiphilic block copolymers were physically loaded with CPT to achieve well-dispersed nanotherapeutics, which allowed the aqueous suspension of CPT at concentrations up to 3.2 mg/mL, significantly exceeding the aqueous solubility of the drug (< 2.0 $\mu\text{g/mL}$ at 37 °C). Cytotoxicity studies revealed enhanced efficacy of the CPT-loaded nanoparticles over free CPT in cancer cells and similar toxicity in normal cells.

In Chapter IV, the development of α -amino acid-based PPAs with acid-triggered backbone degradation was explored. Compared to the β -amino alcohol used in Chapter II and III, the carboxylate group of α -amino acid, particularly methyl carboxylate of methyl L-serinate, complicated the annulation to achieve cyclic monomers (Figure I-7). The cyclic phosphoramidate monomer, which was afforded *via* a state-of-the-art one-step synthesis directly from methyl L-serinate hydrochloride, could be controlled polymerized to afford well-defined PPAs based on α -amino acids. The resulted PPAs were highly water-soluble, the hydrolytic degradation of which was studied, revealing a faster degradation rate compared to analogs without methyl carboxylate groups. Furthermore, the introduction of methyl carboxylate groups endowed PPAs with intumescence, which made it a potential candidate for advanced coatings.

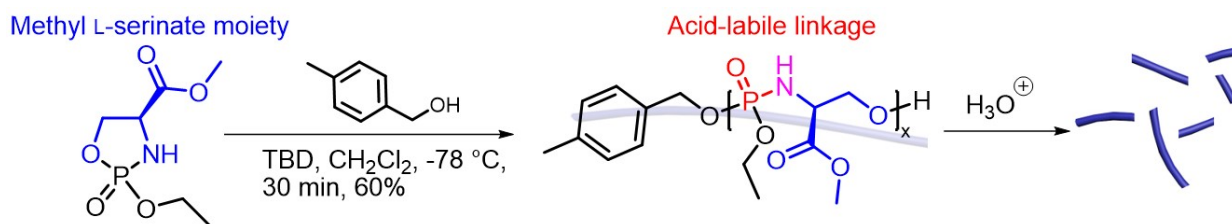


Figure I-7. ROP to afford α -amino acid-based PPAs and its hydrolytic degradation.

CHAPTER II
POLYPHOSPHORAMIDATES THAT UNDERGO ACID-TRIGGERED BACKBONE
DEGRADATION¹

2.1 Introduction

Polymeric systems with the ability to degrade under acidic conditions, while being stable under neutral pH, hold great promise for biomedical applications, for instance, the triggered release of therapeutics in cancer and inflammation, among other diseased tissues.³⁶⁻³⁸ The key to such acid-labile polymeric systems is the cleavage of acid-labile bonds, including but not limited to orthoesters,³⁹ acetals/ketals,⁴⁰ hydrazones⁴¹ and phosphoramidates.⁴² Furthermore, the introduction of acid-labile linkages along the entire polymer backbone could lead to rapid degradation of the polymer backbone, and partial degradation of the backbone linkages could result in a sharp decrease in molecular weights.⁴³ The majority of studies on polymers with acid-degradable backbones have focused on acetals/ketals⁴⁴⁻⁴⁶ and orthoesters,^{43, 47, 48} with a few others on hydrazone linkages.^{49, 50} However, the labilities of those linkages have limited the choice of polymerization methods, with polycondensation used in most of these reported polymers, resulting in broad molecular weight distributions (\mathcal{D}) and potentially impeding their applications. Besides polycondensation, polyacetals have also been achieved by acid-catalyzed acetal metathesis (\mathcal{D} ranging from 1.23-2.88, varied by polymer)⁵¹ and cationic ring-opening polymerization (ROP) (\mathcal{D}

¹Adapted with permission from “Polyphosphoramidates That Undergo Acid-Triggered Backbone Degradation” by Wang, H.; Su, L.; Li, R.; Zhang, S.; Fan, J.; Zhang, F.; Nguyen, T. P.; Wooley, K. L., *ACS Macro Lett.*, **2017**, 6 (3), 219-223. Copyright 2018 American Chemical Society

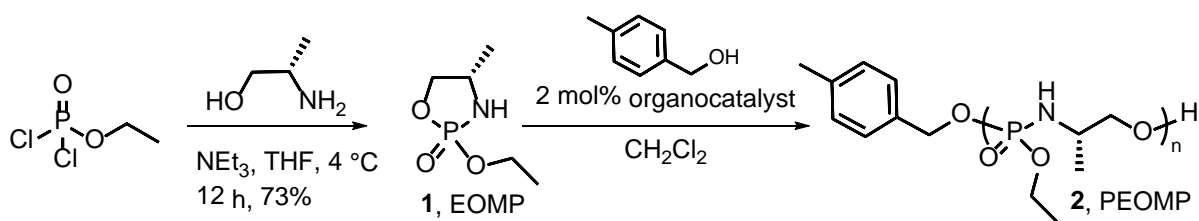


Figure II-1. Synthesis and polymerization of (4*S*)-2-ethoxy-4-methyl-1,3,2-oxazaphospholidine 2-oxide (EOMP), **1**, to afford polymers (PEOMP) bearing phosphoramidate linkages along the backbone, **2**.

ranging from 1.3-2.0, varied by polymer).⁵² Few examples with well-defined polymers containing acid-labile backbone linkages have been reported, including polyacetals achieved by acyclic diene metathesis polymerization,⁵³ and polyesteracetals achieved by cationic ROP.⁵⁴

We perceived that the intrinsic basic reaction conditions of organobase-catalyzed ROP made it especially suitable for polymerization of monomers containing acid-labile linkages. In an earlier study, we had demonstrated that phosphoramidate side chain functionalities along the backbone of a polyphosphoester underwent selective side chain cleavage under acidic conditions.⁹ Herein, we report the design and synthesis of an oxazaphospholidine monomer bearing a phosphoramidate within the cyclic structure to then place that acid-labile linkage along the backbone upon controlled organo-catalyzed ROP to afford well-defined PPAs (Figure II-1).

2.2 Experimental Section

2.2.1 Materials

All chemicals and reagents were used as received from Sigma-Aldrich Co. unless otherwise noted. Tetrahydrofuran (THF), and dichloromethane (DCM) were purified by passage through a

solvent purification system (JC Meyer Solvent Systems). 4-Methylbenzyl alcohol and 1,5,7-triazabicyclo[4.4.0]dec-5-ene (TBD) were dried over CaH₂ in THF, then vacuum dried and stored in a glovebox under Ar atmosphere. 1,8-Diazabicyclo[5.4.0]undec-7-ene (DBU) was dried over CaH₂, distilled, degassed, and stored in a glovebox under Ar atmosphere.

2.2.2 Instrumentation

¹H NMR, ³¹P NMR and ¹³C NMR spectra were recorded on Varian Inova 500 spectrometer (Varian, Inc., Palo Alto, CA) interfaced to a UNIX computer using VnmrJ software. Chemical shifts for ¹H NMR and ¹³C NMR signals were referenced to the solvent resonance frequencies. Chemical shifts for ³¹P NMR signals were referenced to a sealed capillary containing 85% H₃PO₄ placed in the sample solution.

IR spectra were recorded on an IR Prestige 21 system (Shimadzu Corp., Japan), equipped with an ATR accessory, and analyzed using IRsolution v.1.40 software.

Size exclusion chromatography (SEC) eluting with pre-filtered DMF containing 0.05 M LiBr was conducted on a Waters Chromatography, Inc. (Milford, MA) system equipped with an isocratic pump model 1515, a differential refractometer model 2414, and a four-column set including a 5 μm Guard column (50 × 7.5 mm), a Styragel HR 4 5 μm DMF column (300 × 7.5 mm), a Styragel HR 4E 5 μm DMF column (300 × 7.5 mm), and a Styragel HR 2 5 μm DMF column (300 × 7.5 mm). The system was operated at 70 °C with a flow rate of 1.00 mL/min. Polymer solutions were prepared at a concentration of *ca.* 3 mg/mL and an injection volume of 200 μL was used. Data collection and analysis were performed with Discovery32 v. 1.039.000 software (Precision Detectors, Inc., Bellingham, MA). The system was calibrated with S3 polystyrene standards (Polymer Laboratories, Amherst, MA) ranging from 615 to 442800 Da.

Glass transition temperatures (T_g) were measured by differential scanning calorimetry (DSC) on a Mettler-Toledo DSC822 (Mettler-Toledo, Inc., Columbus, OH) under N_2 . Measurements of T_g were performed with a heating rate of 5 °C/min and analyzed using Mettler-Toledo STAR^e v. 10.00 software. The T_g was taken as the midpoint of the inflection tangent of the third heating scan.

Thermogravimetric analysis (TGA) was performed under N_2 atmosphere using a Mettler-Toledo TGA/SDTA851^e, with a heating rate of 5 °C /min. Measurements were analyzed by using Mettler-Toledo STAR^e v. 10.00 software.

Matrix-assisted laser desorption ionization-time of flight (MALDI-Tof) mass spectrometry was performed on an Applied Biosystems Voyager-DE STR (Thermo Fisher Scientific, Inc., Waltham, MA) in reflector ion mode by use of laser pulses at 337 nm. Trans-2-[3-(4-*tert*-butylphenyl)-2-methyl-2-propylidene]malonitrile (DCTB) was used as a matrix.

Electrospray ionization mass spectrometry (ESI-MS) experiments were performed using a Bruker amaZon SL instrument (Bruker Corp., Billerica, MA). The sample was directly infused at a flow rate of 10 μ L/min. The spray voltage was set at 4.5 kV, nebulizer was set at 29 psi and dry gas flow was 10 L/min, respectively. Dry temperature was held at 250 °C. Tandem mass spectrometry (MS/MS) experiments were performed on the same instrument. Bruker Compass DataAnalysis v. 4.2.383.1 software was used for data acquisition and processing.

2.2.3 Synthesis

Synthesis of (4*S*)-2-ethoxy-4-methyl-1,3,2-oxazaphospholidine 2-oxide (EOMP)

A solution of (*S*)-(+)-2-amino-1-propanol (2.31 g, 30.8 mmol) with triethylamine (6.53 g, 64.7 mmol) in 50 mL of anhydrous THF and a solution of ethyl dichlorophosphate (5.02 g, 30.8

mmol) in 50 mL of anhydrous THF were simultaneously added to a stirred solution of 200 mL of neat anhydrous THF at 0 °C with a rate of 12 mL/h for each solution; then the reaction mixture was allowed to stir for 12 h. After complete conversion of ethyl dichlorophosphate, as confirmed by thin-layer chromatography, the reaction mixture was filtered and the filtrate was concentrated. The concentrated filtrate was passed through a silica gel plug of pure THF, and then concentrated to obtain the pure product (3.68 g, 22.3 mmol, 72.6% yield). ¹H NMR (500 MHz, CDCl₃) δ ppm (see assignments in Figure II-2), 4.38-4.28 (m, 1H), 4.11-3.96 (m, 4H), 3.94-3.86 (m, 1H), 3.85-3.61 (m, 5H), 1.37-1.20 (m, 9H), 1.20-1.09 (m, 3H); ¹³C NMR (126 MHz, CDCl₃) δ ppm, 72.90-72.75 (d, *J*_{p-c} = 3.3 Hz), 72.51-72.36 (d, *J*_{p-c} = 3.0 Hz), 63.69-63.55 (d, *J*_{p-c} = 6.4 Hz), 63.52-63.36 (d, *J*_{p-c} = 6.6 Hz), 50.34-49.89 (d, *J*_{p-c} = 9.5 Hz), 49.89-49.50 (d, *J*_{p-c} = 9.7 Hz), 20.97-20.62 (d, *J*_{p-c} = 7.8 Hz), 20.44-20.15 (d, *J*_{p-c} = 6.7 Hz), 16.49-15.97 (d, *J*_{p-c} = 6.8 Hz; d, *J*_{p-c} = 7.1 Hz); ³¹P NMR (202 MHz, CDCl₃) δ ppm, 25.97, 25.20; FT-IR (ATR) (Figure II-3) 3476-3079, 3012-2847, 1452, 1404, 1296, 12360, 1147, 1099, 1051, 997, 957, 903, 866, 831, 763 cm⁻¹; HRMS C₅H₁₂NO₃PH⁺ 166.0633, found (M+H⁺) 166.0619.

General procedure for the organobase-catalyzed ROP of EOMP to afford PEOMP

All polymerizations were carried out using standard glovebox and Schlenk line techniques. EOMP was vacuum dried over P₂O₅ for 0.5 day before transferring to a glovebox for storage under an inert atmosphere. All the reagents were weighed inside a glovebox and the reactions were conducted in a fume hood. EOMP was distributed into flame-dried 5-mL shell vials equipped with rubber septa and stir bars (*ca.* 0.200 g, 1.21 mmol for each). A solution of a given amount of 4-methylbenzyl alcohol (0.0121 mmol to 0.0242 mmol) in anhydrous DCM (210 μL) was transferred *via* syringe into the shell vial while stirring. Organocatalyst TBD or DBU (2 mol%

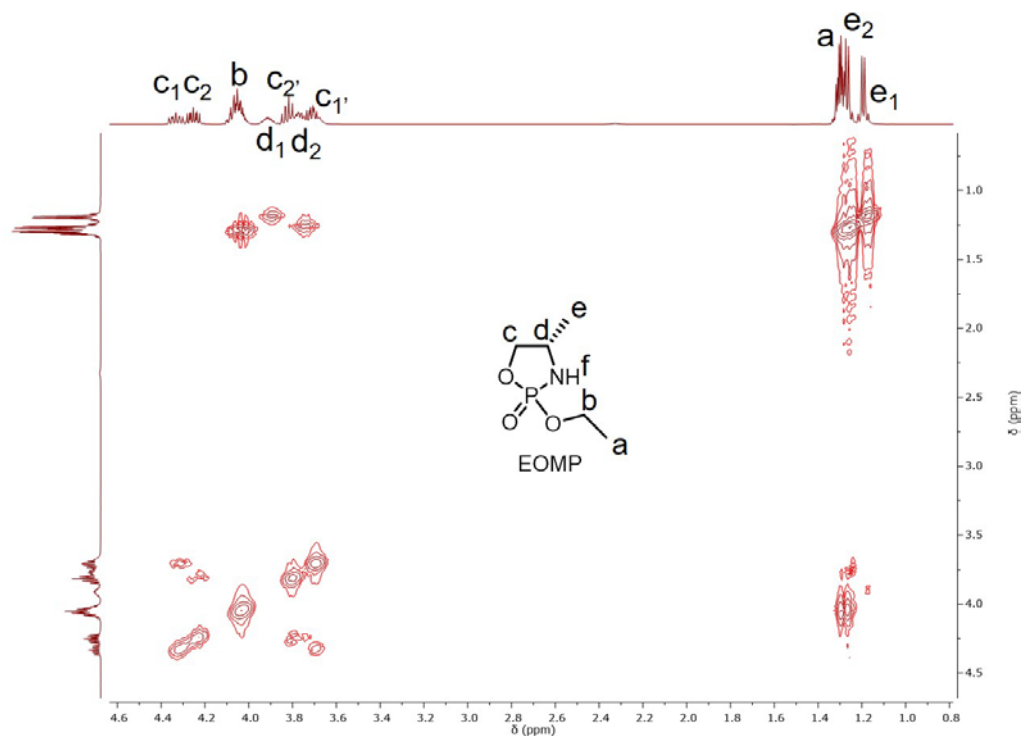


Figure II-2. COSY spectrum of EMOP in CDCl_3 . Protons at the same position but belonging to different isomers were assigned as H_{x1} and H_{x2} , H_{c1} and H_{c2} for example. If signals of the protons labelled as H_{x1} and H_{x2} overlapped with each other and were not distinguishable, H_x would be used as the assignment, H_b for example. Enantiotopic protons were assigned as H_{c1} and $\text{H}_{c1'}$ and H_{c2} and $\text{H}_{c2'}$. Signals of the protons labelled as H_f were overlapped with those of protons labelled as $\text{H}_{c2'}$, H_{d2} and $\text{H}_{c1'}$.

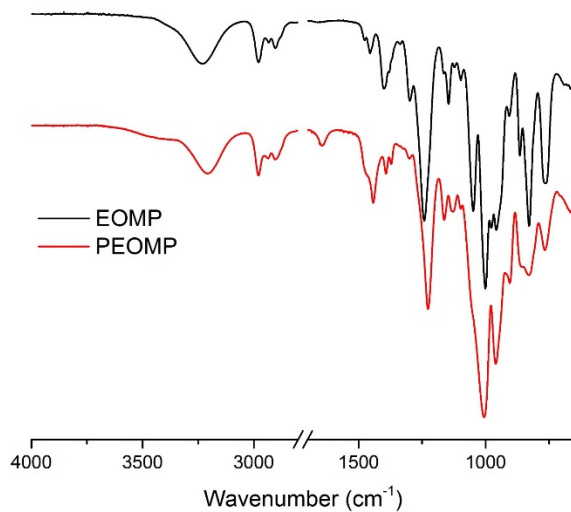


Figure II-3. FT-IR spectra of EOMP and PEOMP ($DP_n = 90$).

relative to monomer, 0.0242 mmol) in anhydrous DCM (210 μ L) was transferred *via* syringe into the shell vial with stirring at -78 $^{\circ}$ C, while being maintained under a nitrogen gas atmosphere. After stirring for a certain period of time (2 min to 60 min), the reaction vial was unstoppered and quenched by addition of Amberlyst 15 H-form resin (20 mg) and 2 mL of DCM. The reaction mixture was then removed from resin, purified by precipitation from DCM into diethyl ether (3x) and vacuum dried to give an average yield of 85%. ^1H NMR (500 MHz, CDCl_3) δ ppm 7.25 (d, $J = 7.5$ Hz, 2H, Ar), 7.15 (d, $J = 7.5$ Hz, 2H, Ar), 4.96 (m, 2H, OCH_2Ar), 4.57-3.68 (m, 5nH), 3.63-3.16 (m, nH), 2.33 (s, 3H, CH_3Ar), 1.53-0.98 (m, 6nH); ^{13}C NMR (126 MHz, CDCl_3) δ ppm, 129.30, 127.95, 70.46, 62.58, 47.64, 21.32, 19.53, 16.54-16.10 (d, $J_{\text{p-c}} = 7.2$ Hz); ^{31}P NMR (202 MHz, CDCl_3) δ ppm, 10.26; FT-IR (ATR) 3600-3035, 3015-2853, 1647, 1442, 1392, 1368, 1227, 1160, 1129, 1006, 959, 902, 827 (Figure II-3); $T_g = 32$ -36 $^{\circ}$ C ($DP_n = 20$ -93); TGA in Ar, 201-500 $^{\circ}$ C, 60% weight loss (Figure II-4).

Model reaction for the ring opening of EOMP with $[\text{M}]_0/[\text{I}]_0$ of 1

To a shell vial equipped with a rubber septum and a stir bar containing EOMP (0.100 g, 0.606 mmol), a solution of 4-methylbenzyl alcohol (0.606 mmol) in anhydrous DCM (105 μ L) was transferred *via* syringe into the shell vial while stirring. TBD (2 mol% to monomer, 0.0121 mmol) in anhydrous DCM (105 μ L) was then transferred *via* syringe into the shell vial with stirring at 0 $^{\circ}$ C, while being maintained under a nitrogen gas atmosphere. After stirring for 5 min, the reaction vial was unstoppered and quenched by addition of Amberlyst 15 H-form resin (10 mg) and 1 mL of CDCl_3 . The reaction mixture was then removed from the resin and directly analyzed by ^{31}P NMR spectroscopy without purification. ^{31}P NMR (202 MHz, CDCl_3) δ ppm, 9.72, 9.57, 8.54 (Figure II-5).

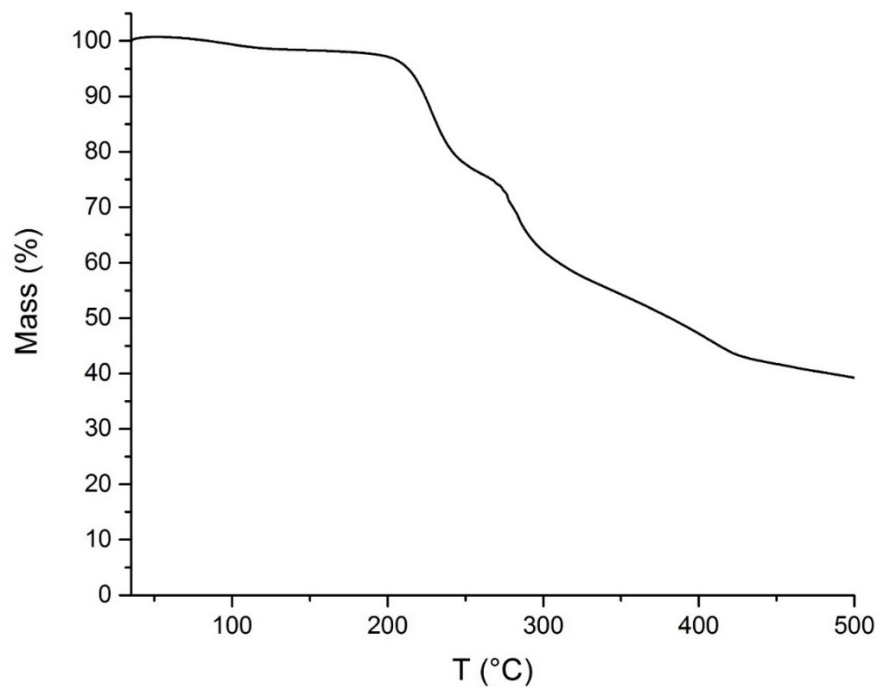


Figure II-4. TGA trace of PEOMP ($DP_n = 90$).

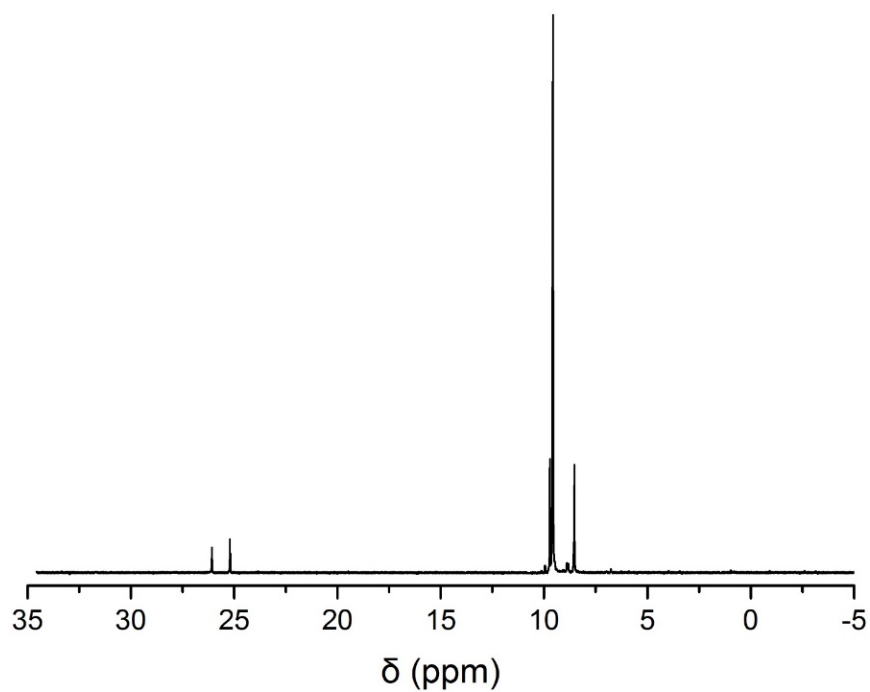


Figure II-5. ^{31}P NMR spectrum of the model reaction mixture for the ring opening of EOMP with $[\text{M}]_0/[\text{I}]_0$ of 1, at a monomer concentration of 2.2 M (same as the polymerization) after 5 min.

Kinetic study of the organobase-catalyzed ROP of EOMP

To a shell vial equipped with a rubber septum and a stir bar containing EOMP (0.400 g, 2.42 mmol), a solution of 4-methylbenzyl alcohol (0.0242 mmol) in anhydrous DCM (420 μ L) was transferred *via* syringe into the shell vial while stirring. TBD (2 mol% to monomer, 0.0484 mmol) in anhydrous DCM (420 μ L) was then transferred *via* syringe into the shell vial with stirring at -78 °C, while being maintained under a nitrogen gas atmosphere. At 2, 5, 8, 15, 30, 45 and 60 min, 150 μ L of the reaction mixture was removed and quenched over Amberlyst 15 H-form resin in CDCl₃ (10 mg in 1 mL CDCl₃). The reaction mixture at each time point was removed from the resin and directly analyzed by ³¹P NMR spectroscopy without purification. The reaction mixture was then purified by precipitation into diethyl ether (3x) and vacuum dried, which was further characterized by DMF SEC and ¹H NMR spectroscopy. The kinetic study was triplicated.

Chain extension of PEOMP

Follow the kinetic study procedure for ROP of EOMP, 0.401 g EOMP was polymerized with 2.25 mol% TBD and 2 mol% 4-methylbenzyl alcohol under -78 °C. After 40 min, an aliquot taken from the reaction mixture was analyzed by ³¹P NMR and DMF SEC and ¹H NMR spectroscopy, which confirmed the conversion to be 95%. Another 0.399 g EOMP dissolved in 210 μ L DCM was added to the reaction mixture *via* syringe at the 40 min time point, and the reaction was allowed to stirred for another 40 min. The reaction mixture was then analyzed ³¹P NMR and DMF SEC and ¹H NMR spectroscopy. The SEC traces were shown in Figure II-6.

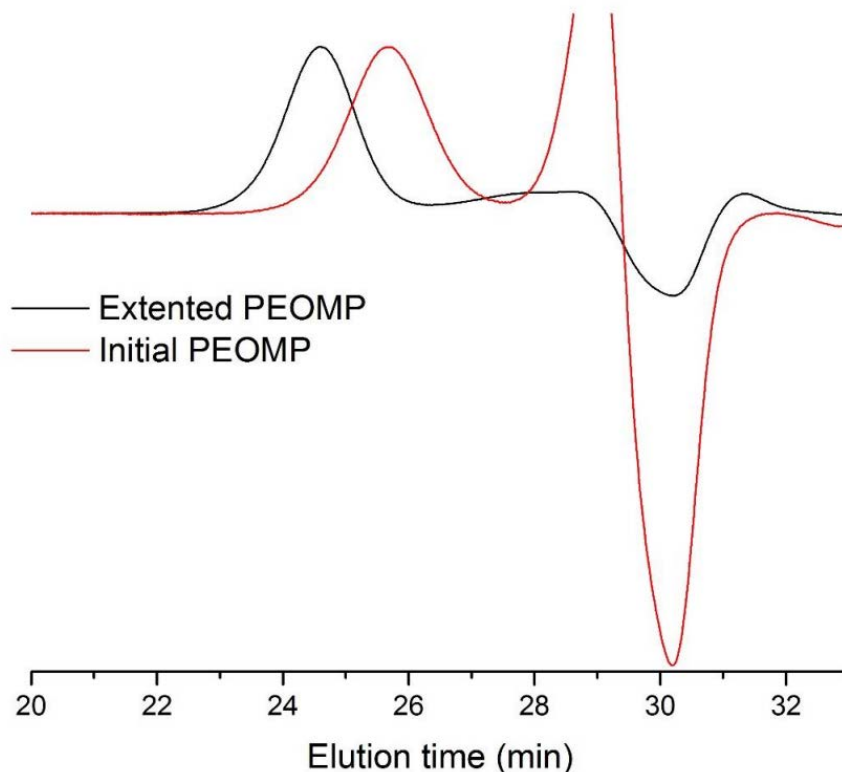


Figure II-6. SEC traces of the chain extension experiment of EOMP. Initial PEOMP achieved with $[M]_0/[I]_0$ of 50, at a monomer concentration of 2.2 M. Extended PEOMP achieved with addition of EOMP with $[M]_0/[I]_0$ of 50, at a monomer concentration of 1.5 M.

Kinetic study of the backbone cleavage of PEOMP in aqueous solution by ^{31}P NMR spectroscopy

In a typical backbone cleavage experiment, PEOMP ($DP_n = 90$, 5.0 mg) was dissolved into 1 mL of buffer solutions (100 mM citric acid - sodium citrate buffer solutions at pH 3.0 and pH 5.0, and 10 mM 3-(N-morpholino)propanesulfonic acid (MOPS) buffer solution at pH 7.4), and 10 vol% of D_2O (0.1 mL) was added to the buffer solutions. The solutions were incubated at 37 °C allowing for the degradation. The ^{31}P chemical shifts were monitored by ^{31}P NMR spectroscopy during the degradation study. Each degradation study was triplicated.

Preparation and identification of the degradation products of PEOMP under acidic conditions

PEOMP ($DP_n = 90$, 5.0 mg) was dissolved into 1 mL of hydrochloric acid (1.1 mM), and 10 vol% of D₂O (0.1 mL) was added to the solution. The solution was incubated at 37 °C allowing for the degradation. The ³¹P chemical shifts were monitored by ³¹P NMR spectroscopy during the degradation. After the degradation reached a certain degree, 100 μL of the reaction mixture was removed, diluted by 1 mL of methanol and directly analyzed by ESI-MS. Peaks showed at certain m/z were further analyzed by MS/MS. To the rest of the reaction mixture was added a trace amount of trimethylamine to adjust the pH value to 7.4, and the reaction mixture was further lyophilized into a powder, followed by analysis by DMF SEC.

Note:

Since ESI-MS is sensitive to salts (buffers) and to eliminate undesired buffer signals, hydrochloric acid was used instead of buffer solutions in this experiment.

2.3 Results and Discussion

The monomer, (4*S*)-2-ethoxy-4-methyl-1,3,2-oxazaphospholidine 2-oxide (EOMP), was synthesized by annulation of ethyl dichlorophosphate with (*S*)-(+)-2-amino-1-propanol in the presence of trimethylamine (Figure II-1). The annulation reaction was highly efficient, as evidenced by only the EOMP peak being observed in the ³¹P NMR spectrum of the crude product. Purification was then accomplished simply by filtration through a silica gel plug to remove the slight excess amount of trimethylamine to give pure EOMP as a highly viscous colorless liquid after concentration. The purity of the monomer was confirmed by mass spectrometry. The ³¹P NMR spectrum of EOMP exhibited resonances at 25.97 and 25.20 ppm (Figure II-7c), similar to

the ^{31}P chemical shift values of reported cyclic phospholane amidate structures.⁹ The two distinct resonances were attributed to possible geometric isomers arising from the 2-position ethoxy and 4-position methyl groups. The ^1H NMR and ^{13}C NMR spectra (Figure II-7a and b) of the monomer also showed two sets of resonances belonging to those two isomers. Resonances in the ^1H NMR spectrum were able to be distinguished through homonuclear correlation spectroscopy (COSY) (Figure II-2), and the intensities of the resonances revealed the two isomers to be roughly at proportions of 1:1 in the mixture.

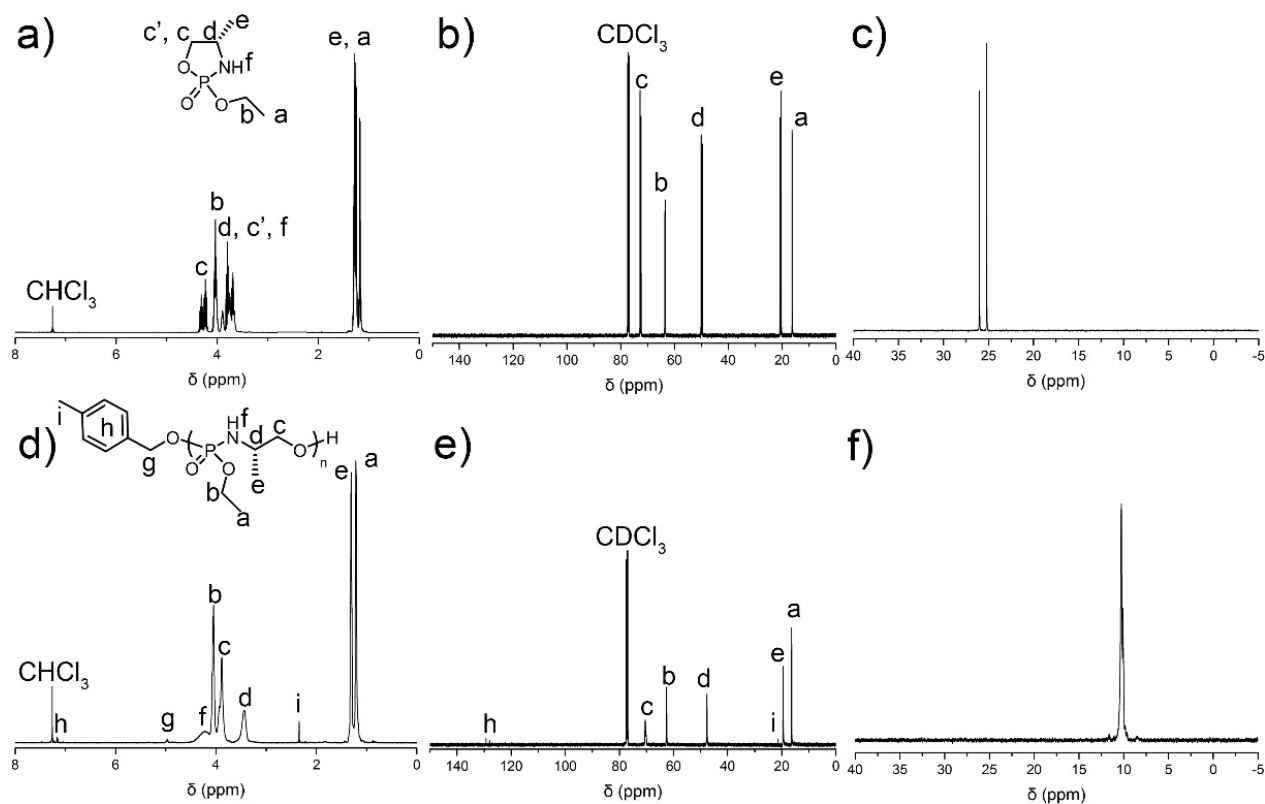


Figure II-7. NMR spectra of EOMP in CDCl_3 (ppm): a) ^1H NMR (500 MHz) (see detailed assignments in Fig. S1.), b) ^{13}C NMR (126 MHz), c) ^{31}P NMR (202 MHz). NMR spectra of PEOMP in CDCl_3 (ppm): d) ^1H NMR (500 MHz), e) ^{13}C NMR (126 MHz), f) ^{31}P NMR (202 MHz).

Table II-1. Polymerization of EOMP Catalyzed by TBD under Different Conditions^a

entry	cat.	<i>T</i> (°C)	[M]/[I]	time (min)	conv. ^b (%)	<i>M</i> _{n, NMR} ^c (kDa)	<i>D</i> ^d
1	TBD	0	100	5	55	9.0	1.10
2	TBD	0	100	10	75	12.2	1.23
3	TBD	0	100	15	88	14.3	1.30
4	TBD	-78	100	60	94	15.2	1.12
5	TBD	-78	50	40	95	7.6	1.08
6	TBD	-78	25	30	94	3.9	1.10

^aThe initiator was 4-methylbenzyl alcohol, the solvent was anhydrous dichloromethane, the monomer concentration was 2.2 M, and catalyst was 2 mol % to monomer for all entries. ^bConversions (conv.) were obtained from ³¹P NMR spectra on aliquots taken from the polymerization mixtures. ^c*M*_{n, NMR} was calculated from the monomer to initiator ratio based on ¹H NMR of final polymer products. ^d*D* was measured by DMF SEC calibrated using polystyrene standards.

Two organocatalysts, 1,8-diazabicyclo[5.4.0]undec-7-ene (DBU) and 1,5,7-triazabicyclo[4.4.0]dec-5-ene (TBD), which had previously shown excellent control in the ROP of several cyclic phosphorus-containing monomers,^{9, 24, 55-57} were used to test the ROP of EOMP (Figure II-1, Table II-1). Initially, DBU was employed as the organocatalyst for the polymerization of EOMP, initiated by 4-methylbenzyl alcohol at room temperature. However, these conditions failed to convert EOMP into its polymer form (PEOMP), even at a relatively high catalyst-to-monomer ratio of 10 mol%. Therefore, DBU was replaced by the stronger catalyst TBD, which has dual activation effects: simultaneously serving as a hydrogen-bond donor to the monomer *via* the N–H site and also as a hydrogen-bond acceptor to the hydroxyl proton of the propagating alcohol chain end.^{23, 25, 58} In the presence of TBD, EMOP polymerization proceeded within 10 min at 0 °C (entries 1-3, Table II-1). However, broadening of *D* (1.2-1.3) was observed after the conversion reached greater than 70%, indicating the occurrence of adverse backbiting or transesterification reactions. Therefore, the reaction temperature was decreased to -78 °C (entries

4-6, Table II-1). At this reduced temperature, the polymerization remained sufficiently fast to reach over 90% conversion within 1 h, and a narrower \bar{D} (1.08-1.15) was achieved over all conversions from 10% to 94%, indicating the side reactions were successfully avoided.

Unlike most cyclic phospholane ester monomers or reported phosphoramidate monomers,^{9, 25} EMOP has two distinct directions to open the oxazaphospholidine ring during the polymerization, where either the P-O bond or P-N bond would be cleaved. Since the pK_a of an amine (*ca.* 38) is significantly larger than that of an alcohol (*ca.* 16), it was hypothesized that the P-O bond cleavage would be more preferable. A model reaction was carried out at the same condition of the polymerization, while the monomer/initiator feed ratio ($[M]_0/[I]_0$) was set to be 1. The ^{31}P NMR spectrum of the reaction mixture exhibited resonances at 9.72, 9.57 and 8.54 ppm (Figure II-5), which correlated to the phosphoramidate and were consistent with the ^{31}P chemical shift values of PEOMP (10.26 ppm) (Figure II-7f). Furthermore, the ^{31}P NMR spectrum showed no resonance at *ca.* 12 ppm, corresponding to the phosphordiamidate; or *ca.* 0 ppm, corresponding to the phosphoester, respectively. These data provided evidence that EOMP had undergone selective cleavage of the P-O bond during the ROP.

The kinetics of EOMP ROP were studied using $[M]_0/[I]_0$ of 100 in dichloromethane with 4-methylbenzyl alcohol as the initiator and TBD as the organocatalyst to monitor the monomer conversions and the growth of polymer chains as a function of time. Monomer conversions were obtained from ^{31}P NMR spectra on aliquots taken from the polymerization mixtures. Subsequently, number-average molecular weights (M_n) were calculated using ^1H NMR spectra after isolation of the polymer samples by precipitation, with comparison of the intensities of the three 4-methyl protons originating from the initiator on the α -chain end resonating at 2.33 ppm, with the six protons of the two methyl groups on the repeating units resonating at 0.98-1.53 ppm.

The linearity of M_n vs monomer conversion (Figure II-8a) suggested that the numbers of macromolecules in the reactions remained constant during the polymerizations. The size exclusion chromatography (SEC) traces (Figure II-8c) showed unimodal peaks during the reactions, which shifted toward shorter elution times as polymerization progressed while maintaining narrow D ,

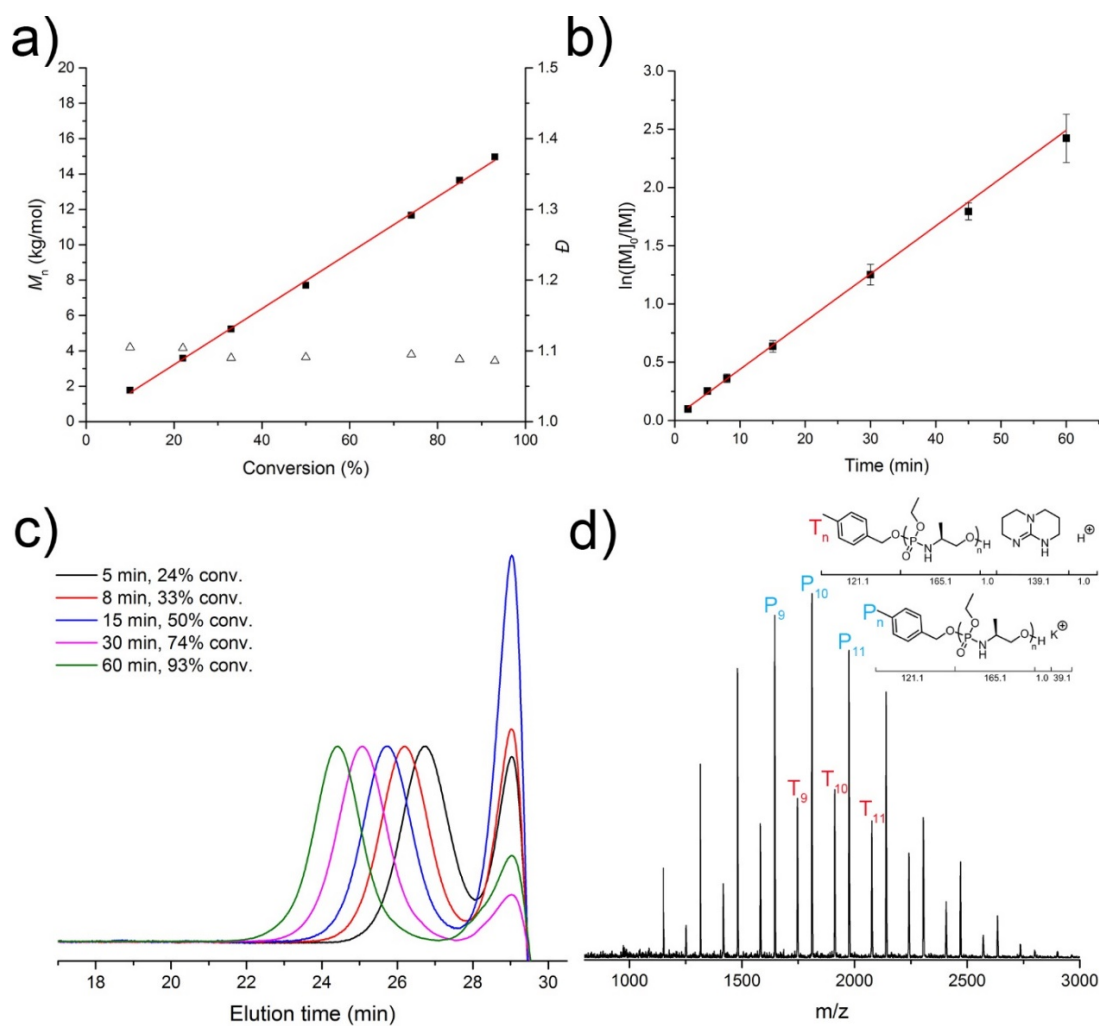


Figure II-8. a) Plot of M_n and D vs monomer conversion for the polymerization of EOMP using TBD as the catalyst and 4-methylbenzyl alcohol as the initiator, obtained from a combination of SEC, ^1H NMR and ^{31}P NMR spectroscopic analyses. The ratio of monomer : initiator : TBD was 100 : 1 : 2. b) Plots of monomer conversion ($\ln([M]_0/[M])$) vs time obtained from ^{31}P NMR spectra. c) SEC traces (DMF as eluent, 1 mL/min) of the ROP of EMOP vs time. d) MALDI-ToF MS spectrum of PEMOP ($DP_n = 10$).

below 1.15. Plots of $\ln([M]_0/[M])$ vs time (Figure II-8b) showed that the polymerization exhibited first order kinetics, also suggesting the characteristics of a controlled polymerization of the EOMP ROP. Further analysis by matrix-assisted laser desorption ionization time-of-flight mass spectrometry (MALDI-Tof MS) (Figure II-8d) of a polymer ($DP_n = 10$ by ^1H NMR spectroscopy), which had undergone termination by treatment with Amberlyst 15 H-form resin and purification by only one time of precipitation into diethyl ether, revealed two populations, each with a spacing of 165.1 m/z, equal to that of the expected monomer repeat unit. Structurally, these two sets of signals were related to the same populations initiated by 4-methylbenzyl alcohol with distinct ionizations. The main peak in the major population at $m/z = 1811.1$ corresponded to a potassium-charged polymer chain of $DP_n = 10$ that had been initiated by 4-methylbenzyl alcohol and terminated by protonation, further confirming the controlled nature of the polymerization. Meanwhile, the main peak in the minor population at $m/z = 1912.2$ was in agreement with a proton-charged polymer chain of $DP_n = 10$ having 4-methylbenzyl oxy and protonated α - and ω -end groups, respectively, and one equivalent of TBD, indicating the strong interaction of TBD with the monomer and the polymer, as well as a possible explanation for the distinct catalytic activity differences between TBD and DBU for the ROP of EOMP. To further investigate the living nature of the polymerization, chain extension of PEOMP polymers was carried out with addition of EOMP, SEC traces (Figure II-6) revealed a shift of the starting PEOMP towards shorter elution time, while maintaining narrow \mathcal{D} , below 1.15.

By controlling the initial ratio of monomer to initiator, $[M]_0/[I]_0$, as well as the reaction time, a series of PEOMPs with different molecular weights was synthesized. ^{31}P NMR spectra clearly showed only one phosphorus environment at a chemical shift of 10.26 ppm (Figure II-7f), and ^1H NMR and ^{13}C NMR spectra (Figure II-7d and e) also confirmed the structure of PEOMP.

PEOMP appeared as a white to pale yellow powder at room temperature, which was attributed to the glass transition temperature (T_g) of 32-36 °C ($DP_n = 20-93$). Compared to the reported polyphosphoester PEMEP ($DP_n = 16-52$, $T_g = -40$ to -37 °C)⁵⁵ and polyphosphoramidate PMOEPA ($DP_n = 17-52$, $T_g = -27$ to -19 °C) analogs,⁹ the T_g of PEOMP was significantly higher, which was attributed to the phosphoramidate linkages along the polymer backbone. PEOMP was highly hygroscopic and would quickly transform from powder to tacky material within minutes and form a viscous solution within hours, if stored open to the air. Furthermore, PEOMP was highly water-soluble, likely attributed to the phosphoramidate backbone linkages and short pendant ethyl groups, with over 800 mg polymer ($DP_n = 90$) easily dissolved into 1.00 mL of nanopure water within minutes at room temperature.

The phosphoramidate linkages along the polymer backbone also endowed PEOMP with acid-lability. The kinetics of the backbone cleavage of PEOMP ($DP_n = 90$) in aqueous solution was studied in three aqueous buffer solutions with different pH values of 3.0, 5.0 and 7.4. Cleavage of the phosphoramidate linkage, having a ³¹P resonance at 10.26 ppm, would generate phosphates with distinct ³¹P chemical shifts at *ca.* 0 ppm, allowing for convenient monitoring of the percentage conversion of backbone cleavage by ³¹P NMR spectroscopy. At pH 7.4 (Figure II-9a), the PEOMP was found to be stable for 12.5 d with negligible changes as expected. In the acidic environment, pH 5.0 (Figure II-9a), *ca.* 27 % of the phosphoramidate bonds were cleaved over 12.5 d, and the cleavage reaction reached a plateau at *ca.* 8.3 d. At pH 3.0 (Figure II-9a), the backbone cleavage was accelerated and *ca.* 90% of the phosphoramidate bonds were cleaved within 8-9 d, reaching a plateau at *ca.* 9.9 d and *ca.* 94% conversion of phosphoramidate-to-phosphate ³¹P resonance frequencies over 12.5 d. The resonance patterns at each frequency of *ca.* 10 and 0 ppm also revealed the progress of backbone cleavage and further breakdown of initial phosphates. As shown

in Figure II-9b, at pH 3.0, over a time range of 4 h to 9.9 d, the conversion increased from 5% to 94% with gradually decreased intensity for the ^{31}P resonance at 10.26 ppm, demonstrating the disappearance of the polymer. Over the same time period, sharp resonance signals appeared at 10.53, 10.39, 10.29 and 10.20 ppm with their intensities first increased then decreased, indicating the formation of oligomers and their further degradation into small molecules. The decrease in overall intensity for the combined signals resonating at *ca.* 10 ppm was coincident with the

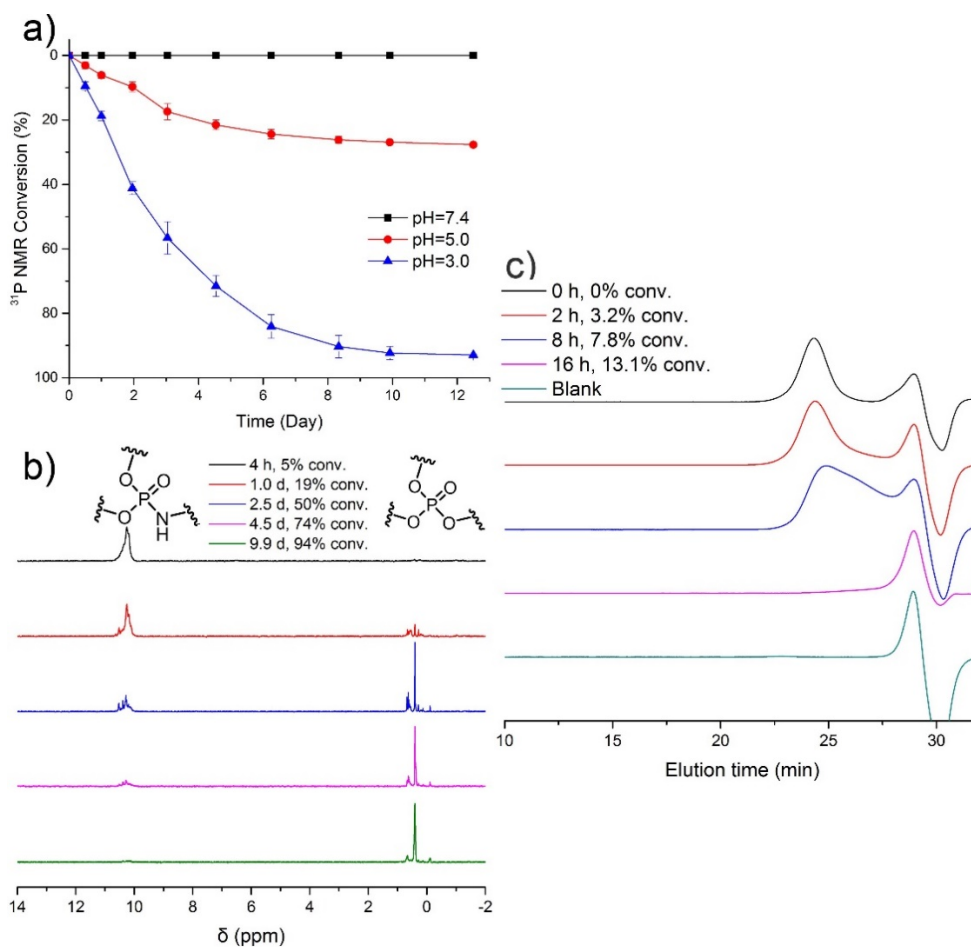


Figure II-9. a) Kinetics of PEOMP degradation at different pH values, as monitored by ^{31}P NMR spectroscopy. b) Transition of ^{31}P NMR resonances of PEOMP over a period of conversion at pH 3.0. c) Progress of the degradation of PEOMP at pH 3.0, as monitored by SEC.

appearance of new resonances at 0.67, 0.63, 0.40, 0.29, 0.13 and -0.11 ppm, and their combined growth in intensities over time, suggesting the formation of phosphates. When monitored by SEC (Figure II-9c), broadening of the peak with increased intensity at longer elution time appeared at 3.2% conversion, while the peak molecular weight (M_p) remained the same, suggesting only a portion of the polymer molecules had been cleaved at this stage. At 7.8% conversion, the M_p shifted to longer elution time with detection of small molecular species, confirming cleavage of a majority of the polymer molecules. At 13.1% conversion, full disappearance of the polymer peak further demonstrated that partial degradation of the backbone linkages resulted in a sharp decrease in molecular weights. Complicating this analysis, however, is the increased affinity to the SEC column for the charged degradation products, relative to the starting PPA.

Therefore, to better understand the molecular weight of the polymer degradation products as a function of % conversion of phosphoramidate backbone linkages, degradation products at different time points were further analyzed by electrospray ionization mass spectrometry (ESI-MS). As shown in Figure II-10b, at 40% conversion, ESI-MS revealed one major population with a spacing of 165 m/z equal to that of a monomer, related to the oligomer series E_b (Ionized form of **4**), which resulted directly from the cleavage of phosphoramidate bonds during degradation (Figure II-10a). The main peak in the major population at $m/z = 512$ corresponding to a trimer was further analyzed by tandem mass spectrometry (MS/MS), and the fragment pattern confirmed the predicted structure (Figure II-11). For the whole series of E_b , the major peaks E_1 , E_2 and E_3 further supported the decrease in molecular weights during backbone degradation, as expected. At 62% conversion (Figure II-10c), the signals of series E_b were still dominant, with intensities increased for E_0 and E_1 (relative to E_2) and decreased for higher molecular weight oligomers. In addition, signal intensities of another two populations increased and became more observable, each

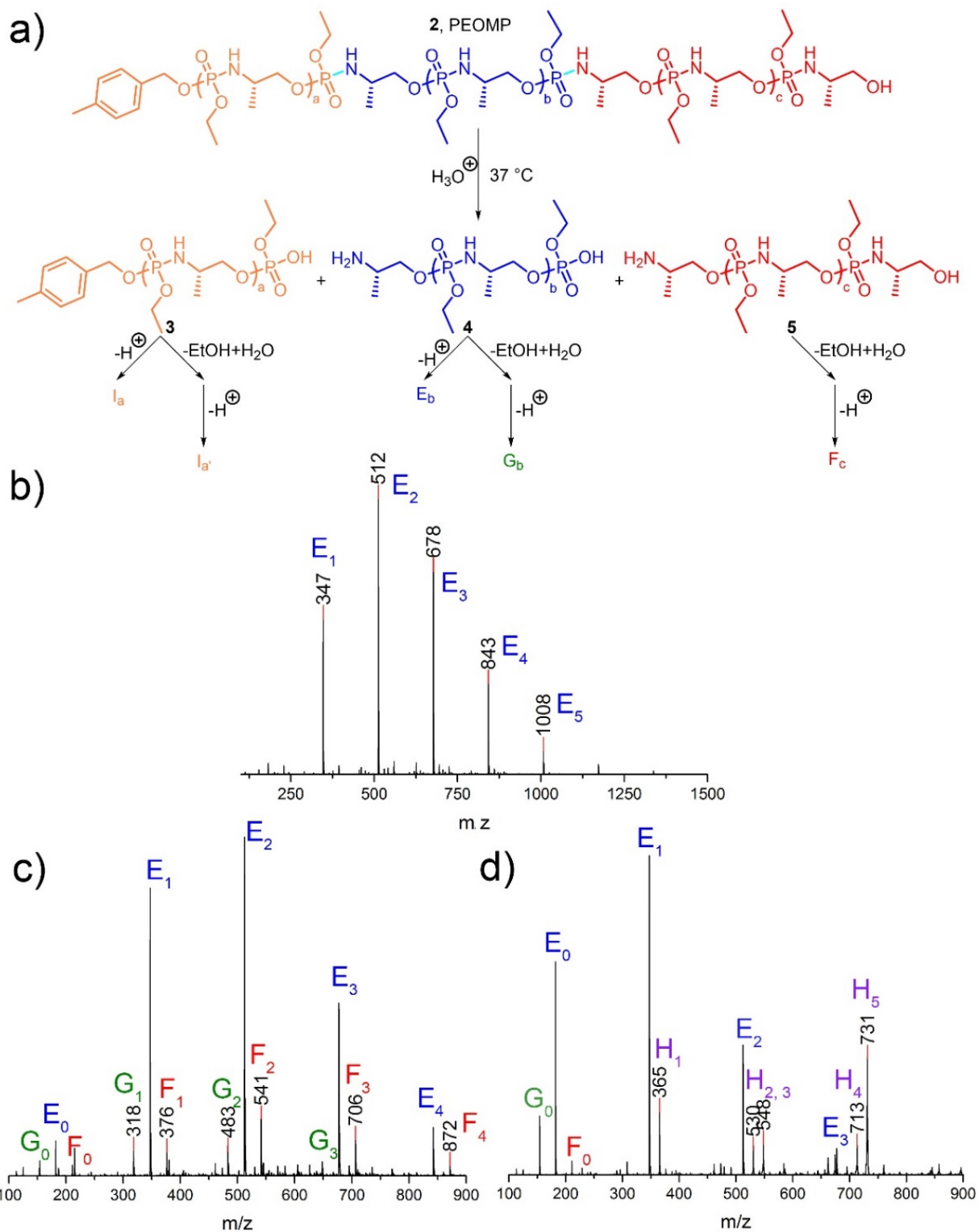


Figure II-10. a) Scheme of hydrolytic degradation of homopolymer 2. ESI-MS analysis (negative ion mode, tested m/z range 50-2000) of the degradation products of 2 under different conversions, b) 40%, c) 62% and d) 94%, obtained from ^{31}P NMR spectra.

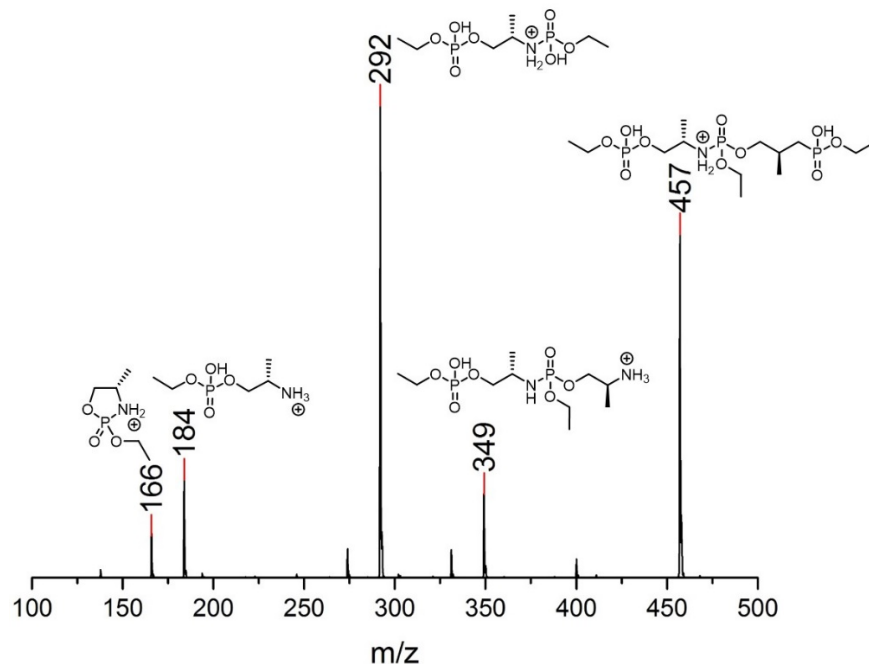


Figure II-11. MS/MS spectrum of E₂ (positive ion mode).

with a spacing of 165 m/z equal to that of a monomer, corresponding to the oligomer series F_c and G_b. A possible route that could derive series F_c was the hydrolysis of one equivalence of ethyl phosphoester bonds from **5** (Figure II-10a), the ω-end counterparts of **4** during the cleavage of the phosphoramidate bond. Unfortunately, signals for the series of **5** were not detected, probably due to their difficulty to be ionized as anions under acidic conditions. Similarly, hydrolysis of one equivalence of ethyl phosphoester bonds from series E_b would result in series G_b (Figure II-10a). At 94% conversion (Figure II-10d), the signals of series E_b were still dominant, with the major peaks shifted from E₁ to E₀, while for series F_c and G_b, only F₀ and G₀ were observable, coincident with the high conversion. Furthermore, there was a new series H, observed at 365, 530, 548, 713, and 731 m/z, attributed to ion clusters formed by E₀ with E₁ or E₀ itself (Figure II-12, 13), probably due to the zwitterionic nature of E₀ and E₁. Series I_a and I_a', derived from **3** (Figure II-10a),

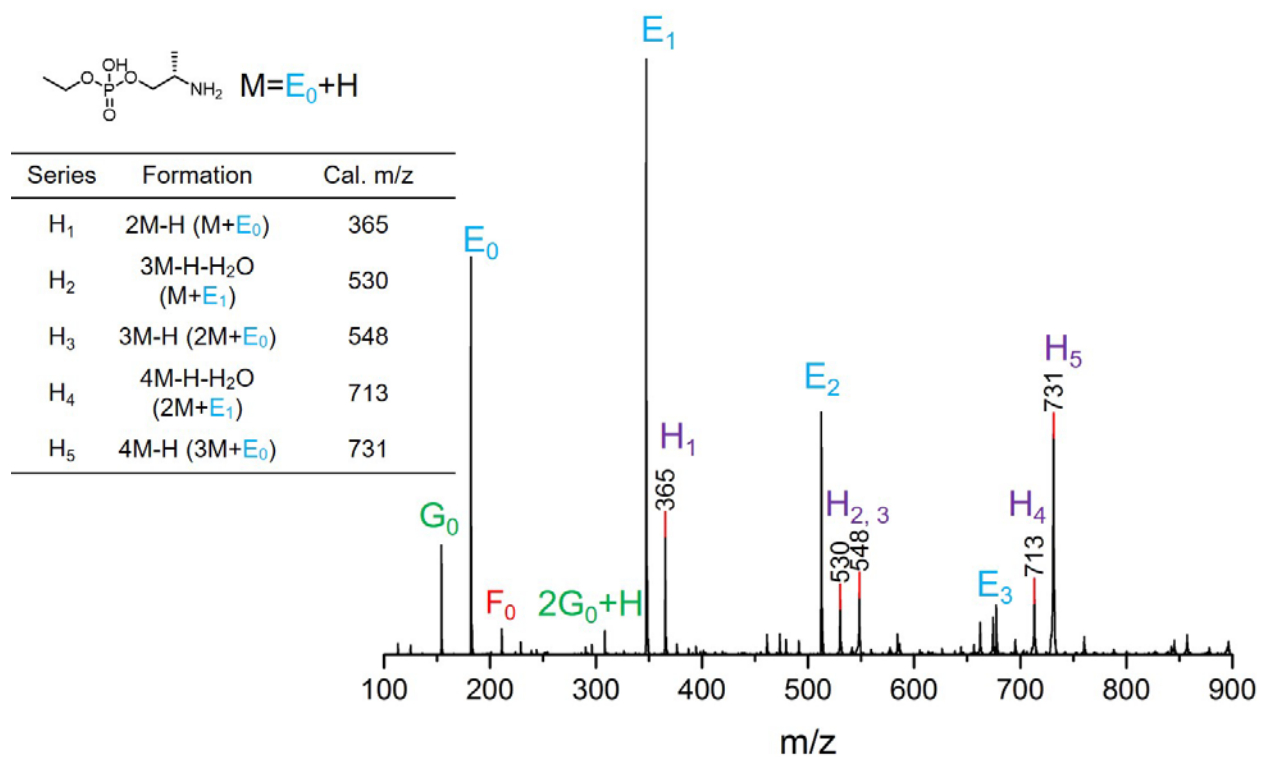


Figure II-12. Analysis of series H in Figure II-10c (negative ion mode).

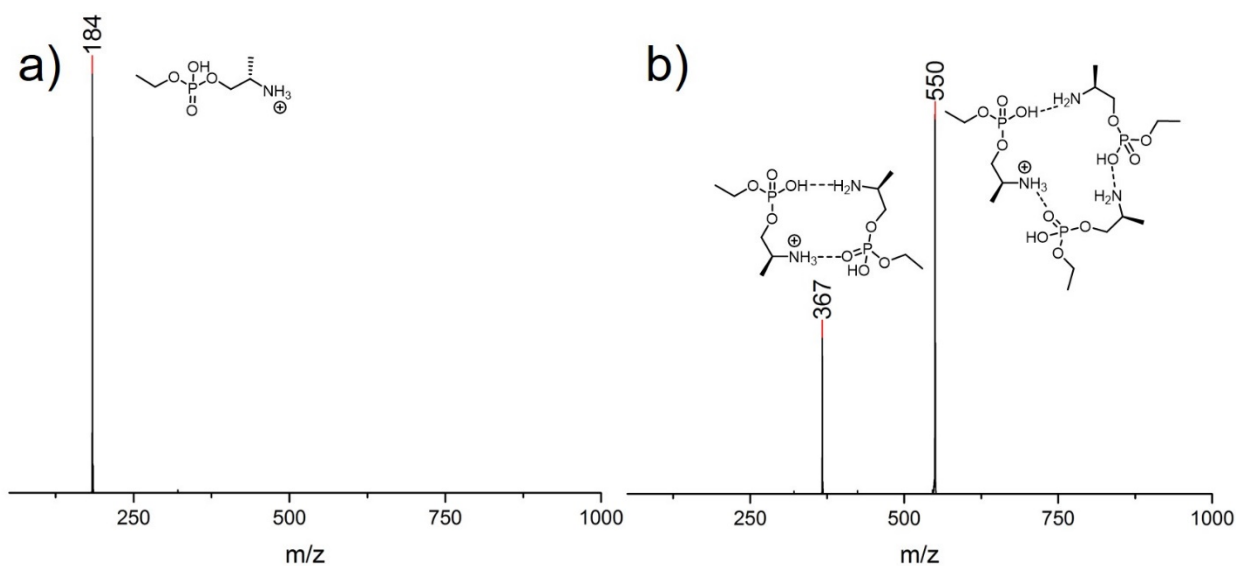


Figure II-13. a) MS/MS spectrum of H₁ (positive ion mode). b) MS/MS spectrum of H₅ (positive ion mode).

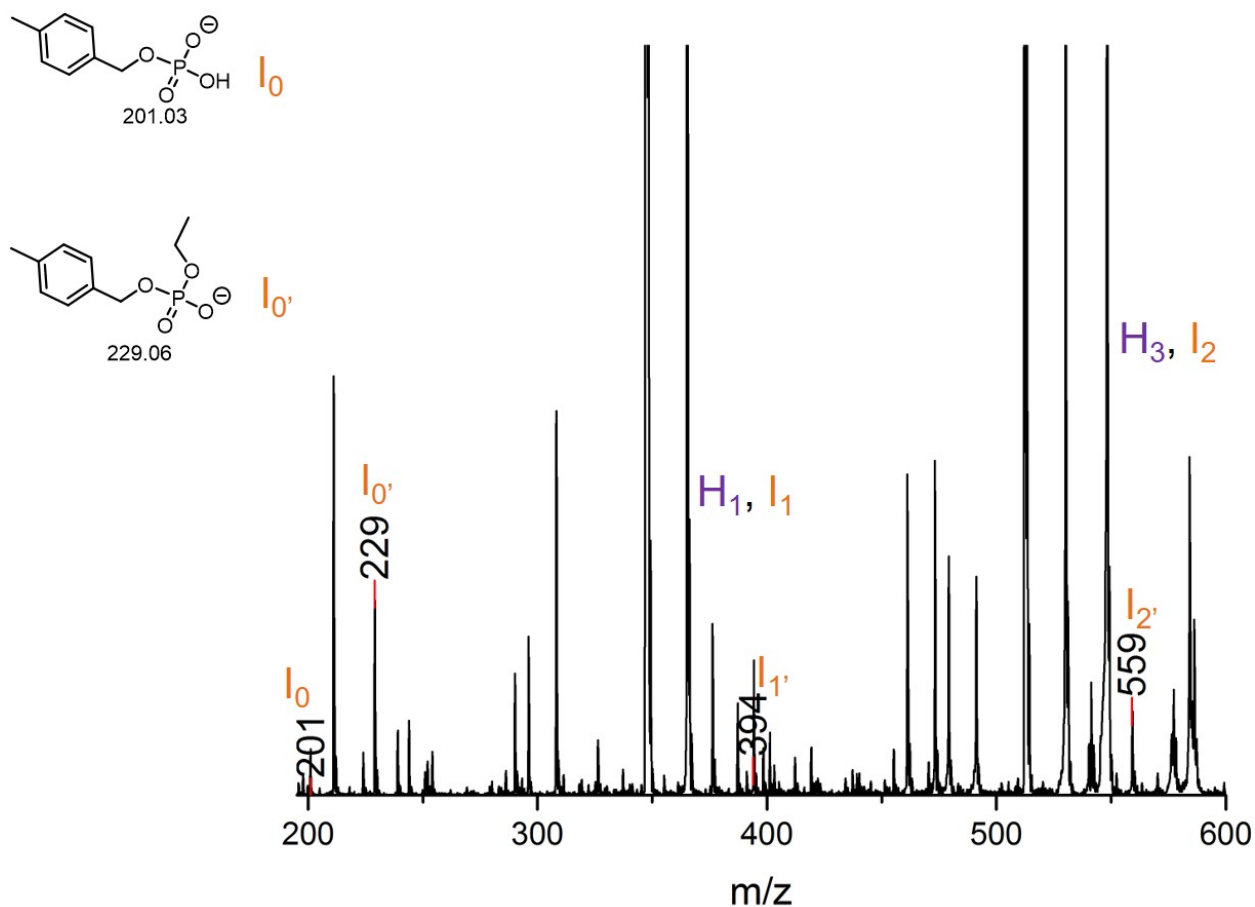


Figure II-14. Analysis of series I and I' (negative ion mode).

the α -end counterparts of **4**, were also detected (Figure II-14); however, the intensities of the signals were relatively low, while some signals of the I_a and I_{a'} overlapped with those of H. Since the signal intensities of series E_b were dominant over all conversions, while no notable signal from product of phosphoester bond cleavage besides series F_c and G_b were observed, the phosphoramidate bonds were demonstrated to be cleaved much faster than the phosphoester bonds under acidic conditions.

2.4 Conclusions

Phosphoramidate polymers having the acid-labile phosphoramidate linkage within the backbone are interesting materials that were shown to be prepared readily under basic condition and then undergo selective backbone cleavage reactions under acidic condition. A unique type of stable oxazaphospholidine monomer was synthesized and its organobase-catalyzed ROP kinetics were explored, showing a controlled manner and selective cleavage of P–O bonds during ROP. The resulting highly water-soluble polymers exhibited much higher T_g than their polyphosphoester analogs. Furthermore, the acid-labile phosphoramidate bonds cleaved much faster than the phosphoester bonds under acidic conditions, which enabled the polymer backbone to breakdown rapidly through the cleavage of P–N bonds under acidic conditions. Future studies, including synthesis of acid-labile nanostructured materials, as well as controlling the acidolysis rate of the polymer, are being actively pursued.

CHAPTER III

ACID-TRIGGERED POLYMER BACKBONE DEGRADATION AND DISASSEMBLY TO ACHIEVE RELEASE OF CAMPTOTHECIN FROM FUNCTIONAL POLYPHOSPHORAMIDATE NANOPARTICLES ²

3.1 Introduction

Polymeric systems with the ability to respond to external stimuli, including pH,^{59, 60} light,⁶¹ temperature,⁶¹⁻⁶⁴ redox,⁶⁵ electric fields,⁶⁶ *etc.*, have great potential for biomedical applications. By taking advantage of such systems, strategies are being pursued to achieve triggered drug release preferentially at pathological sites to lead to higher accumulation of drug in the targeted disease sites and, thus, enhanced efficacy and decreased side effects.⁶⁷ For instance, the higher concentration of glutathione in cancer cells has been extensively exploited to achieve triggered release of therapeutics from reduction-responsive carriers.⁶⁸⁻⁷³ Similarly, the lower pH of cancer and inflammation microenvironments has led to numerous elegant pH-responsive systems.^{71, 72, 74-78}

Camptothecin (CPT), a topoisomerase II inhibitor discovered from the Chinese tree *Camptotheca acuminata* over half a century ago, would benefit greatly from such systems, due to the facile hydrolysis of its therapeutically active lactone form into an inactive carboxylate form at physiological pH (Figure III-1a) and low aqueous solubility (< 2.0 µg/mL at 37 °C).^{79, 80} In the

²Adapted with permission from “Acid-Triggered Polymer Backbone Degradation and Disassembly to Achieve Release of Camptothecin from Functional Polyphosphoramidate Nanoparticles” by Wang, H.; Dong, M.; Khan, S; Su, L.; Li, R.; Song, Y.; Lin, Y.-N.; Kang, N.; Komatsu, H., C.; Elsabahy, M.; Wooley, K. L., *ACS Macro Lett.* **2018**, 7 (7) 783-788. Copyright 2018 American Chemical Society

past several decades, a variety of responsive polymeric systems have been developed to improve the therapeutic efficacy of CPT, among which two major strategies were applied: 1) conjugation of CPT onto polymeric systems through acid/reduction-labile linkages,⁸¹⁻⁸⁷ and 2) physical encapsulation of CPT into an acid/reduction-responsive polymeric system.^{88,89} Generally, the first strategy requires more synthetic steps and has less versatility for adaption to other therapeutics, nevertheless it effectively inhibits the premature release and hydrolysis of CPT. In contrast, the second strategy requires less synthetic effort and is more versatile, however, the premature release of CPT is often unavoidable. As such, highly responsive systems are desired to facilitate cancer cell-specific delivery of therapeutically-active CPT.

Introduction of acid-labile linkages along a polymer backbone is anticipated to lead to rapid acid-triggered degradation, given that even slight degradation of the backbone would markedly decrease molar mass.⁴³ In an earlier study, we demonstrated that the polyphosphoramidate (PPA) poly(4*S*-2-ethoxy-4-methyl-1,3,2-oxazaphospholidine 2-oxide) (PEOMP, **1**) was highly water soluble (> 800 mg dissolved in 1 mL of water) and that it was able to undergo accelerated degradation under acidic conditions, due to the presence of acid-labile phosphoramidate linkages along the backbone (Figure III-1b).⁹⁰ With an interest in expanding this PPA backbone chemistry to hydrophobic polymer blocks and amphiphilic block copolymers that also carry reactive functionalities, we developed a synthetic route to a well-defined amphiphilic diblock copolymer, PEOMP-*b*-PBYOMP, **2**, with acid-labile linkages along the backbone. This block copolymer was afforded *via* a novel oxazaphospholidine monomer bearing a side-chain alkyne functionality upon controlled one-pot sequential organo-catalyzed ring-opening polymerizations (ROPs), and required no further chemical modification to exhibit amphiphilic character (Figure III-1d). Co-assembly of **2** with CPT in aqueous solutions yielded nanotherapeutics, which were evaluated *in*

vitro and revealed enhanced efficacy over free CPT in cancer cells and similar toxicity in normal cells.

3.2 Experimental Section

3.2.1 Materials

Camptothecin (CPT) was purchased from Ark Pharm, Inc. (4*S*)-2-Ethoxy-4-methyl-1,3,2-oxazaphospholidine 2-oxide (EOMP) was synthesized according to the previously reported procedure in Chapter II.⁹⁰ Tetrahydrofuran (THF) and dichloromethane (DCM) were purified by passage through a solvent purification system (JC Meyer Solvent Systems). 4-Methylbenzyl

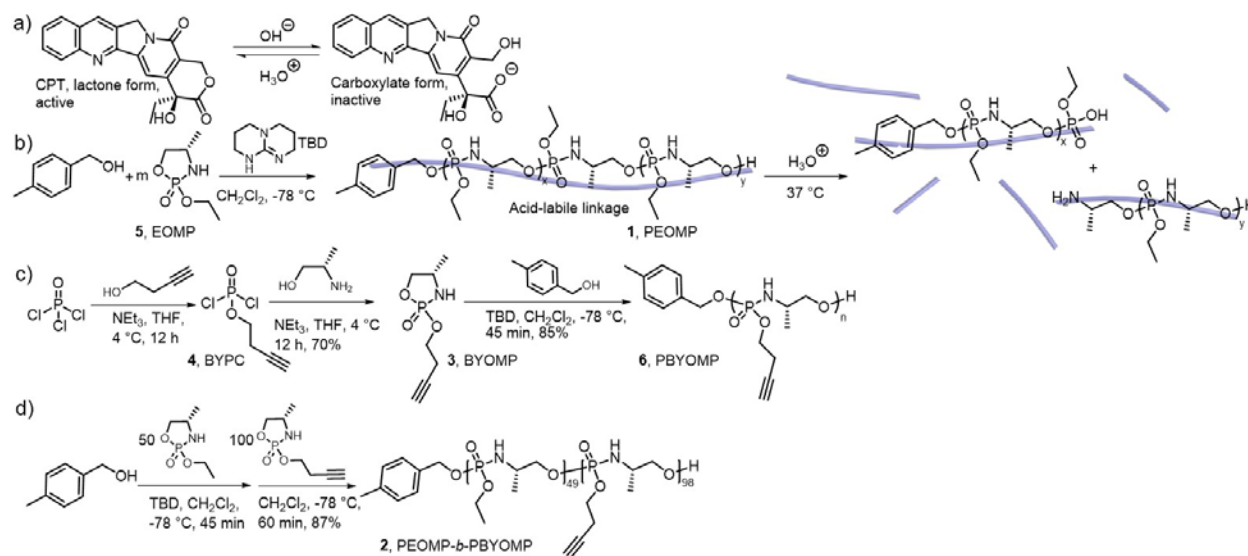


Figure III-1. a) Hydrolysis of CPT. b) Polymerization of EOMP, **5**, to afford PEOMP, **1**, with acid-triggered backbone degradation. c) Synthesis, and polymerization of BYOMP, **3**, to afford alkyne-functionalized polyphosphoramidates, PBYOMP, **6**. d) One-pot sequential polymerization of **5** and **3** to afford the amphiphilic diblock copolymer PEOMP-*b*-PBYOMP, **2**.

alcohol and 1,5,7-triazabicyclo[4.4.0]dec-5-ene (TBD) were dried over CaH_2 in THF, and then vacuum-dried and stored in a glovebox under Ar atmosphere. All other chemicals and reagents were used as received from Sigma-Aldrich Co. unless otherwise noted.

3.2.2 Instrumentation

^1H NMR, ^{31}P NMR, and ^{13}C NMR spectra were recorded on Varian Inova 500 spectrometer (Varian, Inc., Palo Alto, CA) interfaced to a UNIX computer using the VnmrJ software. Chemical shifts for ^1H NMR and ^{13}C NMR signals were referenced to the solvent resonance frequencies. Chemical shifts for ^{31}P NMR signals were referenced to a sealed capillary containing 85% H_3PO_4 placed in the sample solution.

IR spectra were recorded on an IR Prestige 21 system (Shimadzu Corp., Japan), equipped with an ATR accessory, and analyzed using IRsolution v.1.40 software.

Size exclusion chromatography (SEC) eluting with pre-filtered DMF containing 0.05 M LiBr was conducted on a Waters Chromatography, Inc. (Milford, MA) system equipped with an isocratic pump (model 1515), a differential refractometer (model 2414), and a four-column set including a 5 μm Guard column (50 \times 7.5 mm), a Styragel HR 4 5 μm DMF column (300 \times 7.5 mm), a Styragel HR 4E 5 μm DMF column (300 \times 7.5 mm), and a Styragel HR 2 5 μm DMF column (300 \times 7.5 mm). The system was operated at 70 $^\circ\text{C}$ with a flow rate of 1.00 mL/min. Polymer solutions were prepared at *ca.* 3 mg/mL, and an injection volume of 200 μL was used. Data collection and analysis were performed with Discovery32 v. 1.039.000 software (Precision Detectors, Inc., Bellingham, MA). The system was calibrated with S3 polystyrene standards (Polymer Laboratories, Amherst, MA) ranging from 615 to 442800 Da.

Glass transition temperatures (T_g) were measured by differential scanning calorimetry (DSC) on a Mettler-Toledo DSC3/700/1190 (Mettler-Toledo, Inc., Columbus, OH) under a nitrogen gas atmosphere. Measurements were performed with a heating rate of 5 °C/min and the data were analyzed using Mettler-Toledo STAR^e v. 15.00a software. The T_g was taken as the midpoint of the inflection tangent of the second heating scan.

Thermogravimetric analysis (TGA) was performed under Ar atmosphere using a Mettler-Toledo TGA2/1100/464, with a heating rate of 10 °C/min. Data were analyzed using Mettler-Toledo STAR^e v. 15.00a software.

Matrix-assisted laser desorption ionization-time of flight mass spectrometry (MALDI-Tof MS) was performed on a microflexTM LRF mass spectrometer (Bruker Corporation, Billerica, MA) in positive linear mode. Ions were generated by a pulsed nitrogen laser (337 nm, 25 kV) and 100 laser pulses were used per spectrum. Trans-2-[3-(4-*tert*-butylphenyl)-2-methyl-2-propylidene]malonitrile (DCTB) and potassium trifluoroacetate (KTFA) were used as a matrix and cationization reagent, respectively. The sample and matrix were prepared at 1 and 26 mg/mL, respectively, in chloroform, and KTFA was prepared at 1 mg/mL in acetone. The sample solution was mixed with the matrix and KTFA at a volumetric ratio of 2:5:1, and 1 μ L of the mixture was deposited onto a stainless-steel sample holder and dried in air prior to the measurement.

Transmission electron microscopy (TEM) images were collected on a JEOL 1200EX operated at 100 kV, and micrographs were recorded using an SIA-15C CCD camera. Samples for TEM were prepared as follows: 10 μ L of polymer solution in nanopure water (1 mg/mL) was deposited onto a carbon-coated copper grid, and after 1 min, excess solution was quickly wicked away by a piece of filter paper. The samples were then negatively stained with a 1 wt% phosphotungstic acid (PTA) aqueous solution (10 μ L). After 30 s, excess staining solution was

quickly wicked away by a piece of filter paper and the samples were left to dry under ambient conditions prior to imaging.

Dynamic light scattering (DLS) measurements were conducted using a Delsa Nano C instrument from Beckman Coulter, Inc. (Fullerton, CA) equipped with a laser diode operating at 658 nm. Scattered light was detected at 165° and analyzed using a log correlator over 70 accumulations for a 0.5 mL sample in a quartz size cell (0.9 mL capacity). The photomultiplier aperture and attenuator were adjusted automatically to obtain a photon count rate of *ca.* 10 kcps. Number-, volume-, and intensity-based particle size distributions and average diameters were calculated using CONTIN particle size distribution analysis routines in Delsa Nano 2.31 software. All measurements were repeated 10 times.

Loading and release studies were conducted by measuring the concentration of CPT by high-performance liquid chromatography (HPLC) on a Shimadzu Prominence system equipped with an SPD-20AV prominence UV-Vis detector set to 370 and 438 nm, and a Waters X Bridge C8 column (4.6 × 150 mm, 5 μM, 100 Å) eluting in 72% water, 27% acetonitrile and 1% 20 mM ammonium acetate buffer in isocratic mode. The flow rate was set to 1 mL/min with a run time of 20 min, and the column temperature was set to 40 °C. The HPLC method employed an external CPT concentration calibration.

All experiments were performed according to institutional guidelines provided by Texas A&M's Environmental Health and Safety committee. Experiments involving OVCAR-3, SJSA-1, RAW264.7 and MC3T3 cell lines were performed according to guidelines provided by Texas A&M's Institutional Biosafety Committee for biosafety level 2 organisms (Protocol Approval Number IBC2014-075).

3.2.3 Synthesis

Synthesis of but-3-yn-1-yl phosphorodichloridate (BYPC)

A solution of but-3-yn-1-ol (2.26 g, 32.2 mmol) with triethylamine (3.41 g, 33.8 mmol) in anhydrous THF (200 mL) was added to a stirred solution of phosphorus(V) oxychloride (4.94 g, 32.2 mmol) in anhydrous THF (200 mL) in an ice bath. The reaction mixture was allowed to stir at *ca.* 0 °C for 12 h and then warmed to room temperature. After complete conversion of phosphorus(V) oxychloride, as indicated by thin-layer chromatography, the reaction mixture was filtered and the filtrate was concentrated under reduced pressure. The concentrated filtrate was a clear pale-yellow liquid, which was used in the monomer synthesis (described next) without further purification. ¹H NMR (500 MHz, CDCl₃) δ ppm, 4.38 (dt, ⁴J_{P-H} = 17 Hz, ³J_{H-H} = 11.5 Hz, 2H, POCH₂CH₂C≡CH), 2.68 (tdd, ³J_{H-H} = 11.5 Hz, ⁴J_{H-H} = 4.5 Hz, ⁵J_{P-H} = 1 Hz, 2H, POCH₂CH₂C≡CH), 2.08 (t, ⁴J_{H-H} = 4.5 Hz, 1H, POCH₂CH₂C≡CH); ¹³C NMR (126 MHz, CDCl₃) δ ppm, 77.8 (s), 70.9 (s), 69.0 (d, J_{p-c} = 9.1 Hz), 20.1 (d, J_{p-c} = 9.9 Hz); ³¹P NMR (202 MHz, CDCl₃) δ ppm, 7.55.

Synthesis of (4*S*)-2-(but-3-yn-1-yloxy)-4-methyl-1,3,2-oxazaphospholidine 2-oxide (BYOMP)

A solution of (*S*)-(+)-2-amino-1-propanol (2.42 g, 32.2 mmol) with triethylamine (6.83 g, 67.6 mmol) in anhydrous THF (50 mL) and a solution of BYPC (6.02 g, 32.2 mmol) in anhydrous THF (50 mL) were simultaneously added to stirred neat anhydrous THF (200 mL) at 0 °C using a syringe pump at a rate of 10 mL/h. The reaction mixture was allowed to stir for 12 h and was then warmed to room temperature. After complete conversion of but-3-yn-1-yl phosphorodichloridate, as indicated by thin-layer chromatography, the reaction mixture was filtered and the filtrate was

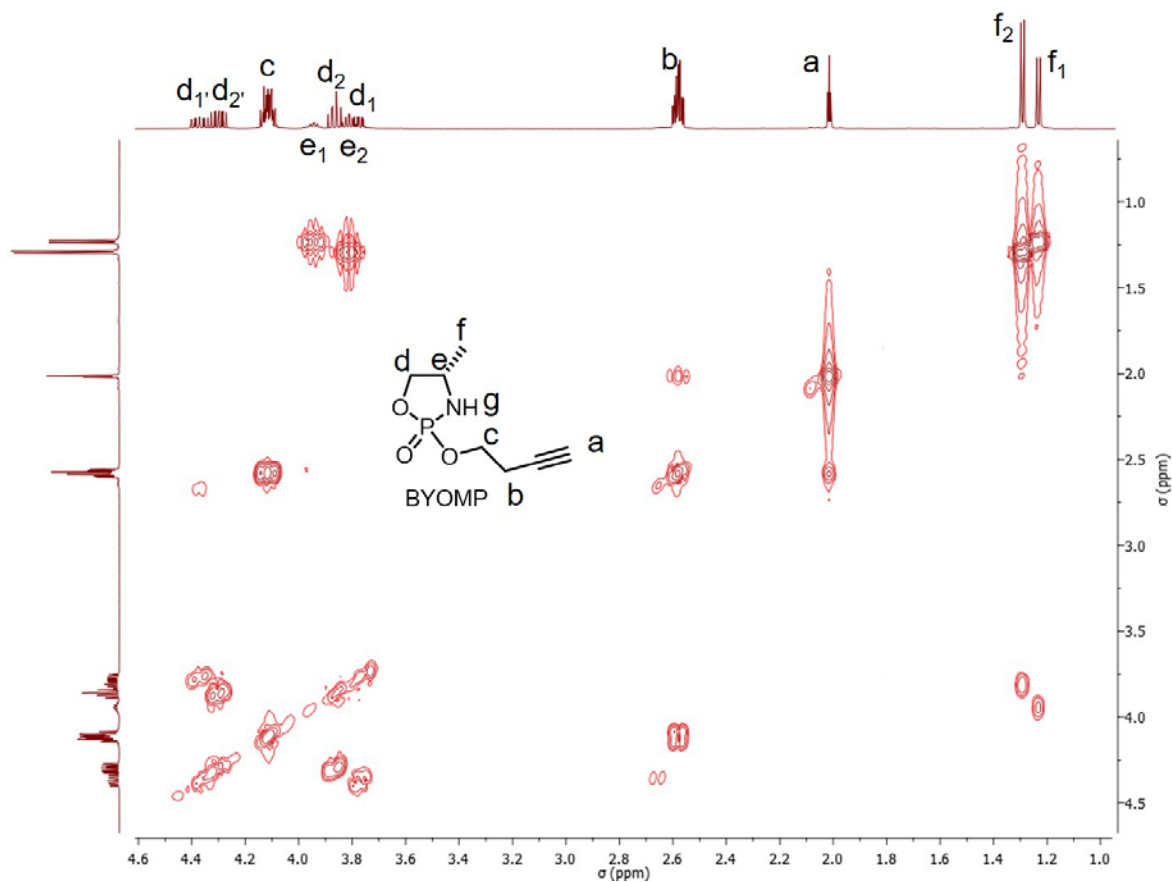


Figure III-2. COSY spectrum of BYOMP in CDCl_3 . Protons at the same position but belonging to different isomers were assigned as H_{x1} and H_{x2} , H_{f1} and H_{f2} for example. If signals of the protons labeled as H_{x1} and H_{x2} overlapped with each other and were not distinguishable, H_x would be used as the assignment, H_b and H_c for example. Enantiotopic protons were assigned as H_{d1} and $\text{H}_{d1'}$ and H_{d2} and $\text{H}_{d2'}$. Signals of the protons labeled as H_g were overlapped with those of protons labeled as H_{d2} , H_{e2} , and H_{d1} .

concentrated under reduced pressure. The concentrated filtrate was passed through a silica gel plug eluting in THF, and then concentrated to obtain the pure product as a clear pale-yellow liquid (4.25 g, 22.5 mmol, 69.9% yield). ^1H NMR (500 MHz, CDCl_3) δ ppm (Figure III-2), 4.46-4.24 (m, 1H), 4.18-4.03 (m, 2H), 3.99–3.73 (m, 3H), 2.70-2.53 (m, 2H), 2.02 (t, $^4J_{\text{H-H}} = 4.5$ Hz), 1.29 (dd, $^4J_{\text{H-H}} = 6$ Hz, $^5J_{\text{P-H}} = 0.5$ Hz, 0.55 H), 1.23 (m, (dd, , $^4J_{\text{H-H}} = 6$ Hz, $^5J_{\text{P-H}}=0.5$ Hz, 0.45 H); ^{13}C NMR (126 MHz, CDCl_3) δ ppm, 79.9 (s), 79.8 (s), 72.9 (d, $J_{\text{p-c}} = 5.1$ Hz), 72.5 (d, $J_{\text{p-c}} = 5.3$ Hz),

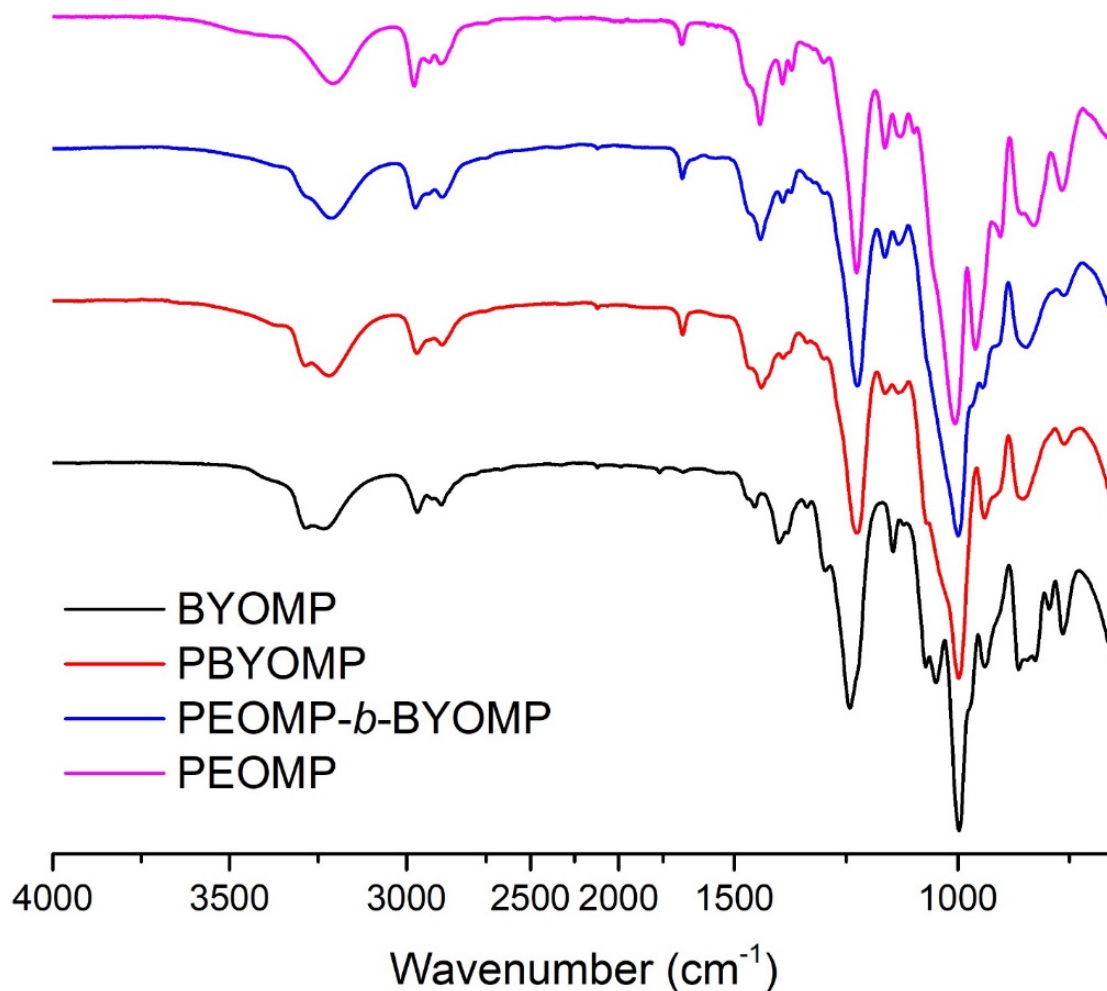


Figure III-3. FT-IR spectra of BYOMP, PBYOMP, PEOMP-*b*-PBYOMP, and PEOMP.

70.3 (s), 65.2 (d, $J_{p-c} = 9.9$ Hz), 65.1 (d, $J_{p-c} = 9.9$ Hz), 50.2 (d, $J_{p-c} = 15.4$ Hz), 49.8 (d, $J_{p-c} = 15.6$ Hz), 20.8 (d, $J_{p-c} = 4.0$ Hz), 20.5 (d, $J_{p-c} = 4.0$ Hz); ³¹P NMR (202 MHz, CDCl₃) δ ppm, 25.62, 24.85; FT-IR (ATR) 3450-3059, 3037-2738, 1454, 1398, 1298, 1240, 1146, 1072, 1047, 995, 937, 864, 795, 764 cm⁻¹ (Figure III-3); HRMS C₇H₁₂NO₃PH⁺ 190.0628, found (M+H⁺) 190.0599.

General procedure for the organobase-catalyzed ring-opening polymerization (ROP) of BYOMP to afford PBYOMP

All polymerizations were carried out using standard glovebox and Schlenk line techniques. BYOMP was vacuum dried over P_2O_5 for 12 h before transferring to a glovebox for storage under an inert Ar atmosphere. All reagents were weighed in the glovebox and the reactions were conducted on a Schlenk line in a fume hood. BYOMP (ca. 0.200 g, 1.06 mmol in each vial) was distributed into flame-dried 5-mL shell vials equipped with rubber septa and stir bars. A solution of a given amount of 4-methylbenzyl alcohol (0.0106-0.0212 mmol) in anhydrous DCM (210 μ L) was transferred *via* syringe into the shell vial of BYOMP while stirring. Organocatalyst TBD (2 mol% relative to monomer, 0.0242 mmol) in anhydrous DCM (210 μ L) was transferred *via* syringe into the shell vial with stirring at -78 $^{\circ}$ C under a nitrogen gas atmosphere. After stirring for a predetermined time (2 to 40 min), the reaction vial was unstoppered and quenched by addition of Amberlyst 15 H-form resin (10 mg) in DCM (1 mL). The reaction solution was then removed from the resin by pipet, and the polymer was isolated by precipitation from DCM into diethyl ether (3x) and dried *in vacuo* to give the polymer as a viscous yellow liquid, with an average yield of 85%. 1H NMR (500 MHz, $CDCl_3$) δ ppm, 7.25 ($1/2AB_q$, $J = 8$ Hz, 2H, Ar), 7.15 ($1/2AB_q$, $J = 8$ Hz, 2H, Ar), 4.96 (m, 2H, OCH_2Ar), 4.77-3.71 (m, 5nH, $POCH_2CH_2C\equiv CH$, $POCH_2CHNH$, $POCH_2CHNH$), 3.69-3.11 (m, nH, $POCH_2CHNH$), 2.79-2.51 (m, 2nH, $POCH_2CH_2C\equiv CH$), 2.34 (s, 3H, CH_3Ar), 2.19-1.91 (m, nH, $POCH_2CH_2C\equiv CH$), 1.44-1.04 (m, 3nH, $POCH_2CHCH_3$); ^{13}C NMR (126 MHz, $CDCl_3$) δ ppm, 151.8, 129.30, 128.0, 80.1, 70.5, 70.1, 64.3, 47.8, 38.0, 21.3, 20.9, 19.5, 15.4, 15.1; ^{31}P NMR (202 MHz, $CDCl_3$) δ ppm, 9.88, 9.04; FT-IR (ATR) 3606-3037, 3015-2779, 1639, 1440, 1390, 1227, 1163, 1122, 997, 939, 850, 764 cm^{-1} (Figure III-3); $T_g = -12$

to -8 °C ($DP_n = 20$ to 98); TGA in Ar, 25-194 °C, 10% weight loss, 194-500 °C, 68% weight loss (Figure III-4).

Kinetic study of the organobase-catalyzed ROP of BYOMP

To a shell vial equipped with a rubber septum and a stir bar containing BYOMP (0.400 g, 2.12 mmol), a solution of 4-methylbenzyl alcohol (0.0212 mmol) in anhydrous DCM (420 μ L) was transferred *via* syringe into the shell vial while stirring. TBD (2 mol% to monomer, 0.0424 mmol) in anhydrous DCM (420 μ L) was then transferred *via* syringe into the shell vial with stirring at -78 °C, while being maintained under a nitrogen gas atmosphere. At 1, 2.5, 5, 10, 20,

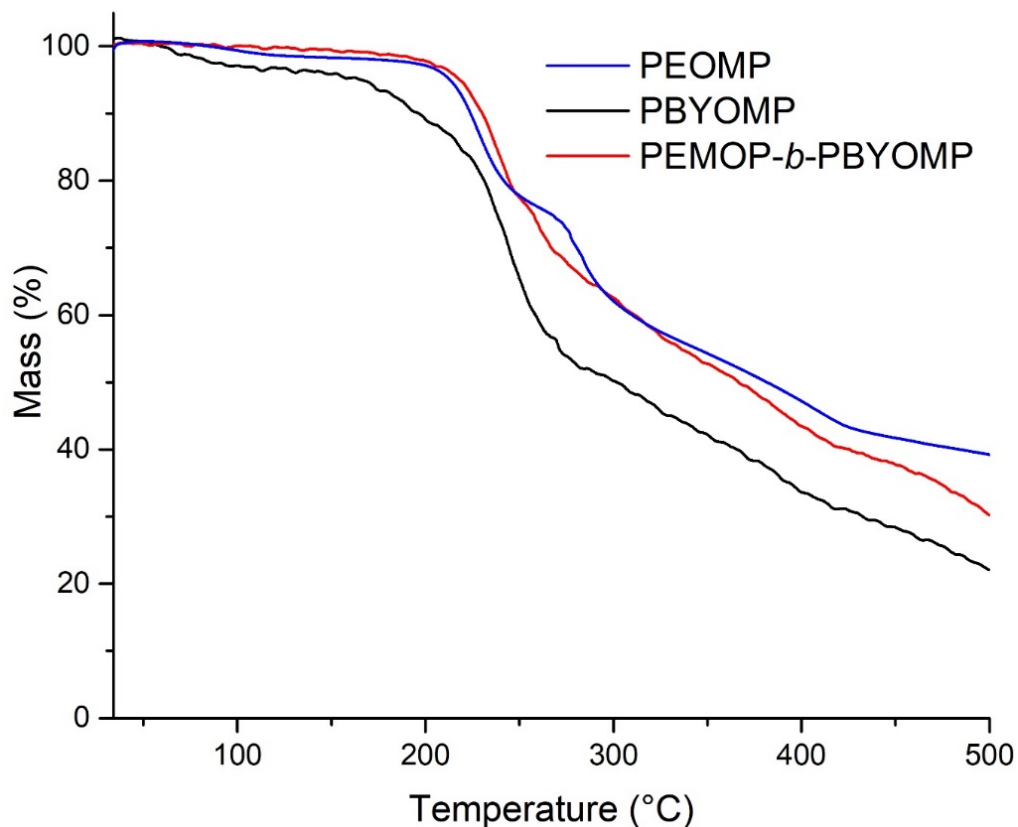


Figure III-4. TGA traces of PEOMP, PBYOMP, and PEOMP-*b*-PBYOMP.

30, and 40 min, 150 μL of the reaction mixture was removed and quenched over Amberlyst 15 H-form resin in CDCl_3 (10 mg in 1 mL CDCl_3). The reaction mixture at each time point was removed from the resin and directly analyzed by ^{31}P NMR spectroscopy without purification. The reaction mixture was then purified by precipitation into diethyl ether (3x) and vacuum dried, which was further characterized by DMF SEC and ^1H NMR spectroscopy. The kinetic study was triplicated.

General procedure for the organobase-catalyzed sequential ROP of EOMP and BYOMP to afford PEOMP_x-*b*-PBYOMP_y

All polymerizations were carried out using standard glovebox and Schlenk line techniques. EOMP was vacuum dried over P_2O_5 for 12 h before transferring to a glovebox for storage under an inert Ar atmosphere. All reagents were weighed in the glovebox and the reactions were conducted on a Schlenk line in a fume hood. EOMP was distributed into flame-dried 5-mL shell vials equipped with rubber septa and stir bars (*ca.* 0.200 g, 1.21 mmol in each vial). A solution of a given amount of 4-methylbenzyl alcohol (0.0242 mmol) in anhydrous DCM (210 μL) was transferred *via* syringe into the shell vial of EOMP while stirring. Organocatalyst TBD (2 mol% relative to monomer, 0.0242 mmol) in anhydrous DCM (210 μL) was transferred *via* syringe into the shell vial with stirring at $-78\text{ }^\circ\text{C}$ while being maintained under a nitrogen gas atmosphere. After stirring for 45 min, a solution of a given amount of BYOMP (0.458 g, 2.42 mmol) in anhydrous DCM (420 μL) was transferred *via* syringe into the shell vial while stirring at $-78\text{ }^\circ\text{C}$. After stirring for 60 min, the reaction vial was unstoppered and quenched by addition of Amberlyst 15 H-form resin (20 mg) in DCM (2 mL). The reaction solution was then removed from the resin by pipet, and the polymer was isolated by precipitation from DCM into diethyl ether (3x) and dried *in vacuo* to give PEOMP_x-*b*-PBYOMP_y as a yellow tacky material, with an average yield of 87%. ^1H NMR

(500 MHz, CDCl₃) δ ppm, 7.24 ($\frac{1}{2}$ AB_q, $J = 8$ Hz, 2H, Ar), 7.15 ($\frac{1}{2}$ AB_q, $J = 8$ Hz, 2H, Ar), 4.96 (m, 2H, OCH₂Ar), 4.77-3.71 (m, 5xH+5yH, yPOCH₂CH₂C \equiv CH, (x+y) POCH₂CHNH, (x+y) POCH₂CHNH, xPOCH₂CH₃), 3.69-3.11 (m, xH+yH, POCH₂CHNH), 2.69-2.50 (m, 2yH, POCH₂CH₂C \equiv CH), 2.34 (s, 3H, CH₃Ar), 2.17-1.96 (m, yH, POCH₂CH₂C \equiv CH), 1.54-1.06 (m, 6xH+3yH, (x+y) POCH₂CHCH₃, xPOCH₂CH₃); ¹³C NMR (126 MHz, CDCl₃) δ ppm, 129.30, 128.0, 80.1, 70.5, 70.1, 64.4, 62.6, 47.8, 38.0, 21.3, 20.8, 19.3, 16.31, 15.0; ³¹P NMR (202 MHz, CDCl₃) δ ppm, 10.32, 9.89, 9.03; FT-IR (ATR) 3600-3037, 3015-2696, 1643, 1440, 1393, 1371, 1225, 1163, 1134, 999, 943, 906, 846, 761 cm⁻¹ (Figure III-3); $T_g = 17$ °C (PEOMP₄₉-*b*-PBYOMP₉₈); TGA in Ar, 205-500 °C, 67% weight loss (Figure III-4).

CPT loading into PEOMP₄₉-*b*-PBYOMP₉₈ micelles to afford CPT@PPA

To a solution of PEOMP₄₉-*b*-PBYOMP₉₈ in ethanol (4 mL, 4 mg/mL), a predetermined amount of CPT solution in ethanol (1.6 to 6.4 mL, 1 mg/mL) was added. The vial was shaken vigorously to mix the solution, and then ethanol was removed *in vacuo*. Subsequently, the polymer/CPT solid mixture was resuspended in 2.0 mL of nanopure water and sonicated 10 min to obtain a well-dispersed suspension of nanoparticles (CPT@PPA). DLS and TEM were used to characterize these CPT-loaded nanoparticles, and HPLC was used to determine CPT loading relative to a CPT calibration curve.

CPT release from CPT@PPA

Release profiles of the CPT@PPA were obtained by monitoring the decrease of CPT concentration over time in dialysis cassettes by HPLC. In a typical experiment, a prepared solution of CPT@PPA (2.0 mL, 8 mg/mL polymer and 0.8 mg/mL CPT) was transferred into a presoaked

dialysis cassette (Slide-A-Lyzer, 10 kDa MWCO, Pierce Biotechnology, Rockford IL). The cassette was allowed to stir in a beaker containing 3 L phosphate buffered saline buffer (PBS, pH 7.4) or 3 L citric acid – Na₂HPO₄ buffer (pH 5.0) at 37 °C. Aliquots (0.1 mL) were taken at pre-determined times, diluted to a 1-mL volume with acetonitrile, and analyzed by HPLC.

Cytotoxicity study of CPT@PPA

SJSA human osteosarcoma (5×10^3 cells/well) and MC3T3-E1 mouse osteoblast precursor cells (5×10^3 cells/well) were plated in 96-well plates in DMEM and MEM α medium, respectively (10% fetal bovine serum, and 1% penicillin/streptomycin). OVCAR-3 human ovarian adenocarcinoma cells (5×10^3 cells/well) and RAW 264.7 mouse leukemic monocyte-macrophage cells (5×10^3 cells/well) were plated in 96-well plates in RPMI and DMEM-high glucose medium, respectively (10% fetal bovine serum, and 1% penicillin/streptomycin). Cells were incubated at 37 °C in a humidified atmosphere containing 5% CO₂ for 48 h to adhere. The samples (CPT, CPT@PPA and polymer micelles) were dissolved in PBS to achieve a desired concentration. Then, the medium was replaced with a fresh medium 1 h prior to the addition of stock solutions of the samples to 100 μ L of the medium (final concentrations ranged from 0.02-50 μ M). The cells were incubated with the formulations for 72 h and then the medium was replaced with 100 μ L of fresh medium prior to the addition of 20 μ L MTS combined reagent to each well (Cell Titer 96[®] Aqueous Non-Radioactive Cell Proliferation Assay, Promega Co., Madison, WI). The cells were incubated with the reagent for 2 h at 37 °C in a humidified atmosphere containing 5% CO₂ protected from light. Absorbance was measured at 490 nm using SpectraMax M5 (Molecular Devices Co., Sunnyvale, CA). The cell viability was calculated based on the relative absorbance to the control-untreated cells. The statistical analysis was performed using GraphPad Prism four-

parameter fit, considering the 0% and 100% cell viabilities were for the control medium (no cells) and cells with no treatment, respectively.

3.3 Results and Discussion

Based on our interest in the development of well-defined poly(glucose carbonate)s, The monomer, (4*S*)-2-(but-3-yn-1-yloxy)-4-methyl-1,3,2-oxazaphospholidine 2-oxide (BYOMP, **3**), was synthesized by annulation of but-3-yn-1-yl phosphorodichloridate (BYPC, **4**) with (*S*)-(+)-2-amino-1-propanol in the presence of triethylamine (Figure III-1c). Addition of but-3-yn-1-ol to phosphorus(V) oxychloride yielded **4**, which was initially purified by vacuum distillation prior to use in monomer synthesis. However, given that the reaction proceeded quantitatively, as evidenced by only the peak of **4** at 7.55 ppm being observed in the ³¹P NMR spectrum, annulation reactions were then conducted with crude **4**. Notably, the use of crude **4** afforded little reduction of the yield of **3**, and substantially increased the overall yield of the two reactions from 29% to 70%. The annulation reaction was highly efficient, and purification was accomplished simply by filtration through a silica gel plug to remove the slight excess of triethylamine to give **3** as a highly viscous colorless liquid. The purity of **3** was confirmed by mass spectrometry. The ³¹P NMR spectrum of **3** showed resonances at 25.62 and 24.85 ppm, similar to the ³¹P chemical shift values reported for EOMP (25.97 and 25.20 ppm), **5**,⁹⁰ and other cyclic phospholane amidate structures.^{9,91} The two distinct resonances were attributed to diastereomers formed during the annulation. The ¹H and ¹³C NMR spectra of the monomer also showed two sets of resonance frequencies corresponding to the two diastereomers. Resonances in the ¹H NMR spectrum were able to be distinguished through homonuclear correlation spectroscopy (COSY) (Figure III-2), and the intensities of the 4-methyl

proton resonances at 1.23 and 1.29 ppm, respectively, revealed the two diastereomers to be present at roughly equal proportions in the mixture (45:55).

Conditions to allow for controlled ROP of **3** were then investigated. Initially, the polymerization was conducted in the presence of the organocatalyst 1,8-diazabicyclo[5.4.0]undec-7-ene (DBU), which had previously provided excellent control of the ROP of cyclic carbonate and cyclic phosphotriester monomers.^{56, 92, 93} However, similarly as observed in the ROP of **5**,⁹⁰ DBU failed to yield appreciable conversion of **3** to polymer in dichloromethane (DCM), even at relatively high catalyst loadings (10 mol% relative to monomer). Thus, DBU was replaced by the more active catalyst 1,5,7-triazabicyclo[4.4.0]dec-5-ene (TBD), which has successfully mediated the controlled ROP of several cyclic phosphorus-containing monomers.^{90, 56, 94, 95} Using a TBD loading of 2 mol% with respect to monomer and 4-methylbenzyl alcohol as the initiator, ROP of **3** in DCM was studied, monitoring monomer conversion and the growth of polymer chains as a function of time by NMR spectroscopy and *N,N*-dimethylformamide size exclusion chromatography (DMF SEC). Monomer conversions were obtained from ³¹P NMR spectra on aliquots taken from the polymerization mixtures. Subsequently, number-average molar masses (M_n) were calculated from the ¹H NMR spectra after isolation of the polymers by precipitation from dichloromethane into diethyl ether, by comparison of the intensities of the 4-methyl protons originating from the initiator on the α -chain end resonating at 2.34 ppm with the methylene protons adjacent to the alkyne on the repeating units resonating at 2.58 ppm. Molar mass distribution (dispersity, \mathcal{D}) was measured by DMF SEC calibrated using polystyrene standards. At 0 °C, the polymerization proceeded to 94% conversion within 5 min (entries 1-3, Table III-1). However, broadening of \mathcal{D} (1.2-1.3) was observed at conversions exceeding 75%, indicating the occurrence of adverse backbiting or transesterification reactions. Hence, the reaction temperature was

Table III-1. Polymerization of BYOMP catalyzed by TBD under different conditions^a

entry	T (°C)	$[M]/[I]$	conv. ^b	$M_{n, \text{NMR}}^c$ (kDa)	\bar{D}^d	time (min)
1	0	100	60%	11.2	1.08	2
2	0	100	77%	14.2	1.26	3
3	0	100	94%	17.8	1.32	5
4	-78	100	98%	18.6	1.15	40
5	-78	50	98%	9.2	1.12	30
6	-78	25	96%	4.4	1.16	20

^aPolymerizations were conducted with 4-methylbenzyl alcohol as the initiator and TBD as the catalyst in anhydrous dichloromethane at a monomer concentration of 2.0 M. ^bConversions (conv.) were obtained from ³¹P NMR spectra of aliquots taken from the polymerization mixtures. ^c $M_{n, \text{NMR}}$ was determined by end group analysis by ¹H NMR spectroscopy of the polymer. ^d \bar{D} was measured by DMF SEC calibrated using polystyrene standards.

decreased to -78 °C (entries 4-6, Table III-1). At this reduced temperature, the polymerization reached > 90% conversion within 30 min, and a narrow \bar{D} (1.1-1.2) was achieved at monomer conversions from 15 to 98%, indicating successful restriction of the side reactions.

The kinetics of polymerization were then studied in detail under these optimized conditions at -78 °C in the presence of 2 mol% TBD with a monomer concentration of 2.0 M in DCM and a monomer/initiator feed ratio ($[M]_0/[I]_0$) of 100. The linearity of M_n vs monomer conversion (Figure III-5a) suggested that the numbers of growing macromolecules in the reactions remained constant during the polymerizations. Plots of $\ln([M]_0/[M])$ vs time (Figure III-5b) showed that the polymerization exhibited first order kinetics, also suggesting the characteristics of a controlled polymerization. Further analysis by matrix-assisted laser desorption ionization time-of-flight mass spectrometry (MALDI-ToF MS) of **6** ($DP_n = 8$ by ¹H NMR spectroscopy, Figure III-6), revealed two populations, each with a spacing of 189 m/z, equal to that of the expected monomer repeat unit. Structurally, these two sets of signals were assigned to populations having the same end

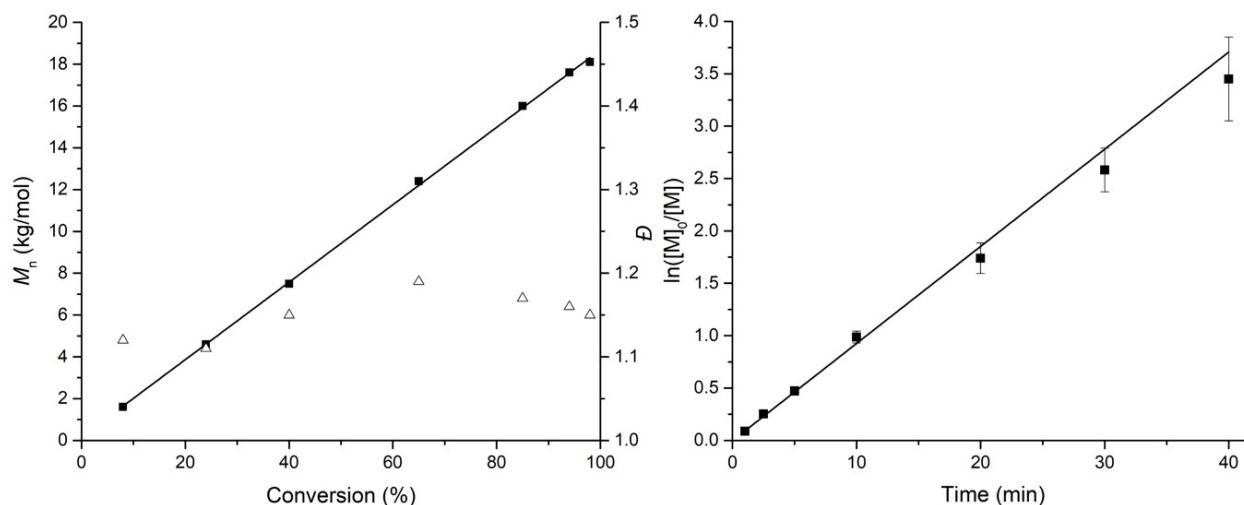


Figure III-5. a) Plot of M_n and D vs monomer conversion for the polymerization of BYOMP using TBD as the catalyst and 4-methylbenzyl alcohol as the initiator, obtained from a combination of SEC, ^1H NMR and ^{31}P NMR spectroscopic analyses. The ratio of monomer : initiator : TBD was 100 : 1 : 2. b) Plots of monomer conversion ($\ln([M]_0/[M])$) vs time obtained from ^{31}P NMR spectra.

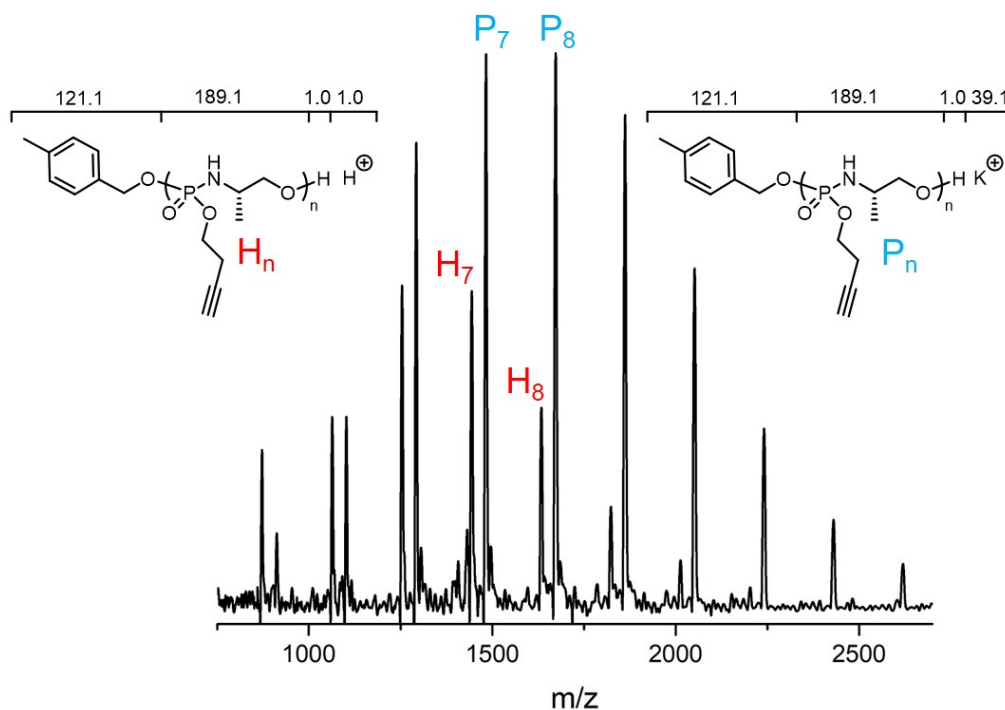


Figure III-6. MALDI-Tof MS spectrum of PBYOMP ($DP_n = 8$).

groups but distinct ionizations. The main peak in the major population at $m/z = 1673$ corresponded to a potassium-charged polymer chain of $DP_n = 8$ that had been initiated by 4-methylbenzyl alcohol and terminated by protonation, further confirming the controlled nature of the polymerization. Meanwhile, the main peak in the minor population at $m/z = 1444$ was in agreement with a proton-charged polymer chain of $DP_n = 7$ having 4-methylbenzyl oxy and protonated α - and ω -end groups, respectively.

By controlling the $[M]_0/[I]_0$ and the reaction time, a series of **6** with different molar masses was synthesized (*ca.* 2-to-18 kg/mol, Table III-1 and Figure III5a). Across this range of molar masses, the polymers were soluble in common organic solvents but did not display water solubility. ^{31}P NMR spectra clearly indicated two chemically-distinct phosphorus environments, resonating at 9.88 and 9.04 ppm, corresponding to the chiral phosphorous atoms. ^1H NMR and ^{13}C NMR spectra further confirmed the structure of **6**. Polymer **6** was a pale-yellow viscous liquid at room temperature, and exhibited a glass transition temperature (T_g) of -12 to -8 °C ($DP_n = 20$ -98). Compared to the T_g of -35 °C reported for an analogous polyphosphoester with alkyne side chains ($DP_n = 50$),⁵⁶ the T_g of **6** was higher, which was attributed to the phosphoramidate linkages along the polymer backbone. Yet, the T_g of **6** was significantly lower than that of **1** ($DP_n = 20$ -93, $T_g = 32$ -36 °C),⁹⁰ likely due to the increased free volume provided by the larger butynyl side chains.

Having demonstrated that both **5** and **3** could undergo controlled ROPs under similar conditions to afford hydrophilic **1** and hydrophobic **6**, respectively, we then designed a synthetic route to produce amphiphilic diblock copolymers that would serve as acid-labile hosts for CPT in water. Given the high water solubility and hydrophilicity of **1**, it was expected that hydrophobic chain segments derived from **3** should be of greater relative length, to provide sufficient hydrophobicity to drive the assembly process and create a hydrophobic domain to maintain

packaging of the drug molecules. After testing different block ratios, a 1:2 block ratio of PEOMP to PBYOMP was determined to yield aqueous assembly. The amphiphilic diblock copolymer **2**, was obtained *via* one-pot sequential ROP of **5** and **3**, in which the sequence of the polymerization was the key to success (Figure III-1d). Due to the dilution of the solution mixture of the first block, the decreased concentration of the second monomer would likely result in a slower polymerization rate and lower polymerization conversion. The two-fold amount of **3** used compared to **5** at this block ratio was also able to compensate for the dilution and be polymerized at the concentration of 2.0 M. Therefore, **3** was selected as the monomer for the second block, the higher activity of which further benefited these polymerizations. In contrast, selection of **5** as the second monomer suffered from dilution effects and resulted in lower than expected conversion (*ca.* 40%). Using an initially-prepared **1** as a macroinitiator maintained as a reaction mixture at -78 °C, addition of **3** as a solution in DCM to afford a concentration of **3** at 2.0 M, resulted in chain extension as observed by the peak in the SEC trace shifting towards shorter elution time relative to **1** (Figure III-7). The increased molar mass as measured by SEC was consistent with the increased degree of polymerization determined by ¹H NMR spectroscopy. Although the molar mass distribution remained narrow ($D < 1.2$), indicative of a well-controlled polymerization, there was consistently a minor high molecular weight shoulder with several synthetic runs, which may be due to mixing complications because of the high viscosity of the polymerization mixture. To limit the breadth of the molar mass distribution and the presence of high molar mass impurities, the solution of monomer **3** was pre-cooled to 0 °C and added as quickly as possible. This one-pot sequential synthesis of well-defined diblock PPAs provides several advantages over chain extension from purified macroinitiators, with fewer steps, shorter experimental time, and higher yields.

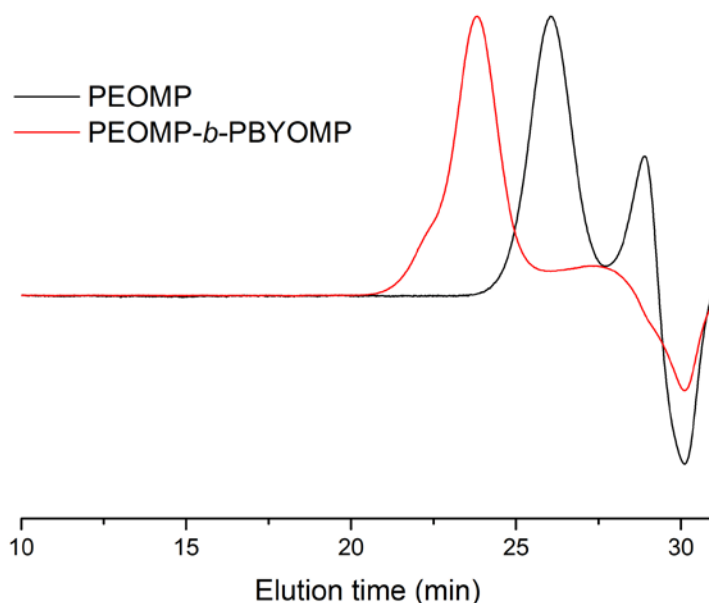


Figure III-7. SEC traces of PEOMP and PEOMP₄₉-*b*-PBYOMP₉₈. PEOMP was synthesized with $[M]_0/[I]_0 = 50$ at $[M] = 2.2$ M. Chain extension of BYOMP from PEOMP macroinitiator at $[M]_0/[I]_0 = 100$ at $[M] = 2.0$ M yielded PEOMP-*b*-PBYOMP.

Aided by the hydrophilic PEOMP block, **2** dispersed readily into aqueous solution, while the alkynyl side chain groups on the hydrophobic PBYOMP block promoted assembly into nanostructures. The size and morphology of the nanostructures were characterized by dynamic light scattering (DLS) and transmission electron microscopy (TEM). DLS showed unimodal size distributions of the PPA nanoparticles, with a number-average hydrodynamic diameter ($D_{h(\text{number})}$) of 15 ± 4 nm (Figure III-8b). TEM images of PPA nanoparticles showed circular structures, with an average diameter (D_{av}) of 22 ± 4 nm (counting > 50 nanoparticles, Figure III-8a) suggesting the formation of core-shell micelles. CPT-loaded PPA nanoparticles (**CPT@PPA**) were prepared in a facile manner (Figure III-9a), by dissolution of the polymer and CPT in ethanol, followed by

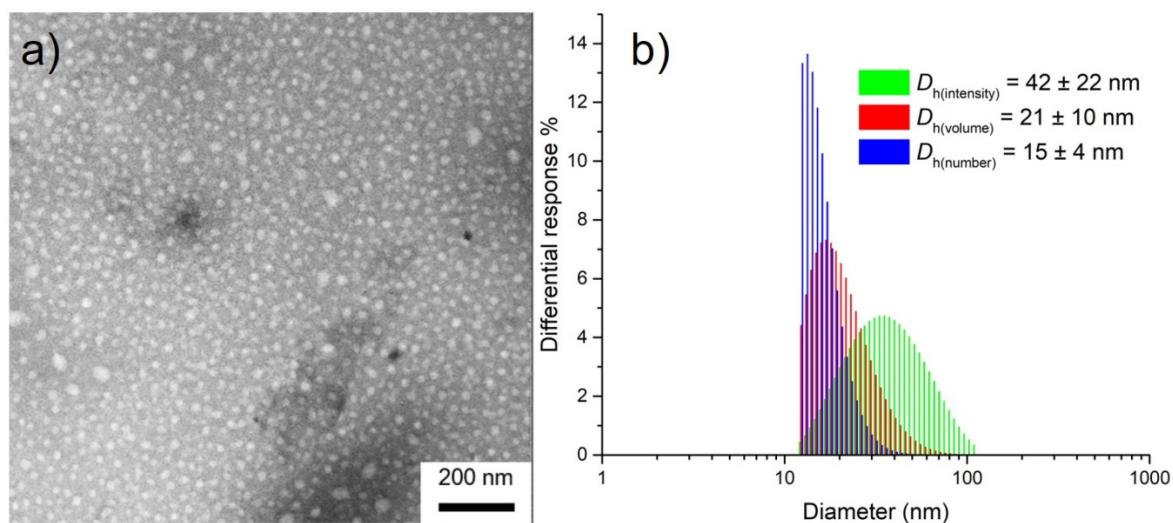


Figure III-8. a) TEM images of PPA micelles negatively stained by 1 wt% phosphotungstic acid aqueous solution (10 μ L) with an average diameter (D_{av}) of 22 ± 4 nm (counting > 50 nanoparticles). b) Number-, volume- and intensity-based hydrodynamic diameter of PPA micelles in nanopure water measured by DLS.

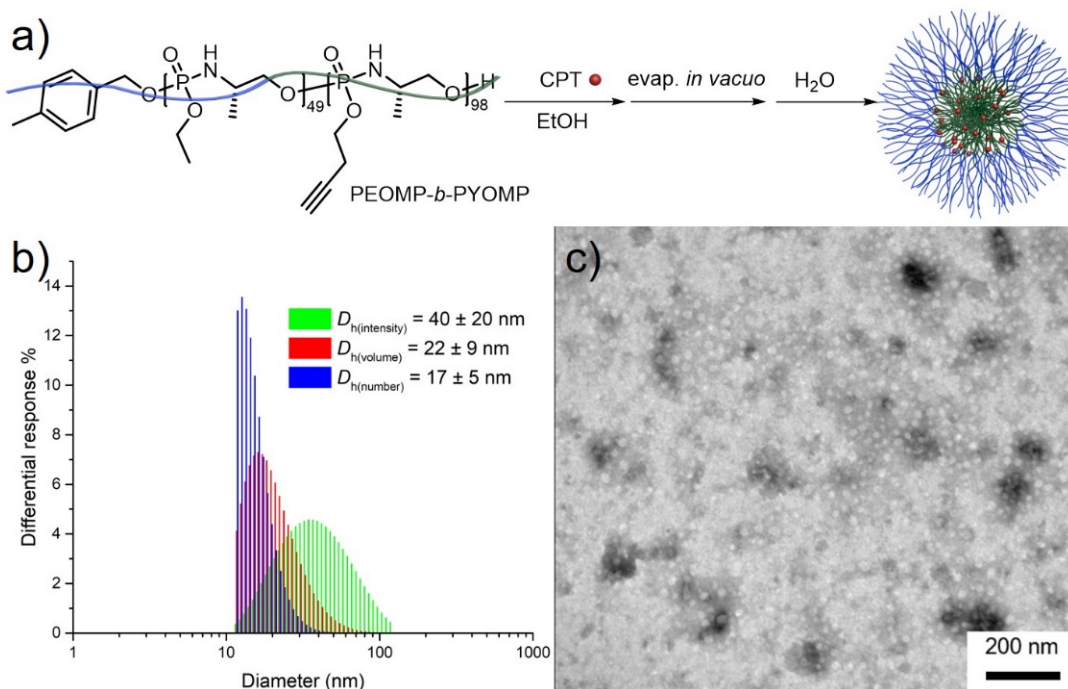


Figure III-9. a) Schematic representation of the formation of **CPT@PPA** by physical encapsulation of CPT into PPA. b) Number-, intensity- and volume-based hydrodynamic diameter distributions of **CPT@PPA** in nanopure water measured by DLS. c) TEM images of **CPT@PPA** negatively stained by 1 wt% phosphotungstic acid aqueous solution (10 μ L), $D_{av} = 24 \pm 4$ nm (counting > 50 nanoparticles). The dark spots are artifacts from phosphotungstic acid.

removal of ethanol *in vacuo* and resuspension in nanopure water with sonication. The CPT concentration and loading capacity were optimized by tuning CPT and polymer concentrations. CPT loading was determined using high-performance liquid chromatography (HPLC), while the size and morphology of the loaded nanostructures were characterized by DLS and TEM. Preliminary experiments showed loading of CPT in the PPA nanoparticles of up to *ca.* 40 wt%, while for optimized stability of the system and inhibition of premature hydrolysis of CPT, a loading of 10 wt% was selected for morphological and biological characterization. DLS showed unimodal size distributions of the **CPT@PPA** nanocarriers, with a number-average hydrodynamic diameter ($D_{h(\text{number})}$) of 17 ± 5 nm (Figure III-9b). TEM images of **CPT@PPA** showed circular structures, with an average diameter (D_{av}) of 24 ± 4 nm (counting > 50 nanoparticles, Figure III-9c) suggesting the formation of micelles. The low T_g of PBYOMP ($DP_n = 20\text{-}98$, $T_g = -12$ to -8 °C) promoted flattening of the micellar structures in the dry state on TEM grids, leading to larger dry state diameters than those observed in solution.

The drug release profiles of CPT from **CPT@PPA** were measured in phosphate buffered saline (PBS, pH 7.4) and citric acid – Na_2HPO_4 (pH 5.0) at 37 °C over 2.5 d. As depicted in Figure III-9a, at pH 7.4, sustained release of CPT was observed over 2.5 d, while at pH 5.0, burst release of CPT was observed, with 98% of CPT released within 8 h. These distinct release profiles at different pH values are consistent with the acid-triggered degradation of the PPA backbone.⁹⁰

The *in vitro* cytotoxicities of drug-equivalent loading **CPT@PPA** were investigated in three cancer and one non- cancer cell lines, and compared to cell viabilities for free CPT as a positive control with each cell line (Figure III-9b, c and Table III-2). The polymer micelles of **2** were found to be nontoxic at all concentrations tested (up to 175 $\mu\text{g}/\text{mL}$). In human osteosarcoma cells (SJSA-1), **CPT@PPA** exhibited a lower IC_{50} (2.2 μM) compared to free CPT (4.6 μM),

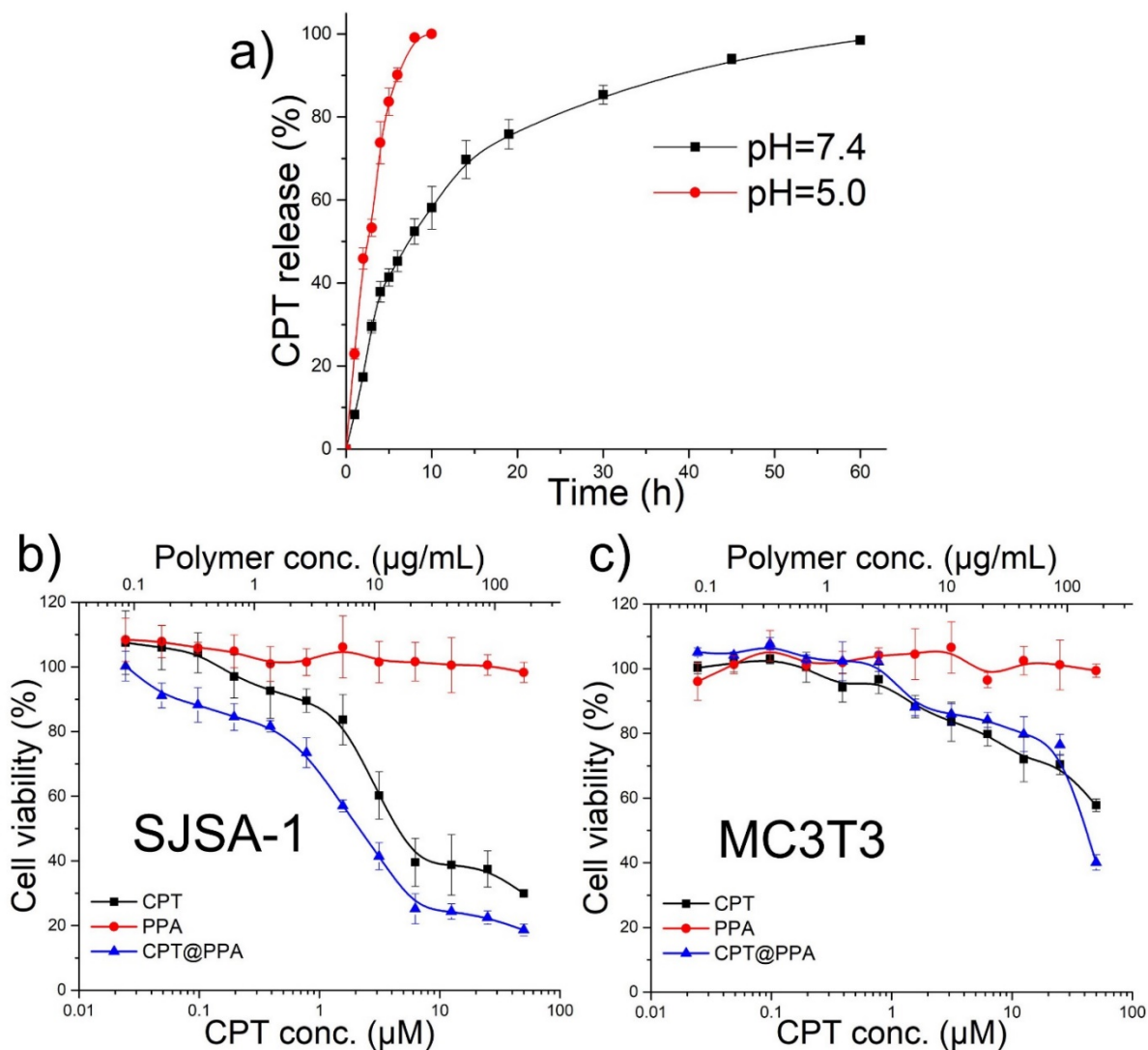


Figure III-10. a) Release of CPT from **CPT@PPA** (10 wt%) at pH 5.0 and pH 7.4, that studied by a dialysis method over 2.5 d at 37 °C in citric acid – Na_2HPO_4 and PBS buffers, respectively, measured in triplicates. Cytotoxicity of CPT, PPA micelles, and **CPT@PPA** in (b) SJSA-1 and (c) MC3T3 cells. Cell viabilities are reported as an average of three measurements.

potentially indicating a protection against hydrolysis of CPT into the open, inactive carboxylate form. In addition, similarly lower IC_{50} values were observed for **CPT@PPA** in comparison to free CPT in human ovarian adenocarcinoma cells (OVCAR-3) and mouse leukemic monocyte-macrophage cells (RAW 264.7). In contrast, in mouse osteoblast precursor cells (MC3T3), IC_{50}

Table III-2. Comparison of the IC₅₀ values of CPT, PPA micelles and **CPT@PPA** in OVCAR-3, RAW264.7, and SJSA-1 cell lines.

	IC ₅₀ (μM)		
	OVCAR-3	RAW264.7	SJSA-1
CPT	3.4	4.2	4.6
PPA	N/A	N/A	N/A
CPT@PPA	1.5	3.1	2.2

values were not calculable up to the concentrations of CPT in both the **CPT@PPA** and free CPT formulations that had led to the cancer cell killing. Taken together, these studies demonstrate the advantages of **CPT@PPA** as anticancer agents, highlighting the potential for reduced side effects in healthy cells without sacrificing efficacy in cancer cells.

3.4 Conclusions

In summary, polymeric nanotherapeutics that display acid-triggered release were successfully obtained *via* the coassembly of PPA-based diblock copolymers and CPT into degradable, functional nanocarriers. An alkyne-functionalized oxazaphospholidine monomer was synthesized and polymerized in a controlled manner by its organobase-catalyzed ROP. One-pot sequential ROP yielded well-defined amphiphilic diblock polymers with acid-labile linkages along the backbone, good biocompatibility, and functionality. The alkyne-functionalized block provided both hydrophobicity to promote aqueous solution assembly and versatile reactive groups that allow for future manipulations, such as attachment of a dye and/or crosslinking of the core. Well-dispersed CPT-loaded nanoparticles with a $D_{h(\text{number})}$ of 17 ± 5 nm were achieved through co-

assembly of the diblock copolymer with CPT, which exhibited sustained release of CPT at pH 7.4 and burst release at pH 5.0. Cytotoxicity assays demonstrated the biocompatibility of the polymer and enhanced efficacy of the CPT-loaded nanoparticles towards cancer cells, with minimal toxicity towards healthy cells. Future studies, including further modification of the polymer *via* alkyne groups and preparation of PPA-based nanoparticles loaded with different drugs, are underway.

CHAPTER IV

CONSTRUCTION OF POLYPHOSPHORAMIDATES WITH ACID-TRIGGERED BACKBONE DEGRADATION USING α -AMINO ACIDS AS BUILDING BLOCKS

4.1 Introduction

Biodegradable polymers are of great interest due to their great potential in a wide range of applications, such as drug delivery, gene transfer, tissue engineering, and regenerative medicine.¹⁻⁶ The most important criteria for their use as biomedical materials are great biocompatibility, suitable degradation rate in particular applications, and nontoxic degradation products. α -Amino acids, based on their wide bioavailability, inherent biocompatibility are attractive starting materials for the development of novel synthetic biodegradable polymers. In addition, the introduction of α -amino acids may endow the polymer with additional advantages.⁹⁶ Interactions of the polymer with bioactive molecules, such as proteins and genes, introduced by α -amino acids may lead to desirable biological properties of the material, including cell adhesion, enzyme inhibition, and enzymatic degradability.⁹⁷ The strong intermolecular hydrogen-bond interactions may also enhance the mechanical and thermal properties of the polymers. Furthermore, the high chemical functionalities of α -amino acids enable easy post-polymerization modification of the polymer for applications like targeting, cell imaging, *etc.*⁹⁸ The origination from renewable feedstocks also increases the value of polymers containing α -amino acids for environmental purposes.

In the past decades, different synthetic approaches, including condensation polymerization,⁹⁹⁻¹⁰¹ ring-opening polymerization (ROP) of N-carboxyanhydrides (NCAs),¹⁰² and ROP of cyclic depsipeptides (morpholine-2,5-dione derivatives),¹⁰³ have been explored for the

synthesis of biodegradable polymers containing α -amino acids with varying structures and properties. For example, Zhong *et al.* reported the synthesis of enzymatically and reductively degradable poly(ester amide)s derived from L-phenylalanine *via* solution polycondensation, which was demonstrated with excellent cell compatibility and great potential as a drug carrier.¹⁰⁴ Fu *et al.* reported an unusual micelle-to-vesicle transformation of cholesterol-decorated poly(L-cysteine) copolymer assemblies, afforded by ROP of NCAs, in response to reactive oxygen species.¹⁰⁵ The interesting morphological transition correlates with the alteration in conformations from β -sheet to α -helix, which grants an attractive “on–off” switch for triggered release and cellular interaction. Recently, Schubert *et al.* reported the controlled ROP of alkyl-substituted morpholine-2,5-dione derivatives to afford well-defined polydepsipeptides derived from valine, leucine, and isoleucine. Among those approaches, controlled ROP of NCAs and depsipeptides are widely exploited due to the great control over the molar mass, molar mass distribution (dispersity, \mathcal{D}), molecular structures of the polymers.¹⁰⁶ However, besides these two categories, ROP of NCAs and cyclic depsipeptides, other approaches to achieve polymers containing α -amino acids *via* a controlled polymerization have rarely been reported.

Introduction of acid-labile linkages along a polymer backbone is anticipated to lead to rapid acid-triggered degradation, given that even slight degradation of the backbone would markedly decrease molar mass. In an earlier study, as shown in Figure IV-1a, we demonstrated that well-defined polyphosphoramides (PPAs) were achieved through ROP of cyclic monomers derived from a β -amino alcohol and that they were able to undergo accelerated degradation under acidic conditions, due to the presence of acid-labile phosphoramidate linkages along the backbone.⁹⁰ Inspired by this research, we perceived that α -amino acids with β -amino alcohol moiety in their

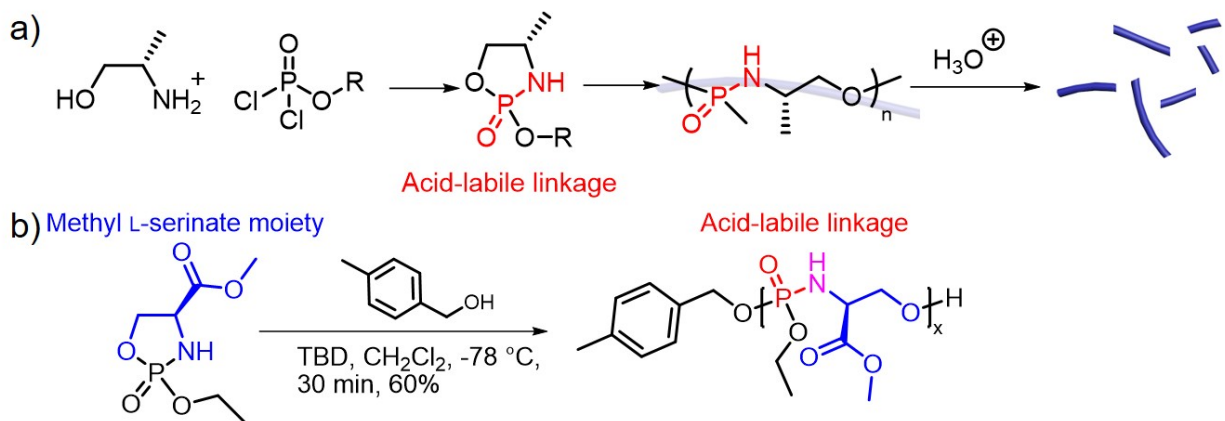


Figure IV-1. a) Well-defined PPAs achieved through ROP of cyclic monomers derived from a β -amino alcohol, which were able to undergo accelerated degradation under acidic conditions. b) ROP of a novel cyclic monomer derived from methyl L-serinate to afford well-defined PPAs with acid-labile linkages along the backbone.

structures, such as L-serine and L-threonine, could be adapted to the developed synthetic methodology to afford well-defined PPAs based on α -amino acids, which could undergo accelerated degradation under acidic conditions with nontoxic phosphates and α -amino acids as the degradation products. Herein, we report the design and synthesis of a novel oxazaphospholidine monomer based on methyl L-serinate (MLS) bearing a phosphoramidate within the cyclic structure to then place that acid-labile linkage along the backbone upon controlled organo-catalyzed ROP to afford well-defined PPAs containing α -amino acids (Figure IV-1b).

4.2 Experimental Section

4.2.1 Materials

All chemicals and reagents were used as received from Sigma-Aldrich Co. unless otherwise noted. Tetrahydrofuran (THF), and dichloromethane (DCM) were purified by passage through a

solvent purification system (JC Meyer Solvent Systems). 4-Methylbenzyl alcohol and 1,5,7-triazabicyclo[4.4.0]dec-5-ene (TBD) were dried over CaH₂ in THF, then vacuum dried and stored in a glovebox under Ar atmosphere. 1,8-Diazabicyclo[5.4.0]undec-7-ene (DBU) was dried over CaH₂, distilled, degassed, and stored in a glovebox under Ar atmosphere.

4.2.2 Instrumentation

¹H NMR, ³¹P NMR, and ¹³C NMR spectra were recorded on Varian Inova 500 spectrometer (Varian, Inc., Palo Alto, CA) interfaced to a UNIX computer using the VnmrJ software. Chemical shifts for ¹H NMR and ¹³C NMR signals were referenced to the solvent resonance frequencies. Chemical shifts for ³¹P NMR signals were referenced to a sealed capillary containing 85% H₃PO₄ placed in the sample solution.

Size exclusion chromatography (SEC) eluting with pre-filtered DMF containing 0.05 M LiBr was conducted on a Waters Chromatography, Inc. (Milford, MA) system equipped with an isocratic pump (model 1515), a differential refractometer (model 2414), and a four-column set including a 5 μm Guard column (50 × 7.5 mm), a Styragel HR 4 5 μm DMF column (300 × 7.5 mm), a Styragel HR 4E 5 μm DMF column (300 × 7.5 mm), and a Styragel HR 2 5 μm DMF column (300 × 7.5 mm). The system was operated at 70 °C with a flow rate of 1.00 mL/min. Polymer solutions were prepared at *ca.* 3 mg/mL, and an injection volume of 200 μL was used. Data collection and analysis were performed with Discovery32 v. 1.039.000 software (Precision Detectors, Inc., Bellingham, MA). The system was calibrated with S3 polystyrene standards (Polymer Laboratories, Amherst, MA) ranging from 615 to 442800 Da.

Glass transition temperatures (T_g) were measured by differential scanning calorimetry (DSC) on a Mettler-Toledo DSC3/700/1190 (Mettler-Toledo, Inc., Columbus, OH) under a

nitrogen gas atmosphere. Measurements were performed with a heating rate of 5 °C/min and the data were analyzed using Mettler-Toledo STAR^e v. 15.00a software. The T_g was taken as the midpoint of the inflection tangent of the second heating scan.

Thermogravimetric analysis (TGA) was performed under Ar atmosphere using a Mettler-Toledo TGA2/1100/464, with a heating rate of 10 °C/min. Data were analyzed using Mettler-Toledo STAR^e v. 15.00a software.

4.2.3 Synthesis

Two-step trial synthesis of methyl (4S)-2-ethoxy-1,3,2-oxazaphospholidine-4-carboxylate 2-oxide (MEOPC)

MLS·HCl (3.00 g, 19.3 mmol) was added to 100 mL of anhydrous THF and formed a suspension, followed by the dropwise addition of triethylamine (6.14 g, 60.8 mmol) in anhydrous THF (50 mL) at room temperature. The reaction mixture was allowed to stir for 12 h and was then filtered. The filtrate was concentrated under reduced pressure to less than 50 mL. The concentrated filtrate was then transferred into a syringe, and neat anhydrous THF was used to adjust the total solution volume to 50 mL. This solution, together with another solution of ethyl dichlorophosphate (3.14 g, 19.3 mmol) in anhydrous THF (50 mL) were simultaneously added to stirred neat anhydrous THF (200 mL) at 0 °C using a syringe pump at a rate of 10 mL/h. The reaction mixture was allowed to stir for 12 h and was then warmed to room temperature. After complete conversion of ethyl phosphorodichloridate, as indicated by ³¹P NMR, the reaction mixture was filtered, and the filtrate was concentrated under reduced pressure. The concentrated filtrate was passed through a silica gel plug eluting in THF and then concentrated to obtain the crude product as a clear yellow liquid. ³¹P NMR (202 MHz, CDCl₃) δ ppm (Figure IV-2), 24.08, 23.85, 8.90-7.20, 6.58, -0.70.

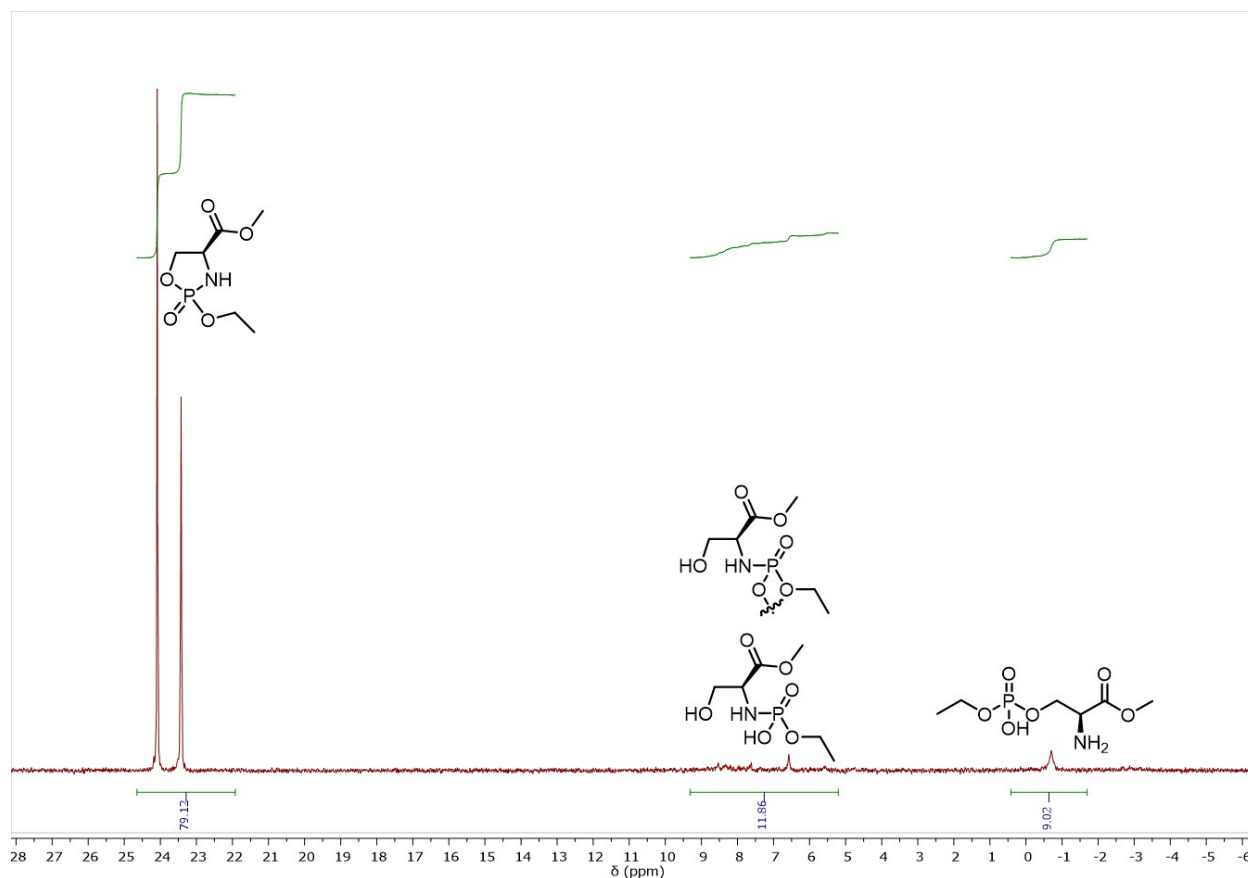


Figure IV-2. ^{31}P NMR (202 MHz, CDCl_3) of the crude products achieved by the two-step trial synthesis. Representative structures of impurities and the product are labeled to the corresponding peaks.

One-step synthesis of MEOPC

MLS·HCl (3.00 g, 19.3 mmol) was added to a solution of ethyl dichlorophosphate (3.14 g, 19.3 mmol) in anhydrous THF (300 mL) and formed a suspension with vigorous stirring, followed by the dropwise addition of a solution of triethylamine (6.14 g, 60.8 mmol) in anhydrous THF (50 mL) at 0°C with a rate of 6 mL/h. The reaction mixture was allowed to stir for 12 h and was then warmed to room temperature. After complete conversion of ethyl phosphorodichloridate, as indicated by ^{31}P NMR, the reaction mixture was filtered and the filtrate was concentrated under

reduced pressure. The concentrated filtrate was passed through a silica gel plug eluting in THF, and then concentrated to obtain the pure product as a clear colorless to pale-yellow liquid (2.34 g, 11.2 mmol, 58.0% yield). ^1H NMR (500 MHz, CDCl_3) δ ppm, 4.56-4.48 (m, 1H), 4.43-4.13 (m, 7H), 4.13-3.98 (m, 4H), 3.77-3.70 (m, 6H), 1.32-1.24 (m, 6H); ^{13}C NMR (126 MHz, CDCl_3) δ ppm, 171.29-171.07 (d, $J_{\text{p-c}} = 6.9$ Hz), 170.96-170.73 (d, $J_{\text{p-c}} = 5.5$ Hz), 67.39-67.21 (d, $J_{\text{p-c}} = 2.0$ Hz), 67.07-66.90 (d, $J_{\text{p-c}} = 2.0$ Hz), 64.23-64.09 (d, $J_{\text{p-c}} = 6.7$ Hz), 64.00-63.84 (d, $J_{\text{p-c}} = 6.2$ Hz), 55.33-55.10 (d, $J_{\text{p-c}} = 11.2$ Hz), 54.79-54.53 (d, $J_{\text{p-c}} = 12.0$ Hz), 53.09, 52.77, 16.31-16.06 (d, $J_{\text{p-c}} = 7.7$ Hz; d, $J_{\text{p-c}} = 7.7$ Hz); ^{31}P NMR (202 MHz, CDCl_3) δ ppm, 24.08, 23.85; HRMS $\text{C}_6\text{H}_{13}\text{NO}_5\text{PH}^+$ 210.0526, found ($\text{M}+\text{H}^+$) 210.0706.

General procedure for the organobase-catalyzed ROP of MEOPC to afford PMEOPC

All polymerizations were carried out using standard glovebox and Schlenk line techniques. MEOPC was vacuum dried over P_2O_5 for 0.5 d before transferring to a glovebox for storage under an inert atmosphere. All the reagents were weighed inside a glovebox, and the reactions were conducted in a fume hood. MEOPC was distributed into flame-dried 5-mL shell vials equipped with rubber septa and stir bars (*ca.* 0.200 g, 0.956 mmol for each). A solution of a given amount of 4-methylbenzyl alcohol (0.00956 mmol to 0.0191 mmol) in anhydrous DCM (210 μL) was transferred *via* syringe into the shell vial while stirring. Organocatalyst TBD (3 mol% relative to monomer, 0.0287 mmol) in anhydrous DCM (210 μL) was transferred *via* syringe into the shell vial with stirring at -78 $^\circ\text{C}$ while being maintained under a nitrogen gas atmosphere. After stirring for a certain period of time (2 min to 35 min), the reaction vial was unstoppered and quenched by addition of Amberlyst 15 H-form resin (10 mg) and 1 mL of DCM. The reaction mixture was then removed from resin, purified by precipitation from DCM into diethyl ether (3x) and vacuum dried

to give an average yield of 58%. ^1H NMR (500 MHz, CDCl_3) δ ppm, 7.22 (b, $J = 8.5$ Hz, 2H, Ar), 7.11 (b, $J = 8.0$ Hz, 2H, Ar), 5.39-3.99 (m, 6nH+2H (OCH_2Ar)), 3.88-3.66 (m, 3nH, COOCH_3), 2.29 (s, 3H, CH_3Ar), 1.34-1.12 (m, 3nH); ^{13}C NMR (126 MHz, CDCl_3) δ ppm, 170.93, 129.17, 127.92, 67.65, 63.14, 54.82, 52.68, 21.23, 16.09; ^{31}P NMR (202 MHz, CDCl_3) δ ppm, 8.37, 7.44, 5.59; $T_g = 15$ °C ($DP_n = 69$); TGA in Ar (Figure IV-2), 25-130, 5% total weight loss, 130-300 °C, 63% total weight loss., 300-500 °C, 74% total weight loss.

Kinetic study of the organobase-catalyzed ROP of MEOPC

To a shell vial equipped with a rubber septum and a stir bar containing MEOPC (0.400 g, 1.91 mmol), a solution of 4-methylbenzyl alcohol (0.0191 mmol) in anhydrous DCM (420 μL) was

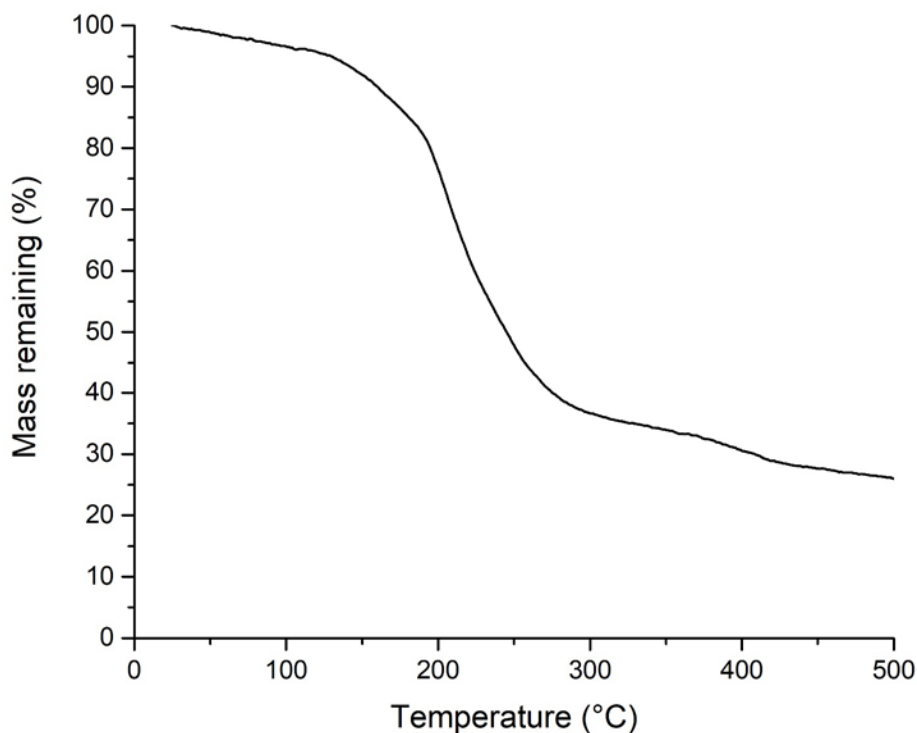


Figure IV-3. TGA trace of PMEOPC₆₉.

transferred *via* syringe into the shell vial while stirring. TBD (3 mol% to monomer, 0.0574 mmol) in anhydrous DCM (420 μ L) was then transferred *via* syringe into the shell vial with stirring at -78 $^{\circ}$ C, while being maintained under a nitrogen gas atmosphere. At 2, 4, 8, 12, 15, 25 and 35min, 150 μ L of the reaction mixture was removed and quenched over Amberlyst 15 H-form resin in CDCl_3 (10 mg in 1 mL CDCl_3). The reaction mixture at each time point was removed from the resin and directly analyzed by ^{31}P NMR spectroscopy without purification. The reaction mixture was then purified by precipitation into diethyl ether (3x) and vacuum dried, which was further characterized by DMF SEC and ^1H NMR spectroscopy.

Kinetic study of the backbone cleavage of PMEOPC in aqueous solution by ^{31}P NMR spectroscopy

PMEOPC ($DP_n = 69$, 5.0 mg) was dissolved into 1 mL of buffer solutions (100 mM citric acid - sodium citrate buffer solutions at pH 3.0, and 10 mM 3-(N-morpholino)propanesulfonic acid (MOPS) buffer solution at pH 7.4), and 10 vol% of D_2O (0.1 mL) was added to the buffer solutions. The solutions were incubated at 37 $^{\circ}$ C allowing for the degradation. The ^{31}P chemical shifts were monitored by ^{31}P NMR spectroscopy during the degradation study.

4.3 Results and Discussion

Based on our efforts to achieve PPAs with acid-triggered backbone degradation,^{90, 107} the monomer MEOPC was designed to be synthesized by annulation of ethyl dichlorophosphate with methyl L-serinate (MLS) in the presence of trimethylamine (Figure IV-1a). Unlike (*S*)-(+)-2-

amino-1-propanol used in our previous studies, MLS is often sold in its salt form, MLS·HCl. Thus, a two-step synthesis was designed to transform MLS·HCl into MLS first, followed by the annulation reaction. MLS·HCl is only soluble in polar protic solvents like water, methanol, and ethanol due to its ionic nature. The neutralization of MLS·HCl was carried out successfully in methanol with sodium hydroxide or sodium methoxide as the base. Protic solvents like methanol would cause severe side reactions with ethyl dichlorophosphate in the annulation reaction and thus needed to be completely removed. However, after the removal of methanol, the achieved MLS could no longer be re-dissolved into polar aprotic solvents like dichloromethane (DCM), tetrahydrofuran (THF), *N,N*-dimethylformamide (DMF), *etc.*, which was likely due to the strong hydrogen bond interactions between MLS molecules. In addition, due to the relatively high boiling point of methanol and its strong hydrogen bond interaction with MLS, there was always a peak of methanol contamination observed from the ¹H NMR spectra of crude products.

Therefore, a new two-step route was designed to achieve MLS *via* a heterogeneous reaction (Figure IV-4a), in which 3 equivalence of triethylamine was added to a suspension of MLS·HCl in THF. Although MLS·HCl was barely dissolved in THF, the trace amount of the dissolved salt could react with triethylamine and generate soluble MLS, which drove the reaction to completion. The annulation was then conducted on the achieved MLS solution. In our previous studies, when (*S*)-(+)-2-amino-1-propanol was applied, the annulation reaction was highly efficient, as evidenced by only the cyclic monomer peaks being observed in the ³¹P NMR spectra of the crude products.⁹⁰
¹⁰⁷ When MLS was applied, as shown in Figure IV-2, the peaks of MEOPC at 24.08 and 23.85 ppm were observed in the ³¹P NMR spectrum, similar to the ³¹P chemical shift values of reported cyclic phosphoramidate structures.^{90, 107} The two distinct resonances were attributed to possible geometric isomers arising from the 2-position ethoxy and 4-position methyl carboxylate groups.

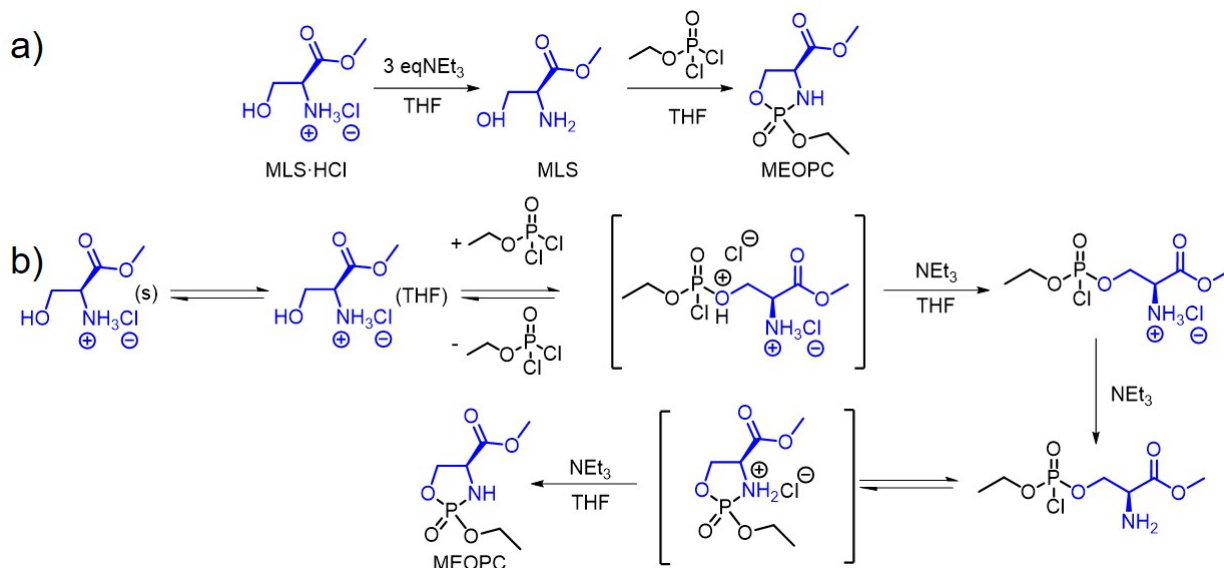


Figure IV-4. a) Two-step trial synthesis of MEOPC from $\text{MLS}\cdot\text{HCl}$ salt. b) One-step synthesis of MEOPC from $\text{MLS}\cdot\text{HCl}$ salt with proposed reaction process and intermediates.

However, there was *ca.* 12% impurity observed at 5.2 to 8.6 ppm, indicating the formation of non-cyclic phosphoramidates. Furthermore, there was another *ca.* 9% impurity observed at -0.9 to -0.2 ppm, suggesting the formation of non-cyclic phosphoesters. Combining these observations, the switch from methyl to methyl carboxylate complicated the ring-closure process and increased intermolecular reactions, likely due to the increased steric hindrance. Multiple purification methods, including column chromatography, recrystallization, precipitation, were applied but failed to sufficiently purify the product due to the hygroscopic and prone to hydrolysis nature of MEOPC.

We perceived that the inhibition of the intermolecular reactions was key to success and finally designed a one-step synthesis method. In this method, $\text{MLS}\cdot\text{HCl}$ was premixed with ethyl dichlorophosphate in THF to form a suspension, followed by the addition of triethylamine in THF at a very slow speed (7.2 mmol/h) at 0 °C. When triethylamine was added to the suspension, it

drove the esterification of MLS·HCl with ethyl dichlorophosphate, neutralization of MLS·HCl, and amidation of MLS with ethyl dichlorophosphate. Due to the pKa difference, with the addition of triethylamine at a slow speed (7.2 mmol/h) at 0 °C, these reactions could be performed stepwise, and this process was proposed in Figure IV-4b. Due to the low solubility of MLS·HCl in THF, during the reaction time, the concentration of MLS·HCl in solution was low, which further inhibited the intermolecular side reactions. Under this condition, the reaction proceeded quantitatively, as evidenced by only the peak of MEOPC at 24.08 and 23.85 ppm being observed in the ^{31}P NMR spectrum (Figure IV-5). Purification was then accomplished simply by filtration through a silica gel plug to remove the slight excess amount of trimethylamine to give pure MEOPC as a highly viscous colorless to pale yellow liquid after concentration. The ^1H NMR and ^{13}C NMR spectra (Figure IV-6b and 7b) of MEOPC also showed two sets of resonances belonging to the two isomers.

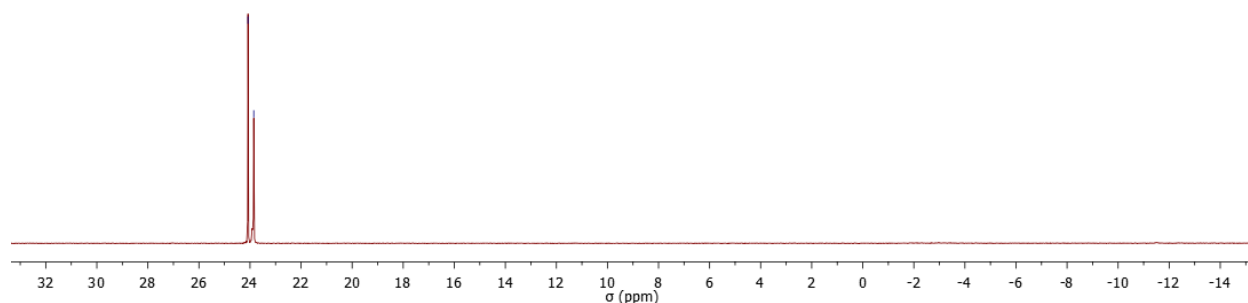


Figure IV-5. ^{31}P NMR (202 MHz, CDCl_3) of the crude products achieved by the one-step synthesis.

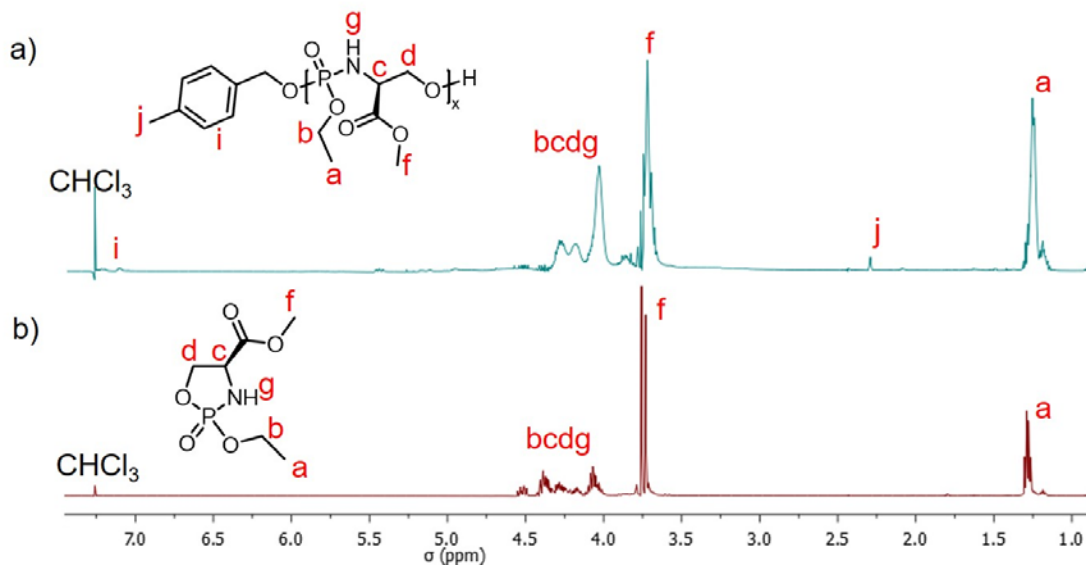


Figure IV-6. a) ^1H NMR (500 MHz, CDCl_3) of PMEOPC. b) ^1H NMR (500 MHz, CDCl_3) of MEOPC.

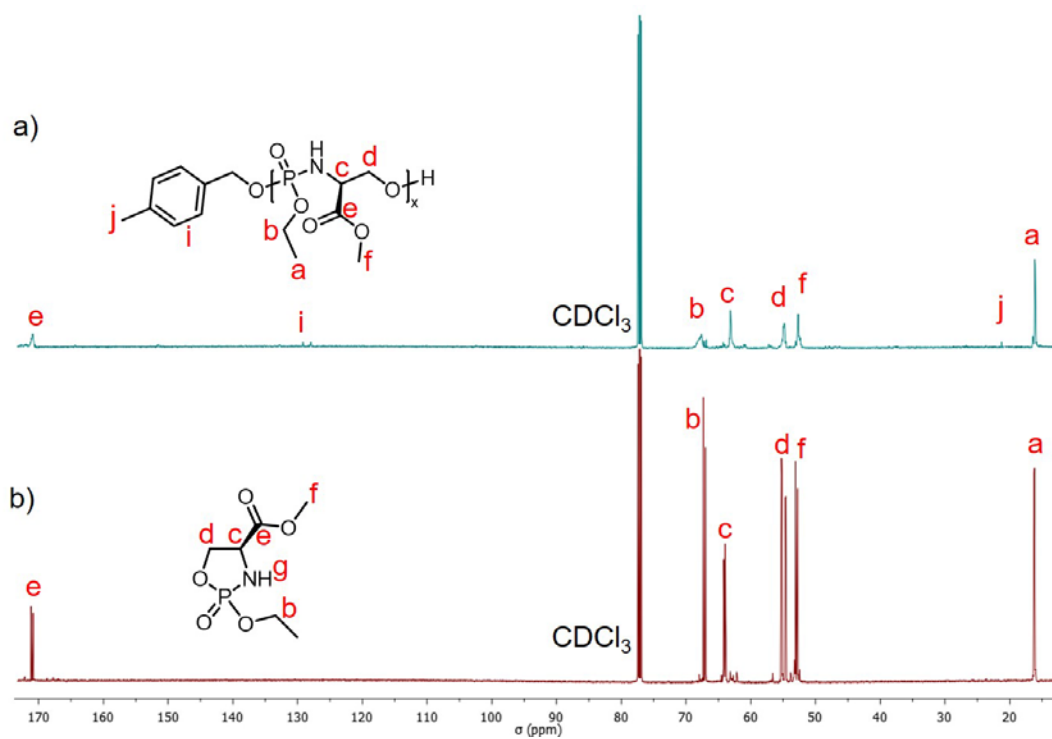


Figure IV-7. a) ^{13}C NMR (126 MHz, CDCl_3) of PMEOPC. b) ^{13}C NMR (126 MHz, CDCl_3) of MEOPC.

Table IV-1. Polymerization of MEOPC catalyzed by TBD under different conditions^a

Entry	T (°C)	[Cat.]/[M]	conv. ^b	M_n NMR (kDa) ^c	\bar{D} ^d	Time (min)
1	0	2%	12%	N. A.	N. A.	30
2	0	2%	14%	N. A.	N. A.	60
3	0	2%	14%	N. A.	N. A.	120
4	0	3%	42%	8.4	1.22	2
5	0	3%	53%	10.5	1.28	3
6	0	3%	68%	13.7	1.39	5
7	-78	3%	65%	13.2	1.24	12
8	-78	3%	74%	14.6	1.31	15
9	-78	3%	91%	18.3	1.35	35

^aPolymerizations were conducted with 4-methylbenzyl alcohol as the initiator and TBD as the catalyst in anhydrous dichloromethane at a monomer concentration of 1.9 M. ^bConversions (conv.) were obtained from ³¹P NMR spectra of aliquots taken from the polymerization mixtures. ^c M_n , NMR was determined by end group analysis by ¹H NMR spectroscopy of the polymer, with a comparison of the intensities of the three 4-methyl protons originating from the initiator on the α -chain end resonating at 2.29 ppm, with the six protons of the two methyl groups on the repeating units resonating at 1.34-1.12 ppm. ^d \bar{D} was measured by DMF SEC calibrated using polystyrene standards.

Two organocatalysts, 1,8-diazabicyclo[5.4.0]undec-7-ene (DBU) and 1,5,7-triazabicyclo[4.4.0]dec-5-ene (TBD), which had previously shown excellent control in the ROP of several cyclic phosphorus-containing monomers,^{9, 24, 55-57} were used to test the ROP of MEOPC (Figure IV-1, Table IV-1). Similar to what we have found for other oxazaphospholidine analogs of MEOPC, DBU was not able to polymerize MEOPC at room temperature even at a relatively high catalyst-to-monomer ratio of 10 mol%. Therefore, the stronger catalyst TBD, which has dual activation effects: simultaneously serving as a hydrogen-bond donor to the monomer *via* the N-H site and also as a hydrogen-bond acceptor to the hydroxyl proton of the propagating alcohol chain end, was applied.^{23, 25, 58} In the presence of TBD, at the previously successful catalyst-to-monomer ratio of 2 mol%, MEOPC polymerization proceeded at 0 °C. However, only relatively low

conversions (<15%) were achieved (entries 1-3, Table IV-1), which might be attributed to two possible reasons: 1) compared to previously reported oxazaphospholidine analogs, the bulkier methyl carboxylate group of MEOPC might lead to weaker binding interactions of TBD with the monomer; 2) The synthetic challenge in the annulation step could lead to more than expected impurities. Thus, the catalyst-to-monomer ratio was increased to 3%, which allow the polymerization to proceed rapidly within 10 min (entries 4-6, Table IV-1). However, for all the polymers achieved, \bar{D} was over 1.2, and broadening of \bar{D} (> 1.3) was observed after the conversion reached greater than *ca.* 50%, indicating the occurrence of adverse backbiting or transesterification reactions. Compared to previously reported analogs, the broader \bar{D} and broadening of \bar{D} at rather an early stage of the polymerization could be attributed to the increased amount of catalyst used, which decreased the control over the ROP. Another possible reason might be the transesterification with the methyl carboxylate group, which required further study to be confirmed. To minimize side relations, the reaction temperature was decreased to -78 °C. At this reduced temperature, the polymerization remained sufficiently fast to reach over 90% conversion within 35 min, and a relatively narrow \bar{D} (<1.3) was achieved under *ca.* 70% conversion, indicating the side reactions were successfully inhibited (entries 7-9, Table IV-1). However, compared to our previously developed PPA systems, ROP of MEOPC was more prone to backbiting or transesterification at higher conversions.

The kinetics of MEOPC ROP were studied using $[M]_0/[I]_0$ of 100 in dichloromethane with 4-methylbenzyl alcohol as the initiator and TBD as the organocatalyst to monitor the monomer conversions and the growth of polymer chains as a function of time. Monomer conversions were obtained from ^{31}P NMR spectra on aliquots taken from the polymerization mixtures. Plots of $\ln([M]_0/[M])$ vs time (Figure IV-8) showed that the polymerization exhibited first-order kinetics,

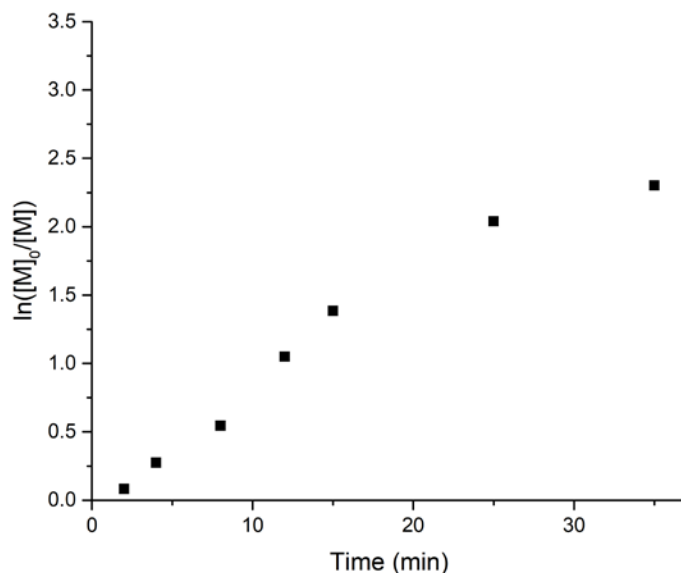


Figure IV-8. Plots of monomer conversion ($\ln([M]_0/[M])$) vs time obtained from ^{31}P NMR spectra.

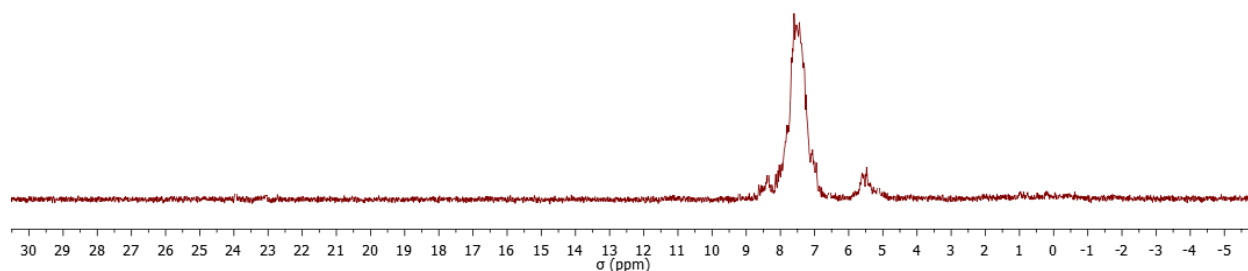


Figure IV-9. ^{31}P NMR (202 MHz, CDCl_3) of the crude products achieved by the one-step synthesis.

especially at <70% conversions, suggesting the characteristics of a controlled polymerization of the MEOPC ROP.

By controlling the initial ratio of monomer to initiator, $[M]_0/[I]_0$, as well as the reaction time, a series of PMEOPCs with different molar mass was synthesized. ^{31}P NMR spectra showed broad peaks with chemical shifts of 8.37, 7.44, 5.59 ppm (Figure IV-9), and ^1H NMR and ^{13}C NMR spectra (Figure IV-6a and 7a) also confirmed the structure of PMEOPC.

PMEOPC appeared as a viscous pale-yellow liquid at room temperature, which was attributed to the glass transition temperature (T_g) of 15 °C ($DP_n = 69$). Compared to the reported PPA analog PEOMP ($T_g = 32-36$ °C, $DP_n = 20-93$),^{90, 107} which shared the same structure with PMEOPC except switching the 4-methyl carboxylate of the MEOPC to a simple methyl, the T_g of PMEOPC was lower. This was likely due to the increased free volume provided by the larger methyl carboxylate chains. Furthermore, the introduction of methyl carboxylate groups endowed PMEOPC with intumescence. As shown in Figure IV-10, during the thermal degradation under argon, PMEOPC swelled into foam-like structures with dramatically increase in volume, which made it a promising material for fire-retardant coatings.

The phosphoramidate linkages along the polymer backbone and short side chains also endowed PMEOPC with acid-lability. The kinetics of the backbone cleavage of PMEOPC ($DP_n = 69$) in aqueous solution was studied in aqueous buffer solutions with different pH values of 3.0



Figure IV-10. A piece of char of PMEOPC after TGA.

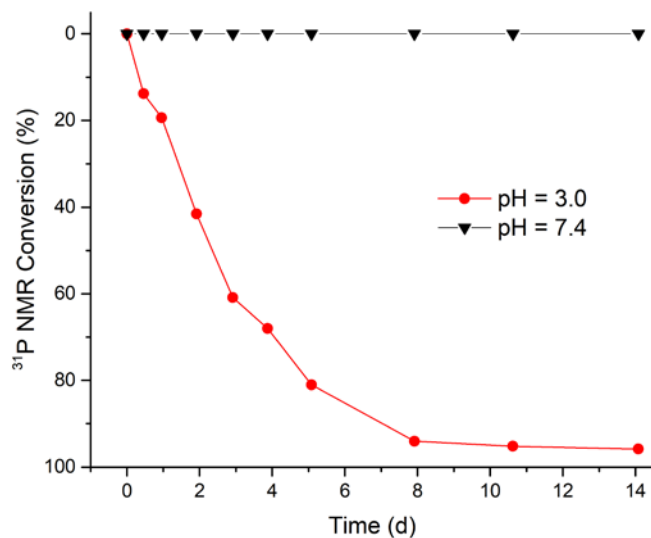


Figure IV-11. Kinetics of PMEOPC degradation at different pH values, as monitored by ^{31}P NMR spectroscopy.

and 7.4. Cleavage of the phosphoramidate linkage, having a ^{31}P resonance at 8.37, 7.44 and 5.59 ppm, would generate phosphates with distinct ^{31}P chemical shifts at *ca.* 0 ppm, allowing for convenient monitoring of the percentage conversion of backbone cleavage by ^{31}P NMR spectroscopy. At pH 7.4 (Figure IV-11), the P MEOPC was found to be stable for 14 d with negligible changes as expected. In the acidic environment, pH 3.0 (Figure IV-11), *ca.* 90% of the phosphoramidate bonds were cleaved within 5 d, reaching a plateau at *ca.* 8 d and *ca.* 96% conversion of phosphoramidate-to-phosphate ^{31}P resonance frequencies over 14 d. Compared to the reported PPA analog PEOMP (8-9 d to achieve 90% conversion at pH 3.0),⁹⁰ the degradation rate of PMEOPC was slightly accelerated. These observations correlated well with previously reported studies on the degradation of phosphoramidate linkages on small molecules, where the neighboring carboxylic acid, methyl carboxylate, and other groups were found to accelerate the cleavage of phosphoramidate linkage.

4.4 Conclusions

Cyclic phosphoramidate monomer MEOPC was achieved *via* a one-step synthesis directly from an α -amino acid derivative (methyl L-serinate hydrochloride), which could be controlled polymerized to afford PPAs with acid-triggered backbone degradation. The hydrolytic degradation of the resulting highly water-soluble polymer PMEOPC was studied, which revealed a faster degradation rate of PMEOPC compared to analogs without methyl carboxylate groups. Furthermore, the introduction of methyl carboxylate groups endowed PMEOPC with intumescence, which made it a potential candidate for advanced coatings. Future studies, including constructing pH-responsive hydrogels based on PMEOPC, are being actively pursued.

CHAPTER V
CONCLUSIONS AND FUTURE WORK

5.1 Conclusions

This dissertation has presented the design, synthesis, and characterization of a range of unique PPAs with acid-triggered backbone degradation and their application as drug carriers to improve the efficacy of an anticancer drug. Polymers with acid-labile linkage along the backbone is of great interest as their ability to rapidly degrade into small molecules under acidic conditions even at the early stage of the degradation. This work has provided a set of synthetic methodologies to achieve cyclic monomers bearing acid-labile phosphoramidate linkages and their corresponding polymers. Polymer properties, including hydrophilicity/hydrophobicity, functionality, degradation rate, were able to be controlled through the manipulation of the monomer structures.

Chapter II focused on the synthesis of a highly water-soluble PPA with a detailed study of its degradation mechanism under aqueous acid conditions. In this chapter, we developed a methodology in which PPAs were prepared readily under basic conditions via ROP, during which P-O bonds were cleaved to afford the polymer. Under acidic conditions, the acid-labile phosphoramidate bonds cleaved much faster than the phosphoester bonds, which enabled the polymer backbone to breakdown rapidly through the cleavage of P-N bonds under acidic conditions. Degradation study in aqueous solution demonstrated PPAs underwent rapid backbone degradation under acidic conditions, yielding oligomers within days compared to months required for polyphosphoester analogs.

In Chapter III, the synthetic methodology developed in Chapter II was advanced to afford well-defined amphiphilic diblock copolymer. PPA nanoparticles were prepared through the self-assembly of amphiphilic diblock PPA, which had large hydrophobic cores for drug loading and pendant alkyne groups for future modification. To further demonstrate the applicability of this system, an anticancer drug CPT was selected as a model drug. CPT is a promising anticancer drug, yet its therapeutic potential has been limited by poor water solubility and facile hydrolysis of the active lactone form into an inactive carboxylate form at neutral pH. Encapsulation of CPT into PPA nanoparticles achieved CPT-loaded nanotherapeutics, which inhibited the premature hydrolysis of CPT under neutral pH and enabled accelerated CPT release when lower pH of the cancer microenvironment was encountered. The encapsulation also achieved the aqueous suspension of CPT at concentrations up to 3.2 mg/mL, which was more than 1600× higher than the aqueous solubility of free CPT. The performance of CPT-loaded nanotherapeutics was evaluated *in vivo* and revealed enhanced efficacy relative to free CPT in cancer cells and similar toxicity in normal cells. This system is versatile for adoption to other drugs, and the presence of pendant reactive functionality provides a powerful platform for future manipulations, such as conjugation of drugs or imaging agents.

Chapter IV explored the development of α -amino acid-based PPAs with acid-triggered backbone degradation. However, compared to the β -amino alcohol used in Chapter II and III, the carboxylate group of α -amino acid, particularly methyl carboxylate of MLS, complicated the annulation to achieve cyclic monomers. A state-of-the-art experimental design successfully afforded cyclic phosphoramidate monomer MEOPC *via* a one-step synthesis directly from MLS·HCl, which could be controlled polymerized to afford well-defined PPAs based on α -amino acids. The hydrolytic degradation of the resulted highly water-soluble polymer PMEOPC was

studied, which revealed a faster degradation rate of PMEOPC compared to analogs without methyl carboxylate groups. Furthermore, the introduction of methyl carboxylate groups endowed PMEOPC with intumescence, which made it a potential candidate for advanced coatings.

5.2 Future Work

There is significant potential for developing novel monomers and polymers based on the synthetic methodologies developed in this dissertation. For example, by switching the starting material from dichlorophosphate to phosphonic dichloride, phosphoramidate linkage will be generated instead of phosphoramidate (Figure V-1a). The switch of the substitution group on the phosphorous has huge impact on the hydrolysis rate of the P-N bond, giving that a factor of 10^3 rate enhancement has been reported by Haake *et al.*¹⁰⁸ The resulted cyclic monomer may be polymerized to afford polyphosphoramidates, which are expected to be much more acid-sensitive. Similarly, by switching the starting material from dichlorophosphate to phosphoramidic dichloride, two phosphoramidate linkages will be generated upon annulation (Figure V-1b). The

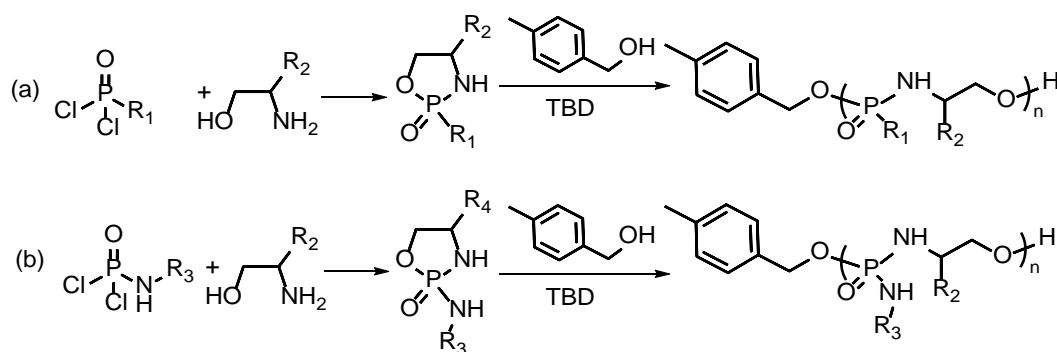


Figure V-1. a) Proposed route to achieve polyphosphoramidates. b) Proposed route to achieve polyphosphordiamidates.

resulted cyclic monomer may be polymerized to afford polyphosphordiamidates, which have the ability to cleave both the backbone and side chains under acidic conditions.

Meanwhile, there is huge potential to be exploited from the developed PPA systems. In Chapter III, different hydrophilic to hydrophobic ratio, side-chains of the polymers could be tuned to study the self-assembly behavior of PPAs. The pendant alkyne side-chain groups could also be used to crosslink the core of the nanoparticle, which is expected to further distinguish the release behavior of PPA-based nanotherapeutics under neutral and acidic conditions. In addition, the alkyne groups could be used to conjugate drugs or imaging agents (Figure V-2).

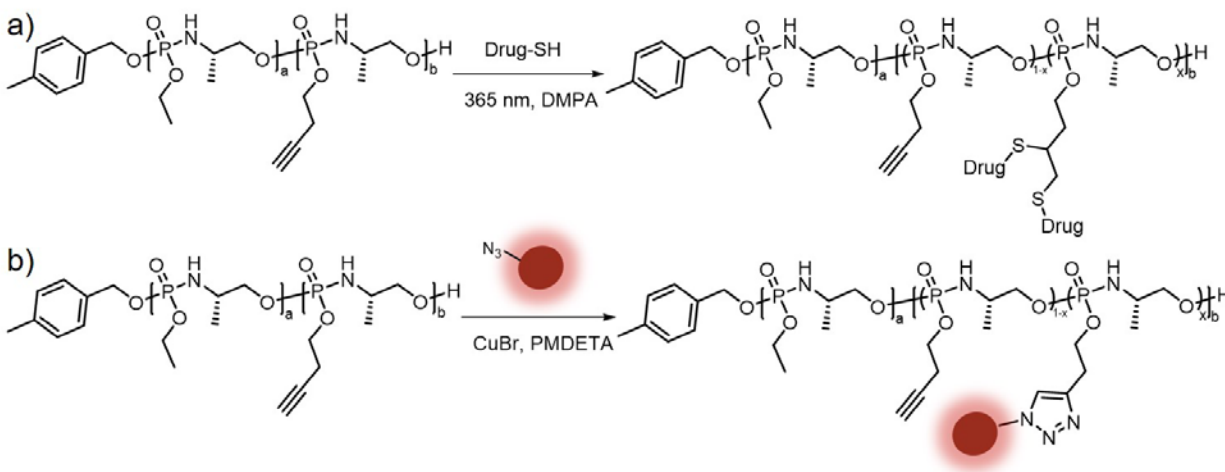


Figure V-2. a) Drug conjugation for PPAs *via* thiol-ene reaction. b) Dye conjugation for PPAs *via* CuAAC.

The α -amino acid-based PPAs of Chapter IV are currently the least explored from this dissertation. Further studies including conducting kinetics of the polymerizations and the degradation in triplicate are necessary. The achieved PMEOPC is water soluble, upon switching the initiator to 1,3-propanediol. PMEOPC diols are expected to be achieved, which could be further modified and crosslinked by a photo-initiator to form pH-responsive hydrogels (Figure

V-3). Drugs, for example, an anti-cancer drug doxorubicin could be further loaded into the PPA hydrogels. The drug-loaded PPA hydrogels are expected to be degraded rapidly under acidic conditions.

Besides, there are also other polymerization methods that is compatible with the developed PPA system and could be utilized to construct complex polymer structures. For example, ring-opening metathesis polymerization (ROMP), could be adapted to afford PPA-based brush copolymers.

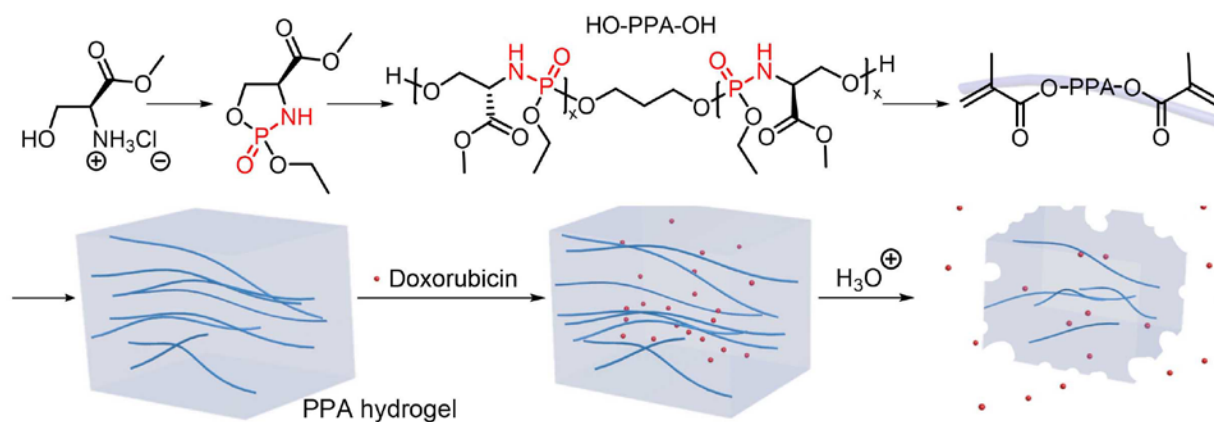


Figure V-3. Schematic synthesis and degradation of PPA hydrogels based on an α -amino acid.

REFERENCES

- (1) Gross, R. A.; Kalra, B., Biodegradable Polymers for the Environment. *Science* **2002**, 297 (5582), 803-807.
- (2) Nair, L. S.; Laurencin, C. T., Biodegradable polymers as biomaterials. *Prog. Polym. Sci.* **2007**, 32 (8), 762-798.
- (3) Laycock, B.; Nikolić, M.; Colwell, J. M.; Gauthier, E.; Halley, P.; Bottle, S.; George, G., Lifetime prediction of biodegradable polymers. *Prog. Polym. Sci.* **2017**, 71, 144-189.
- (4) Asghari, F.; Samiei, M.; Adibkia, K.; Akbarzadeh, A.; Davaran, S., Biodegradable and biocompatible polymers for tissue engineering application: a review. *Artificial Cells, Nanomedicine, and Biotechnology* **2017**, 45 (2), 185-192.
- (5) Pina, S.; Oliveira, J. M.; Reis, R. L., Natural-Based Nanocomposites for Bone Tissue Engineering and Regenerative Medicine: A Review. *Adv. Mater.* **2015**, 27 (7), 1143-1169.
- (6) Pack, D. W.; Hoffman, A. S.; Pun, S.; Stayton, P. S., Design and development of polymers for gene delivery. *Nature Reviews Drug Discovery* **2005**, 4, 581.
- (7) Soppimath, K. S.; Aminabhavi, T. M.; Kulkarni, A. R.; Rudzinski, W. E., Biodegradable polymeric nanoparticles as drug delivery devices. *J. Control. Release* **2001**, 70 (1), 1-20.
- (8) Steinbach, T.; Wurm, F. R., Poly(phosphoester)s: A New Platform for Degradable Polymers. *Angew. Chem. Int. Ed.* **2015**, 54 (21), 6098-6108.
- (9) Zhang, S.; Wang, H.; Shen, Y.; Zhang, F.; Seetho, K.; Zou, J.; Taylor, J.-S. A.; Dove, A. P.; Wooley, K. L., A Simple and Efficient Synthesis of an Acid-Labile Polyphosphoramidate by Organobase-Catalyzed Ring-Opening Polymerization and Transformation to Polyphosphoester Ionomers by Acid Treatment. *Macromolecules* **2013**, 46 (13), 5141-5149.
- (10) Becker, G.; Wurm, F. R., Functional biodegradable polymers via ring-opening polymerization of monomers without protective groups. *Chem. Soc. Rev.* **2018**.
- (11) Kishore, K.; Kannan, P.; Iyanar, K., Synthesis, characterization, and fire retardancy of ferrocene containing polyphosphate esters. *J. Polym. Sci., Part A: Polym. Chem.* **1991**, 29 (7), 1039-1044.
- (12) Kishore, K.; Kannan, P., Synthesis, spectral, thermal, and flammability studies of phenolphthalein polyphosphate esters. *J. Polym. Sci., Part A: Polym. Chem.* **1990**, 28 (12), 3481-3486.

- (13) Richards, M.; Dahiyat, B. I.; Arm, D. M.; Lin, S.; Leong, K. W., Interfacial polycondensation and characterization of polyphosphates and polyphosphonates. *J. Polym. Sci., Part A: Polym. Chem.* **1991**, *29* (8), 1157-1165.
- (14) Nuyken, O.; Pask, S., Ring-Opening Polymerization—An Introductory Review. *Polymers* **2013**, *5* (2), 361-403.
- (15) Xiao, C.-S.; Wang, Y.-C.; Du, J.-Z.; Chen, X.-S.; Wang, J., Kinetics and Mechanism of 2-Ethoxy-2-oxo-1,3,2-dioxaphospholane Polymerization Initiated by Stannous Octoate. *Macromolecules* **2006**, *39* (20), 6825-6831.
- (16) Mespouille, L.; Coulembier, O.; Kawalec, M.; Dove, A. P.; Dubois, P., Implementation of metal-free ring-opening polymerization in the preparation of aliphatic polycarbonate materials. *Prog. Polym. Sci.* **2014**, *39* (6), 1144-1164.
- (17) Nederberg, F.; Lohmeijer, B. G. G.; Leibfarth, F.; Pratt, R. C.; Choi, J.; Dove, A. P.; Waymouth, R. M.; Hedrick, J. L., Organocatalytic Ring Opening Polymerization of Trimethylene Carbonate. *Biomacromolecules* **2007**, *8* (1), 153-160.
- (18) Kamber, N. E.; Jeong, W.; Waymouth, R. M.; Pratt, R. C.; Lohmeijer, B. G. G.; Hedrick, J. L., Organocatalytic Ring-Opening Polymerization. *Chem. Rev.* **2007**, *107* (12), 5813-5840.
- (19) Dove, A. P., Metal-Free Catalysis in Ring-Opening Polymerization. In *Handbook of Ring-Opening Polymerization*, Wiley-VCH Verlag GmbH & Co. KGaA: 2009; pp 357-378.
- (20) Lin, B.; Waymouth, R. M., Organic Ring-Opening Polymerization Catalysts: Reactivity Control by Balancing Acidity. *Macromolecules* **2018**, *51* (8), 2932-2938.
- (21) Dove, A. P., Organic Catalysis for Ring-Opening Polymerization. *ACS Macro Lett.* **2012**, *1* (12), 1409-1412.
- (22) Pratt, R. C.; Lohmeijer, B. G.; Long, D. A.; Waymouth, R. M.; Hedrick, J. L., Triazabicyclodecene: a simple bifunctional organocatalyst for acyl transfer and ring-opening polymerization of cyclic esters. *Journal of the American Chemical Society* **2006**, *128* (14), 4556-7.
- (23) Iwasaki, Y.; Yamaguchi, E., Synthesis of Well-Defined Thermoresponsive Polyphosphoester Macroinitiators Using Organocatalysts. *Macromolecules* **2010**, *43* (6), 2664-2666.
- (24) Zhang, S.; Zou, J.; Zhang, F.; Elsabahy, M.; Felder, S. E.; Zhu, J.; Pochan, D. J.; Wooley, K. L., Rapid and Versatile Construction of Diverse and Functional Nanostructures Derived from a Polyphosphoester-Based Biomimetic Block Copolymer System. *J. Am. Chem. Soc.* **2012**, *134* (44), 18467-18474.

- (25) Clément, B.; Grignard, B.; Koole, L.; Jérôme, C.; Lecomte, P., Metal-Free Strategies for the Synthesis of Functional and Well-Defined Polyphosphoesters. *Macromolecules* **2012**, *45* (11), 4476-4486.
- (26) Bauer, K. N.; Liu, L.; Wagner, M.; Andrienko, D.; Wurm, F. R., Mechanistic study on the hydrolytic degradation of polyphosphates. *Eur. Polym. J.* **2018**, *108*, 286-294.
- (27) Baran, J.; Penczek, S., Hydrolysis of Polyesters of Phosphoric Acid. 1. Kinetics and the pH Profile. *Macromolecules* **1995**, *28* (15), 5167-5176.
- (28) Cankaya, A.; Steinmann, M.; Bülbül, Y.; Lieberwirth, I.; Wurm, F. R., Side-chain poly(phosphoramidate)s via acyclic diene metathesis polycondensation. *Polym. Chem.* **2016**, *7* (31), 5004-5010.
- (29) Wang, J.; Zhang, P.-C.; Lu, H.-F.; Ma, N.; Wang, S.; Mao, H.-Q.; Leong, K. W., New polyphosphoramidate with a spermidine side chain as a gene carrier. *J. Control. Release* **2002**, *83* (1), 157-168.
- (30) Zhang, X.-Q.; Wang, X.-L.; Zhang, P.-C.; Liu, Z.-L.; Zhuo, R.-X.; Mao, H.-Q.; Leong, K. W., Galactosylated ternary DNA/polyphosphoramidate nanoparticles mediate high gene transfection efficiency in hepatocytes. *J. Control. Release* **2005**, *102* (3), 749-763.
- (31) Wang, J.; Gao, S. J.; Zhang, P. C.; Wang, S.; Mao, H. Q.; Leong, K. W., Polyphosphoramidate gene carriers: effect of charge group on gene transfer efficiency. *Gene Therapy* **2004**, *11*, 1001.
- (32) Zhang, X.-Q.; Wang, X.-L.; Huang, S.-W.; Zhuo, R.-X.; Liu, Z.-L.; Mao, H.-Q.; Leong, K. W., In Vitro Gene Delivery Using Polyamidoamine Dendrimers with a Trimesyl Core. *Biomacromolecules* **2005**, *6* (1), 341-350.
- (33) Ren, Y.; Jiang, X.; Pan, D.; Mao, H.-Q., Charge Density and Molecular Weight of Polyphosphoramidate Gene Carrier Are Key Parameters Influencing Its DNA Compaction Ability and Transfection Efficiency. *Biomacromolecules* **2010**, *11* (12), 3432-3439.
- (34) Zhang, P.-C.; Wang, J.; Leong, K. W.; Mao, H.-Q., Ternary Complexes Comprising Polyphosphoramidate Gene Carriers with Different Types of Charge Groups Improve Transfection Efficiency. *Biomacromolecules* **2005**, *6* (1), 54-60.
- (35) Aoshima, S.; Oda, Y.; Matsumoto, S.; Shinke, Y.; Kanazawa, A.; Kanaoka, S., Efficient Design for Stimuli-Responsive Polymers with Quantitative Acid-Degradability: Specifically Designed Alternating Controlled Cationic Copolymerization and Facile Complete Degradation. *ACS Macro Lett.* **2014**, *3* (1), 80-85.
- (36) Binauld, S.; Stenzel, M. H., Acid-degradable polymers for drug delivery: a decade of innovation. *Chem. Commun.* **2013**, *49* (21), 2082-2102.

- (37) Meng, F.; Zhong, Y.; Cheng, R.; Deng, C.; Zhong, Z., pH-sensitive polymeric nanoparticles for tumor-targeting doxorubicin delivery: concept and recent advances. *Nanomedicine* **2014**, *9* (3), 487-499.
- (38) Pang, X.; Jiang, Y.; Xiao, Q.; Leung, A. W.; Hua, H.; Xu, C., pH-responsive polymer–drug conjugates: Design and progress. *J. Control. Release* **2016**, *222*, 116-129.
- (39) Tang, R.; Ji, W.; Panus, D.; Palumbo, R. N.; Wang, C., Block copolymer micelles with acid-labile ortho ester side-chains: Synthesis, characterization, and enhanced drug delivery to human glioma cells. *J. Control. Release* **2011**, *151* (1), 18-27.
- (40) Zhang, Q.; Hou, Z.; Louage, B.; Zhou, D.; Vanparijs, N.; De Geest, B. G.; Hoogenboom, R., Acid-Labile Thermoresponsive Copolymers That Combine Fast pH-Triggered Hydrolysis and High Stability under Neutral Conditions. *Angew. Chem. Int. Ed.* **2015**, *54* (37), 10879-10883.
- (41) Cui, J.; Yan, Y.; Wang, Y.; Caruso, F., Templated Assembly of pH-Labile Polymer-Drug Particles for Intracellular Drug Delivery. *Adv. Funct. Mater.* **2012**, *22* (22), 4718-4723.
- (42) Zhang, L.; Jeong, Y.-I.; Zheng, S.; Jang, S. I.; Suh, H.; Kang, D. H.; Kim, I., Biocompatible and pH-sensitive PEG hydrogels with degradable phosphoester and phosphoamide linkers end-capped with amine for controlled drug delivery. *Polym. Chem.* **2013**, *4* (4), 1084-1094.
- (43) Li, L.; Xu, Y.; Milligan, I.; Fu, L.; Franckowiak, E. A.; Du, W., Synthesis of Highly pH-Responsive Glucose Poly(orthoester). *Angew. Chem. Int. Ed.* **2013**, *52* (51), 13699-13702.
- (44) Jain, R.; Standley, S. M.; Fréchet, J. M. J., Synthesis and Degradation of pH-Sensitive Linear Poly(amidoamine)s. *Macromolecules* **2007**, *40* (3), 452-457.
- (45) Liu, N.; Vignolle, J.; Vincent, J.-M.; Robert, F.; Landais, Y.; Cramail, H.; Taton, D., One-Pot Synthesis and PEGylation of Hyperbranched Polyacetals with a Degree of Branching of 100%. *Macromolecules* **2014**, *47* (5), 1532-1542.
- (46) Paramonov, S. E.; Bachelder, E. M.; Beaudette, T. T.; Standley, S. M.; Lee, C. C.; Dashe, J.; Fréchet, J. M. J., Fully Acid-Degradable Biocompatible Polyacetal Microparticles for Drug Delivery. *Bioconjug. Chem.* **2008**, *19* (4), 911-919.
- (47) Wang, C.; Ge, Q.; Ting, D.; Nguyen, D.; Shen, H.-R.; Chen, J.; Eisen, H. N.; Heller, J.; Langer, R.; Putnam, D., Molecularly engineered poly(ortho ester) microspheres for enhanced delivery of DNA vaccines. *Nat Mater* **2004**, *3* (3), 190-196.
- (48) Schacht, E.; Toncheva, V.; Vandertaelen, K.; Heller, J., Polyacetal and poly(ortho ester)–poly(ethylene glycol) graft copolymer thermogels: Preparation, hydrolysis and FITC-BSA release studies. *J. Control. Release* **2006**, *116* (2), 219-225.

- (49) Jeong, M. J.; Kim, B. J.; Chang, J. Y., Synthesis and characterization of soluble main-chain hydrazone polymers. *J. Polym. Sci., Part A: Polym. Chem.* **2002**, *40* (24), 4493-4497.
- (50) Zhou, L.; Yu, L.; Ding, M.; Li, J.; Tan, H.; Wang, Z.; Fu, Q., Synthesis and Characterization of pH-Sensitive Biodegradable Polyurethane for Potential Drug Delivery Applications. *Macromolecules* **2011**, *44* (4), 857-864.
- (51) Pemba, A. G.; Flores, J. A.; Miller, S. A., Acetal metathesis polymerization (AMP): A method for synthesizing biorenewable polyacetals. *Green Chemistry* **2013**, *15* (2), 325-329.
- (52) Whiting, B. T.; Coates, G. W., Synthesis and Polymerization of Bicyclic Ketals: A Practical Route to High-Molecular Weight Polyketals. *J. Am. Chem. Soc.* **2013**, *135* (30), 10974-10977.
- (53) Khaja, S. D.; Lee, S.; Murthy, N., Acid-Degradable Protein Delivery Vehicles Based on Metathesis Chemistry. *Biomacromolecules* **2007**, *8* (5), 1391-1395.
- (54) Neitzel, A. E.; Petersen, M. A.; Kokkoli, E.; Hillmyer, M. A., Divergent Mechanistic Avenues to an Aliphatic Polyesteracetal or Polyester from a Single Cyclic Esteracetal. *ACS Macro Lett.* **2014**, *3* (11), 1156-1160.
- (55) Steinbach, T.; Schroder, R.; Ritz, S.; Wurm, F. R., Microstructure analysis of biocompatible phosphoester copolymers. *Polym. Chem.* **2013**, *4* (16), 4469-4479.
- (56) Zhang, S.; Li, A.; Zou, J.; Lin, L. Y.; Wooley, K. L., Facile Synthesis of Clickable, Water-Soluble, and Degradable Polyphosphoesters. *ACS Macro Lett.* **2012**, *1* (2), 328-333.
- (57) Steinbach, T.; Ritz, S.; Wurm, F. R., Water-Soluble Poly(phosphonate)s via Living Ring-Opening Polymerization. *ACS Macro Lett.* **2014**, *3* (3), 244-248.
- (58) Dove, A. P., Organic Catalysis for Ring-Opening Polymerization. *ACS Macro Lett.* **2012**, *1* (12), 1409-1412.
- (59) Kocak, G.; Tuncer, C.; Butun, V., pH-Responsive polymers. *Polym. Chem.* **2017**, *8* (1), 144-176.
- (60) Zhang, S.; Bellinger, A. M.; Gletting, D. L.; Barman, R.; Lee, Y.-A. L.; Zhu, J.; Cleveland, C.; Montgomery, V. A.; Gu, L.; Nash, L. D.; Maitland, D. J.; Langer, R.; Traverso, G., A pH-responsive supramolecular polymer gel as an enteric elastomer for use in gastric devices. *Nat. Mater.* **2015**, *14*, 1065.
- (61) Jochum, F. D.; Theato, P., Temperature- and light-responsive smart polymer materials. *Chem. Soc. Rev.* **2013**, *42* (17), 7468-7483.

- (62) Becker, G.; Marquetant, T. A.; Wagner, M.; Wurm, F. R., Multifunctional Poly(phosphoester)s for Reversible Diels–Alder Postmodification To Tune the LCST in Water. *Macromolecules* **2017**, *50* (20), 7852-7862.
- (63) Wolf, T.; Hunold, J.; Simon, J.; Rosenauer, C.; Hinderberger, D.; Wurm, F. R., Temperature responsive poly(phosphonate) copolymers: from single chains to macroscopic coacervates. *Polym. Chem.* **2018**, *9* (4), 490-498.
- (64) Keith, H.; A., W. M.; D., N. L.; L., L. T.; Christine, L.; T., L. A.; C., G. M.; Sarah, U.; O., C. K.; S., W. T.; L., W. K.; J., M. D., A Processable Shape Memory Polymer System for Biomedical Applications. *Adv. Healthc. Mater.* **2015**, *4* (9), 1386-1398.
- (65) Zhang, X.; Han, L.; Liu, M.; Wang, K.; Tao, L.; Wan, Q.; Wei, Y., Recent progress and advances in redox-responsive polymers as controlled delivery nanoplateforms. *Mater. Chem. Front.* **2017**, *1* (5), 807-822.
- (66) Ge, J.; Neofytou, E.; Cahill, T. J.; Beygui, R. E.; Zare, R. N., Drug Release from Electric-Field-Responsive Nanoparticles. *ACS Nano* **2012**, *6* (1), 227-233.
- (67) Mura, S.; Nicolas, J.; Couvreur, P., Stimuli-responsive nanocarriers for drug delivery. *Nat. Mater.* **2013**, *12*, 991.
- (68) Su, L.; Li, R.; Khan, S.; Clanton, R.; Zhang, F.; Lin, Y.-N.; Song, Y.; Wang, H.; Fan, J.; Hernandez, S.; Butters, A. S.; Akabani, G.; MacLoughlin, R.; Smolen, J.; Wooley, K. L., Chemical Design of Both a Glutathione-Sensitive Dimeric Drug Guest and a Glucose-Derived Nanocarrier Host to Achieve Enhanced Osteosarcoma Lung Metastatic Anticancer Selectivity. *J. Am. Chem. Soc.* **2018**, *140* (4), 1438-1446.
- (69) Zhang, F.; Gong, S.; Wu, J.; Li, H.; Oupicky, D.; Sun, M., CXCR4-Targeted and Redox Responsive Dextrin Nanogel for Metastatic Breast Cancer Therapy. *Biomacromolecules* **2017**, *18* (6), 1793-1802.
- (70) Zhong, P.; Meng, H.; Qiu, J.; Zhang, J.; Sun, H.; Cheng, R.; Zhong, Z., $\alpha\beta3$ Integrin-targeted reduction-sensitive micellar mertansine prodrug: Superb drug loading, enhanced stability, and effective inhibition of melanoma growth in vivo. *J. Control. Release* **2017**, *259*, 176-186.
- (71) Zhu, A.; Miao, K.; Deng, Y.; Ke, H.; He, H.; Yang, T.; Guo, M.; Li, Y.; Guo, Z.; Wang, Y.; Yang, X.; Zhao, Y.; Chen, H., Dually pH/Reduction-Responsive Vesicles for Ultrahigh-Contrast Fluorescence Imaging and Thermo-Chemotherapy-Synergized Tumor Ablation. *ACS Nano* **2015**, *9* (8), 7874-7885.
- (72) Li, H.-J.; Du, J.-Z.; Du, X.-J.; Xu, C.-F.; Sun, C.-Y.; Wang, H.-X.; Cao, Z.-T.; Yang, X.-Z.; Zhu, Y.-H.; Nie, S.; Wang, J., Stimuli-responsive clustered nanoparticles for improved tumor penetration and therapeutic efficacy. *Proc. Natl. Acad. Sci.* **2016**, *113* (15), 4164-4169.

- (73) Jiang, X.; Zheng, Y.; Chen, H. H.; Leong, K. W.; Wang, T. H.; Mao, H. Q., Dual - Sensitive Micellar Nanoparticles Regulate DNA Unpacking and Enhance Gene - Delivery Efficiency. *Adv. Mater.* **2010**, *22* (23), 2556-2560.
- (74) Li, H.-J.; Du, J.-Z.; Liu, J.; Du, X.-J.; Shen, S.; Zhu, Y.-H.; Wang, X.; Ye, X.; Nie, S.; Wang, J., Smart Superstructures with Ultrahigh pH-Sensitivity for Targeting Acidic Tumor Microenvironment: Instantaneous Size Switching and Improved Tumor Penetration. *ACS Nano* **2016**, *10* (7), 6753-6761.
- (75) Xiaoding, X.; Jun, W.; Yanlan, L.; Mikyung, Y.; Lili, Z.; Xi, Z.; Sushant, B.; Qing, L.; Emily, H.; Jinjun, S.; C., F. O., Ultra - pH - Responsive and Tumor - Penetrating Nanoplatform for Targeted siRNA Delivery with Robust Anti - Cancer Efficacy. *Angew. Chem. Int. Ed.* **2016**, *55* (25), 7091-7094.
- (76) Yang, G.; Xu, L.; Xu, J.; Zhang, R.; Song, G.; Chao, Y.; Feng, L.; Han, F.; Dong, Z.; Li, B.; Liu, Z., Smart Nanoreactors for pH-Responsive Tumor Homing, Mitochondria-Targeting, and Enhanced Photodynamic-Immunotherapy of Cancer. *Nano Lett.* **2018**, *18* (4), 2475-2484.
- (77) Haijun, Y.; Zhirui, C.; Pengcheng, Y.; Chengyue, G.; Bing, F.; Tongying, J.; Siling, W.; Qi, Y.; Dafang, Z.; Xiangliang, Y.; Zhiwen, Z.; Yaping, L., pH - and NIR Light - Responsive Micelles with Hyperthermia - Triggered Tumor Penetration and Cytoplasm Drug Release to Reverse Doxorubicin Resistance in Breast Cancer. *Adv. Funct. Mater.* **2015**, *25* (17), 2489-2500.
- (78) Li, J.; Li, Y.; Wang, Y.; Ke, W.; Chen, W.; Wang, W.; Ge, Z., Polymer Prodrug-Based Nanoreactors Activated by Tumor Acidity for Orchestrated Oxidation/Chemotherapy. *Nano Lett.* **2017**, *17* (11), 6983-6990.
- (79) Selvi, B.; Patel, S.; Savva, M., Physicochemical Characterization and Membrane Binding Properties of Camptothecin. *J. Pharm. Sci.* **2008**, *97* (10), 4379-4390.
- (80) Pommier, Y., Topoisomerase I inhibitors: camptothecins and beyond. *Nat. Rev. Cancer* **2006**, *6*, 789.
- (81) Cai, K.; He, X.; Song, Z.; Yin, Q.; Zhang, Y.; Uckun, F. M.; Jiang, C.; Cheng, J., Dimeric Drug Polymeric Nanoparticles with Exceptionally High Drug Loading and Quantitative Loading Efficiency. *J. Am. Chem. Soc.* **2015**, *137* (10), 3458-3461.
- (82) Jin, H.; Sun, M.; Shi, L.; Zhu, X.; Huang, W.; Yan, D., Reduction-responsive amphiphilic polymeric prodrugs of camptothecin-polyphosphoester for cancer chemotherapy. *Biomater. Sci.* **2018**.

- (83) Hu, M.; Huang, P.; Wang, Y.; Su, Y.; Zhou, L.; Zhu, X.; Yan, D., Synergistic Combination Chemotherapy of Camptothecin and Floxuridine through Self-Assembly of Amphiphilic Drug–Drug Conjugate. *Bioconjug. Chem.* **2015**, *26* (12), 2497-2506.
- (84) Zhigang, X.; Dongdong, W.; Shuang, X.; Xiaoyan, L.; Xiaoyu, Z.; Haixia, Z., Preparation of a Camptothecin Prodrug with Glutathione - Responsive Disulfide Linker for Anticancer Drug Delivery. *Chem. Asian J.* **2014**, *9* (1), 199-205.
- (85) Zhang, Q.; He, J.; Zhang, M.; Ni, P., A polyphosphoester-conjugated camptothecin prodrug with disulfide linkage for potent reduction-triggered drug delivery. *J. Mater. Chem. B* **2015**, *3* (24), 4922-4932.
- (86) McRae Page, S.; Martorella, M.; Parekar, S.; Kosif, I.; Emrick, T., Disulfide Cross-Linked Phosphorylcholine Micelles for Triggered Release of Camptothecin. *Molecular Pharmaceutics* **2013**, *10* (7), 2684-2692.
- (87) Hu, X.; Hu, J.; Tian, J.; Ge, Z.; Zhang, G.; Luo, K.; Liu, S., Polyprodrug Amphiphiles: Hierarchical Assemblies for Shape-Regulated Cellular Internalization, Trafficking, and Drug Delivery. *J. Am. Chem. Soc.* **2013**, *135* (46), 17617-17629.
- (88) Min, K. H.; Kim, J.-H.; Bae, S. M.; Shin, H.; Kim, M. S.; Park, S.; Lee, H.; Park, R.-W.; Kim, I.-S.; Kim, K.; Kwon, I. C.; Jeong, S. Y.; Lee, D. S., Tumoral acidic pH-responsive MPEG-poly(β -amino ester) polymeric micelles for cancer targeting therapy. *J. Control. Release* **2010**, *144* (2), 259-266.
- (89) Hu, X.; Li, H.; Luo, S.; Liu, T.; Jiang, Y.; Liu, S., Thiol and pH dual-responsive dynamic covalent shell cross-linked micelles for triggered release of chemotherapeutic drugs. *Polym. Chem.* **2013**, *4* (3), 695-706.
- (90) Wang, H.; Su, L.; Li, R.; Zhang, S.; Fan, J.; Zhang, F.; Nguyen, T. P.; Wooley, K. L., Polyphosphoramidates That Undergo Acid-Triggered Backbone Degradation. *ACS Macro Lett.* **2017**, *6* (3), 219-223.
- (91) Nifant'ev, I. E.; Shlyakhtin, A. V.; Bagrov, V. V.; Komarov, P. D.; Kosarev, M. A.; Tavtorkin, A. N.; Minyaev, M. E.; Roznyatovsky, V. A.; Ivchenko, P. V., Controlled ring-opening polymerisation of cyclic phosphates, phosphonates and phosphoramidates catalysed by heteroleptic BHT-alkoxy magnesium complexes. *Polym. Chem.* **2017**, *8* (44), 6806-6816.
- (92) Su, L.; Khan, S.; Fan, J.; Lin, Y.-N.; Wang, H.; Gustafson, T. P.; Zhang, F.; Wooley, K. L., Functional sugar-based polymers and nanostructures comprised of degradable poly(d-glucose carbonate)s. *Polym. Chem.* **2017**.
- (93) Iwasaki, Y.; Yokota, A.; Otaka, A.; Inoue, N.; Yamaguchi, A.; Yoshitomi, T.; Yoshimoto, K.; Neo, M., Bone-targeting poly(ethylene sodium phosphate). *Biomater. Sci.* **2018**, *6* (1), 91-95.

- (94) Bauer, K. N.; Liu, L.; Andrienko, D.; Wagner, M.; Macdonald, E. K.; Shaver, M. P.; Wurm, F. R., Polymerizing Phostones: A Fast Way to In-Chain Poly(phosphonate)s with Adjustable Hydrophilicity. *Macromolecules* **2018**, *51* (4), 1272-1279.
- (95) Zhang, F.; Smolen, J. A.; Zhang, S.; Li, R.; Shah, P. N.; Cho, S.; Wang, H.; Raymond, J. E.; Cannon, C. L.; Wooley, K. L., Degradable polyphosphoester-based silver-loaded nanoparticles as therapeutics for bacterial lung infections. *Nanoscale* **2015**, *7* (6), 2265-2270.
- (96) Xu, H.; Yao, Q.; Cai, C.; Gou, J.; Zhang, Y.; Zhong, H.; Tang, X., Amphiphilic poly(amino acid) based micelles applied to drug delivery: The in vitro and in vivo challenges and the corresponding potential strategies. *J. Control. Release* **2015**, *199*, 84-97.
- (97) Sun, H.; Meng, F.; Dias, A. A.; Hendriks, M.; Feijen, J.; Zhong, Z., α -Amino Acid Containing Degradable Polymers as Functional Biomaterials: Rational Design, Synthetic Pathway, and Biomedical Applications. *Biomacromolecules* **2011**, *12* (6), 1937-1955.
- (98) Deng, C.; Wu, J.; Cheng, R.; Meng, F.; Klok, H.-A.; Zhong, Z., Functional polypeptide and hybrid materials: Precision synthesis via α -amino acid N-carboxyanhydride polymerization and emerging biomedical applications. *Prog. Polym. Sci.* **2014**, *39* (2), 330-364.
- (99) Puiggali, J.; Subirana, J. A., Synthetic polymers containing α -amino acids: from polyamides to poly(ester amide)s. *J. Pept. Sci.* **2005**, *11* (5), 247-249.
- (100) Guo, K.; Chu, C. C., Synthesis, Characterization, and Biodegradation of Novel Poly(ether ester amide)s Based on l-Phenylalanine and Oligoethylene Glycol. *Biomacromolecules* **2007**, *8* (9), 2851-2861.
- (101) Arabuli, N.; Tsitlanadze, G.; Edilashvili, L.; Kharadze, D.; Gogvadze, T.; Beridze, V.; Gomurashvili, Z.; Katsarava, R., Heterochain polymers based on natural amino acids. Synthesis and enzymatic hydrolysis of regular poly(ester amide)s based on bis(L-phenylalanine) α,ω -alkylene diesters and adipic acid. *Macromol. Chem. Phys.* **1994**, *195* (6), 2279-2289.
- (102) Huang, J.; Heise, A., Stimuli responsive synthetic polypeptides derived from N-carboxyanhydride (NCA) polymerisation. *Chem. Soc. Rev.* **2013**, *42* (17), 7373-7390.
- (103) Feng, Y.; Lu, J.; Behl, M.; Lendlein, A., Progress in Depsipeptide-Based Biomaterials. *Macromolecular Bioscience* **2010**, *10* (9), 1008-1021.
- (104) Sun, H.; Cheng, R.; Deng, C.; Meng, F.; Dias, A. A.; Hendriks, M.; Feijen, J.; Zhong, Z., Enzymatically and Reductively Degradable α -Amino Acid-Based Poly(ester amide)s: Synthesis, Cell Compatibility, and Intracellular Anticancer Drug Delivery. *Biomacromolecules* **2015**, *16* (2), 597-605.

- (105) Liu, H.; Wang, R.; Wei, J.; Cheng, C.; Zheng, Y.; Pan, Y.; He, X.; Ding, M.; Tan, H.; Fu, Q., Conformation-Directed Micelle-to-Vesicle Transition of Cholesterol-Decorated Polypeptide Triggered by Oxidation. *J. Am. Chem. Soc.* **2018**, *140* (21), 6604-6610.
- (106) Dirauf, M.; Bandelli, D.; Weber, C.; Görls, H.; Gottschaldt, M.; Schubert, U. S., TBD-Catalyzed Ring-Opening Polymerization of Alkyl-Substituted Morpholine-2,5-Dione Derivatives. *Macromol. Rapid Commun.* *0* (0), 1800433.
- (107) Wang, H.; Dong, M.; Khan, S.; Su, L.; Li, R.; Song, Y.; Lin, Y.-N.; Kang, N.; Komatsu, C. H.; Elsabahy, M.; Wooley, K. L., Acid-Triggered Polymer Backbone Degradation and Disassembly to Achieve Release of Camptothecin from Functional Polyphosphoramidate Nanoparticles. *ACS Macro Lett.* **2018**, *7* (7), 783-788.
- (108) Rahil, J.; Haake, P., Reactivity and mechanism of hydrolysis of phosphonamides. *J. Am. Chem. Soc.* **1981**, *103* (7), 1723-1734.